SC771: Monte Carlo Simulation of Radiation Imaging Systems

Theoretical Session

A Badano,[1] J Sempau,[2] MJ Flynn[3]

[1] NIBIB/CDRH Lab for the Assessment of Medical Imaging Systems
Center for Devices and Radiological Health
U. S. Food and Drug Administration, Rockville
[2] Institut de Tècniques Energètiques
Universitat Politècnica de Catalunya, Barcelona
[3] Henry Ford Health System, Detroit

Short-course at SPIE Medical Imaging Symposium, San Diego, 2/17/07.

The International Society for Optical Engineering

Course syllabus

1. **Fundamentals of Monte Carlo (40 min, AB)**
   - Experiments, theory and numerical modeling
   - Components of the Monte Carlo method
   - The Monte Carlo method
   - Transport coefficients and cross sections
   - Random number generators
   - Variance reduction
2. PENELOPE **(70 min, JS),** *10-min break*
3. MANTIS **(70 min, AB)**
   - Introduction to MANTIS
   - Optical transport methods
   - Validation and examples
   - Applications in indirect x-ray imaging
   - Applications in display devices
   - Other applications
4. **Imaging simulation using** XSPECT **(45, MJF)**
5. **File list and description for the companion CD**
6. **Hands-on demonstrations (afternoon session, AB/JS/MJF)**

Outline

1. **Fundamentals of Monte Carlo (40 min, AB)**
   - Experiments, theory and numerical modeling
   - Components of the Monte Carlo method
   - The Monte Carlo method
   - Transport coefficients and cross sections
   - Random number generators
   - Variance reduction
2. PENELOPE (70 min, JS), *10-min break*
3. MANTIS (70 min, AB)
   - Introduction to MANTIS
   - Optical transport methods
   - Validation and examples
   - Applications in indirect x-ray imaging
   - Applications in display devices
   - Other applications
4. Imaging simulation using XSPECT (45, MJF)
5. File list and description for the companion CD
6. Hands-on demonstrations (afternoon session, AB/JS/MJF)

Experiments, theory and numerical modeling

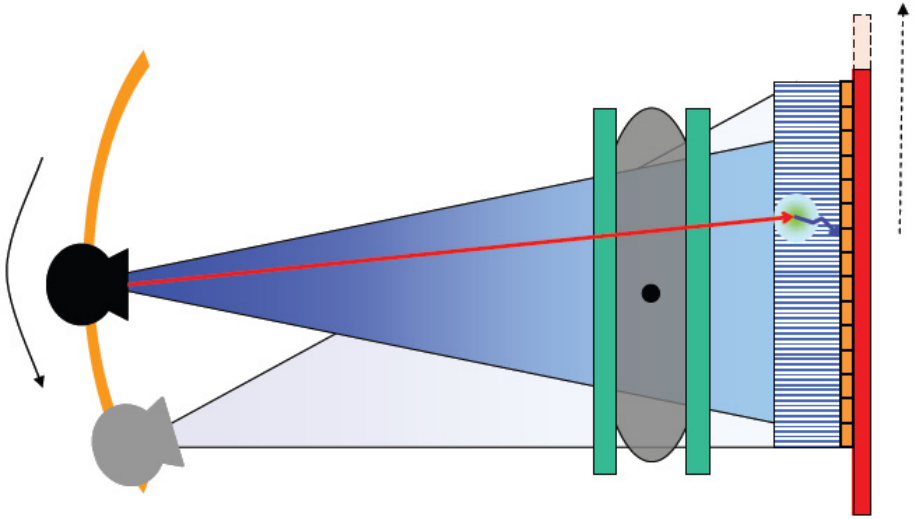

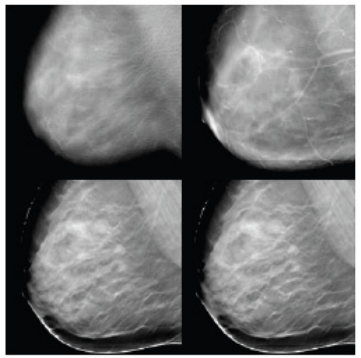

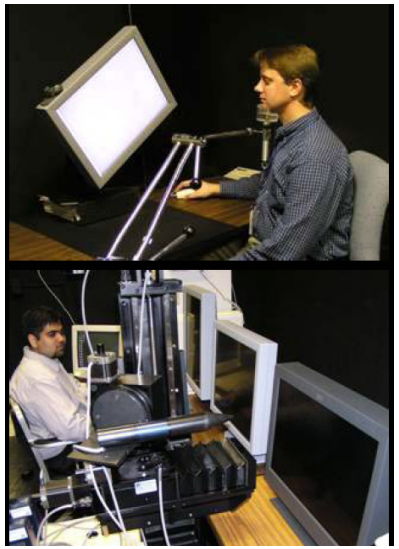

Source

Database of measured spectra & code for generating spectra after arbitrary materials.

Object statistics

Computer models of backgrounds and signals to compute SNR_{input}.

Imaging sensors

Monte Carlo simulation (MANTIS), models and experimental validation of digital detectors.

Display

State-of-the-art medical display characterization lab.

Observer performance

Task performance using mathematical and human observers.

Approaches for numerical modeling I

Simple model (can be analytical)

- No x-ray scatter, no e^- transport
- No phosphor blur, no gain variance
- No optical transport, no depth effects
- Limited to $\perp$ x rays

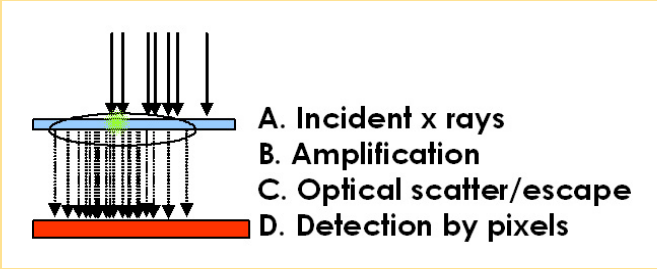

First-order approximation (can be analytical)

- No x-ray scatter, no e^- transport
- Stationary and isotropic phosphor blur
- Gain variance due to conversion (Poisson)
- Optical transport via diffusion approximation
- Limited to $\perp$ x rays

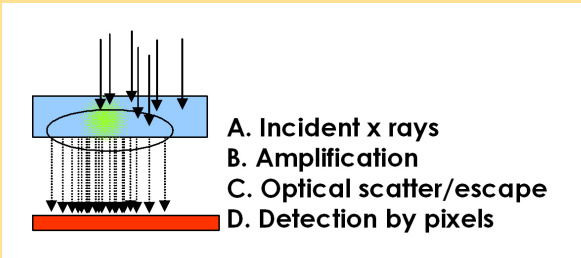

Approaches for numerical modeling II

Second-order approximation [1,2]

- No x-ray scatter in detector, no e^- transport
- Limited to low x-ray energy: no Compton, no atomic relaxation
- Stationary phosphor blur and Poisson gain
- Detailed optical transport with Monte Carlo
- Limited to perpendicular x rays

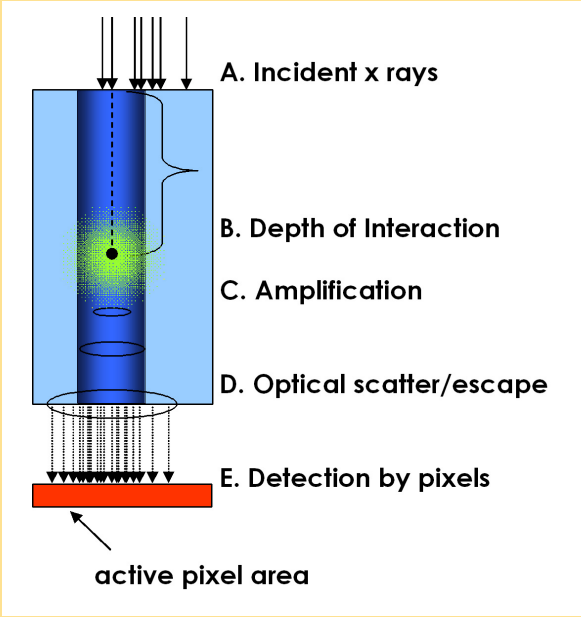

Approaches for numerical modeling III

Detailed simulation [3]

- Particle energy range 100 eV - 1 GeV
- All x-ray interactions including Compton scattering and atomic relaxation (fluorescence and Auger electrons)
- Detailed $e^{\pm}$ transport
- Anisotropic optical blur with realistic columnar model
- Any x-ray incidence angle
- Complex object and detector models
- List-mode operation at interaction level, with simultaneous scoring of dose and imaging performance

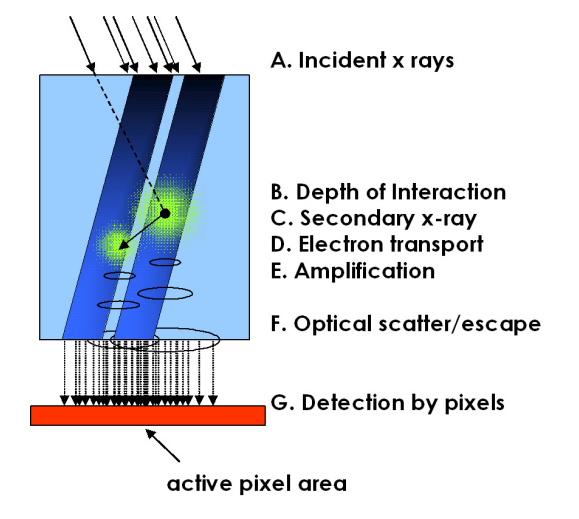

How much detail is required?

Goal of the simulation

- Design, optimization, or knowledge of the limitations of the system?
- What is the imaging task? What is the scale of the imaged object?

Benefits of Monte Carlo simulations

- Knowledge of the forward-problem in shift-variant, non-stationary systems can lead to improved image quality and reconstruction.
- Monte Carlo methods are uniquely positioned to address complex 3D geometries. Moreover, variability in imaging can be represented using massive parallel techniques.

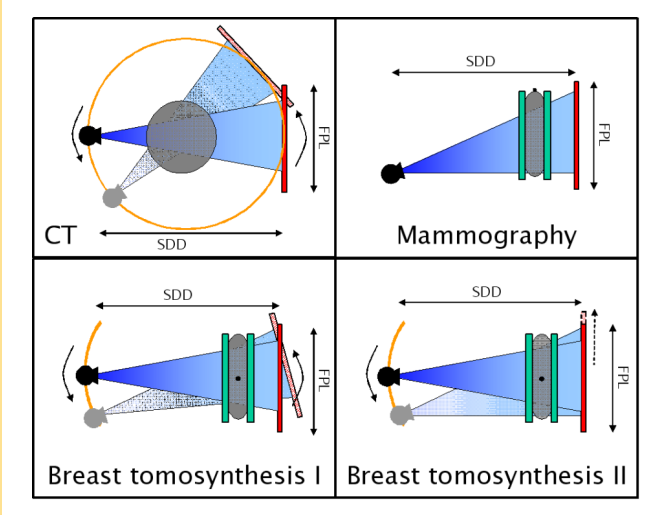

Components of the Monte Carlo method

Components

- Physics models represented by a probability density model
- Geometry of source, object and detector
- Outcome or metric
- Uncertainty

Topics

- Probability distribution functions
- Sampling rules
- Random number generator
- Scoring (tally for output)
- Error estimation (statistical)
- Variance reduction techniques
- Parallelization

Monte Carlo methods I

Stochastic simulation methods

- A quantity is estimated by repetition of a random experiment.
- The mean value of the quantity, over many repetitions, converges to the quantity of interest.
- In computer simulations, random experiments are performed with the help of random number generators.
- Term coined in the early 1940's by Stanislaw Ulam.
- Particularly suited for parallel computation.

Monte Carlo methods II

Monte Carlo integration

$$Q = \int_a^b q(x)p(x)dx$$

where $p(x)$ is the PDF, and Q is the quantity of interest.
The estimate Q_N (after N samples of x_i) is

$$Q_N = \frac{1}{N}\sum_{i=1}^{N} q(x_i)$$

In this case,

$$\lim_{N\to\infty} Q_N = Q$$

$$Var(Q_N) \propto \frac{1}{N}$$

The estimate is unbiased and consistent.

Monte Carlo methods III

Monte Carlo transport methods

Appropriate tracking of particles from source (external or internal) to fate (detection, absorption, scattering).

$$D = \int_0^Z d(z)p(x)dx$$

where $p(x)$ is the PDF, and D is the quantity of interest.
The estimate D_N (after N particles) is

$$D_N = \frac{1}{N}\sum_{i=1}^{N} d_{particle}$$

In this case, the estimate is unbiased provided that the physics models are accurate.

$$\lim_{N\to\infty} D_N = D$$

Cross section and transport coefficients I

Linear attenuation coefficient, μ

The probability of a photon with a given energy to undergo photoelectric absorption or scattering when crossing a layer of material can be expressed quantitatively in terms of the linear attenuation coefficient (cm^{-1}), which is dependent on density, ρ (g/cm^{-1}): $\mu_{tot} = \sum_i \mu_i$, where i represent different interaction types.

Mass attenuation coefficient, μ/ρ

If the mass attenuation coefficients are directly available for individual elements, the linear attenuation coefficients for mixtures and compounds are obtained according to: $\mu = \rho \sum_i w_i (\mu/\rho)_i$, where w_i are the elemental mass fractions.

Cross section and transport coefficients II

Differential cross section, $\mathrm{d}\sigma$

The scattering is specified by the differential (microscopic) cross section: $\frac{\mathrm{d}^2\sigma}{\mathrm{d}W\mathrm{d}\Omega}(E, W, \theta)$, where W is the energy lost by the incident particle, $\mathrm{d}\Omega$ is the solid angle element in the direction (θ, ϕ).

Total cross section, σ

σ is a measure of the probability per unit path length of a specified interaction between an incident radiation and a target particle or system of particles. Units are [L^2, with 1 barn = 10^{-24} cm^2]. With axial symmetry, the total cross section is $\sigma(E) = \int_0^E \mathrm{d}W \int_0^\pi 2\pi \sin\theta \mathrm{d}\theta \frac{\mathrm{d}^2\sigma}{\mathrm{d}W\mathrm{d}\Omega}(E, W, \theta)$.

Macroscopic cross section, Σ

Σ is the cross section per unit volume. The product of the microscopic cross-section and the number of targets per unit volume, $\sigma\mathcal{N} = 1/\lambda$.
For a mixture of nuclides, it is the stoichiometrically weighted sum of such products.

Cross section and transport coefficients III

Total mean free path, λ

The inverse of the interaction probability per unit path length: $\lambda = \frac{1}{\mathcal{N}\sigma}$.

Density of particles

The number of molecules per unit volume is given by $\mathcal{N} = N_A \frac{\rho}{A_M}$ where N_A is Avogadro's number[a] (6.022×10^{23} mol^{-1}) and ρ is the mass density of the material. Use stoichiometry for molecules and compounds.

[a] Number of atoms in a mass equal to the substance's atomic mass A_M, in grams.

Random number generators I

Anyone who considers arithmetical methods of producing random digits is, of course, in a state of sin. – John von Neumann (1951)

Anyone who has not seen the above quotation in at least 100 places is probably not very old. – D. V. Pryor (1993)

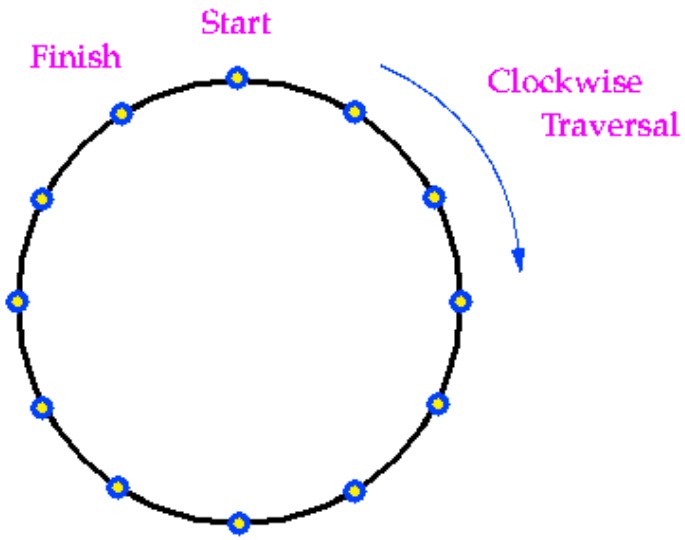

Figure 2: Illustration of Random Number Cycle

Random number generators II

Desired attributes

- Pseudo-randomness (emulation of stochastic natural phenomena): correlations (hyperplanes [4]) in fine scale ($0.500 < x < 0.501$, $0.400 < y < 0.401$) for congruential (left), Marsaglia/James (center), and Mersenne Twister[a] [5, 6] (right). 538 points in each plot.

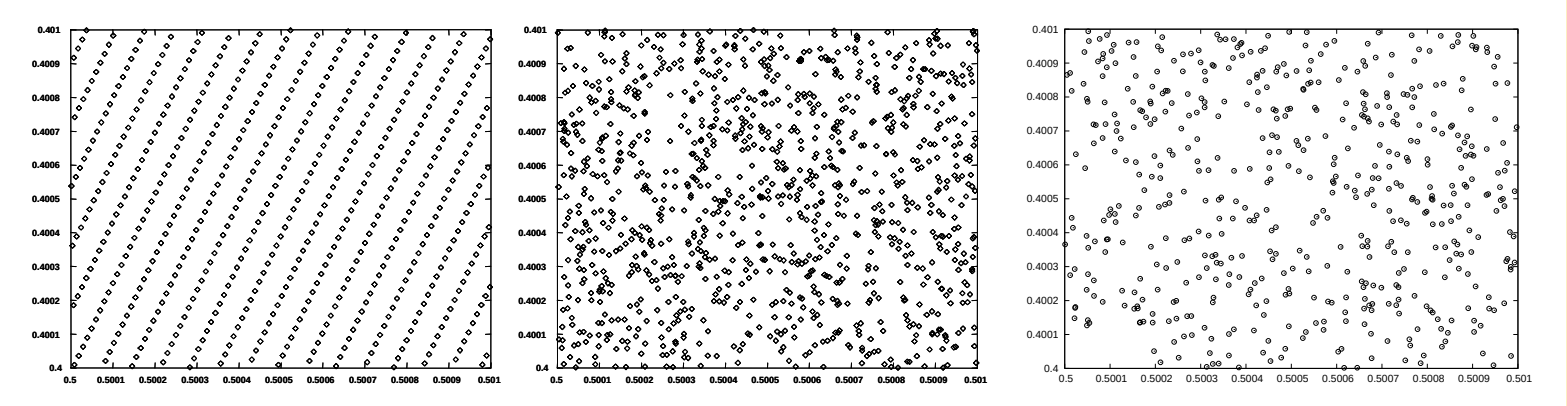

- Portability and repeatability (across architectures and OS)
- Long period (beware of periodicity in asymptotic behavior)
- Computational efficiency and parallel overhead

[a] Intel's implementation in IMKL.

Variance reduction I

Statistical uncertainty

- Any quantity of interest (energy deposited, $E_d = \int e p_e de$) is evaluated as the average of a large number N of simulated random events:

$$\overline{E_d} = \frac{1}{N} \sum_{i=1}^{N} e_i,$$

with a statistical uncertainty given by,

$$\sigma_{E_d} = \sqrt{\frac{1}{N} \left[\frac{1}{N} \sum_{i=1}^{N} e_i^2 - \overline{E_d}^2 \right]}.$$

Variance reduction

Used to reduce the number of histories necessary to achieve the desired statistical uncertainty in a Monte Carlo calculation.

Variance reduction II

Statistical efficiency [7]

$$FOM = \frac{1}{\sigma^2_{E_d} T}$$

- T computation time

Techniques

- Interaction forcing
- Stratified sampling
- Splitting and Russian roulette
- Importance sampling
- Range rejection

Outline

1. Fundamentals of Monte Carlo (40 min, AB)
   - Experiments, theory and numerical modeling
   - Components of the Monte Carlo method
   - The Monte Carlo method
   - Transport coefficients and cross sections
   - Random number generators
   - Variance reduction
2. PENELOPE **(70 min, JS),** *10-min break*
3. MANTIS (70 min, AB)
   - Introduction to MANTIS
   - Optical transport methods
   - Validation and examples
   - Applications in indirect x-ray imaging
   - Applications in display devices
   - Other applications
4. Imaging simulation using XSPECT (45, MJF)
5. File list and description for the companion CD
6. Hands-on demonstrations (afternoon session, AB/JS/MJF)

Overview of PENELOPE

Francesc Salvat

José M. Fernández-Varea
Univ. de Barcelona

Josep Sempau
Univ. Politècnica de Catalunya

Penelope
Statue in the Vatican, Rome

Summary

- Physics
  - Photons
  - Electrons & positrons
  - Mixed simulation
- Code operation
- Variance reduction
- Bechmarks and applications

What is PENELOPE?

Software package for MC simulation of the
coupled transport of e± and γ

- **50 eV** < E < 1 GeV
- Arbitrary material systems and complex geometries
- Subroutine package in FORTRAN
- Auxiliary tools (geometry viewers, EMF, etc)

Photon interactions

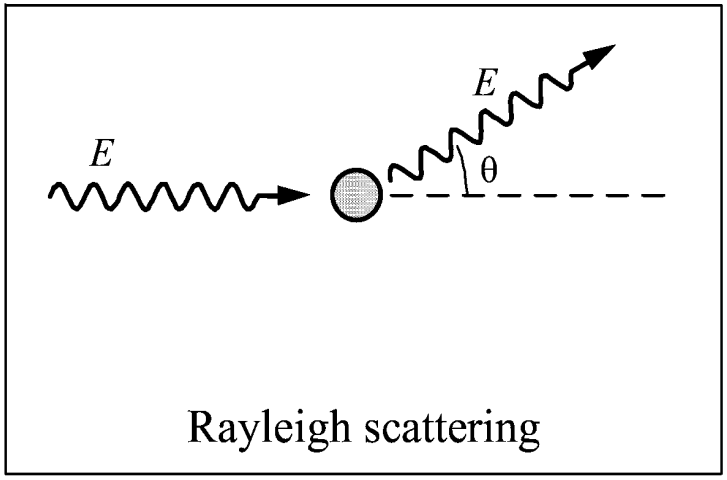

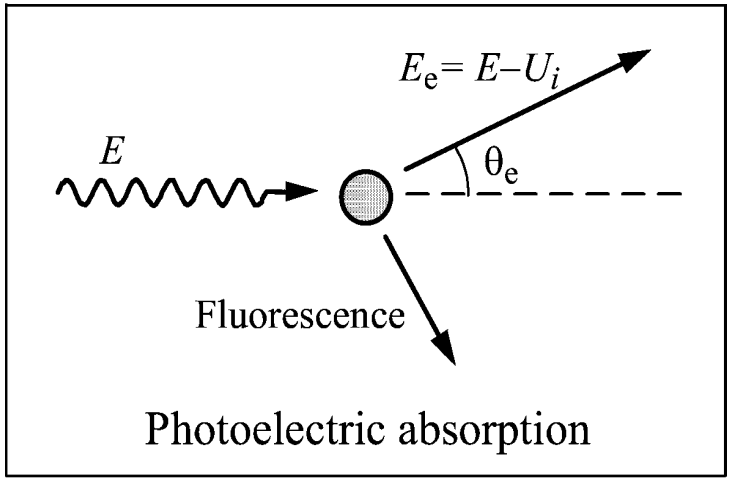

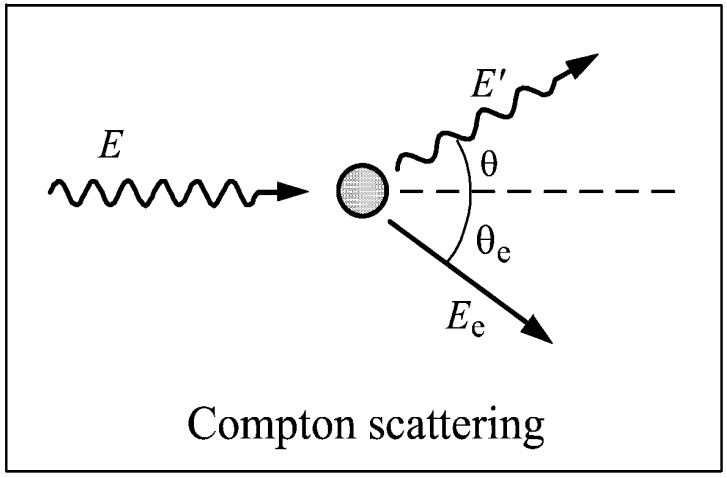

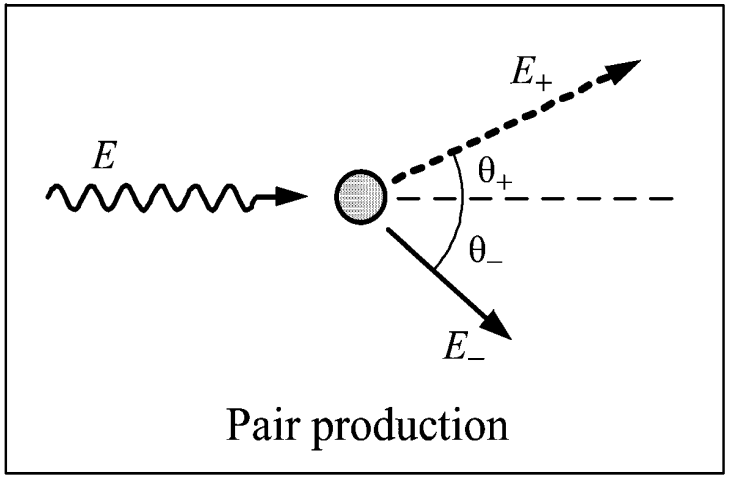

Rayleigh scattering

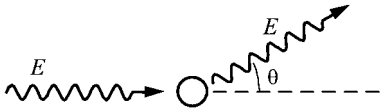

$$\frac{d\sigma_{ra}}{d\Omega} = r_e^2 \frac{1+\cos^2\theta}{2} |F(q,Z)|^2$$

Analytical approx to $F(q,Z)$ from Hubbell et al (1975)

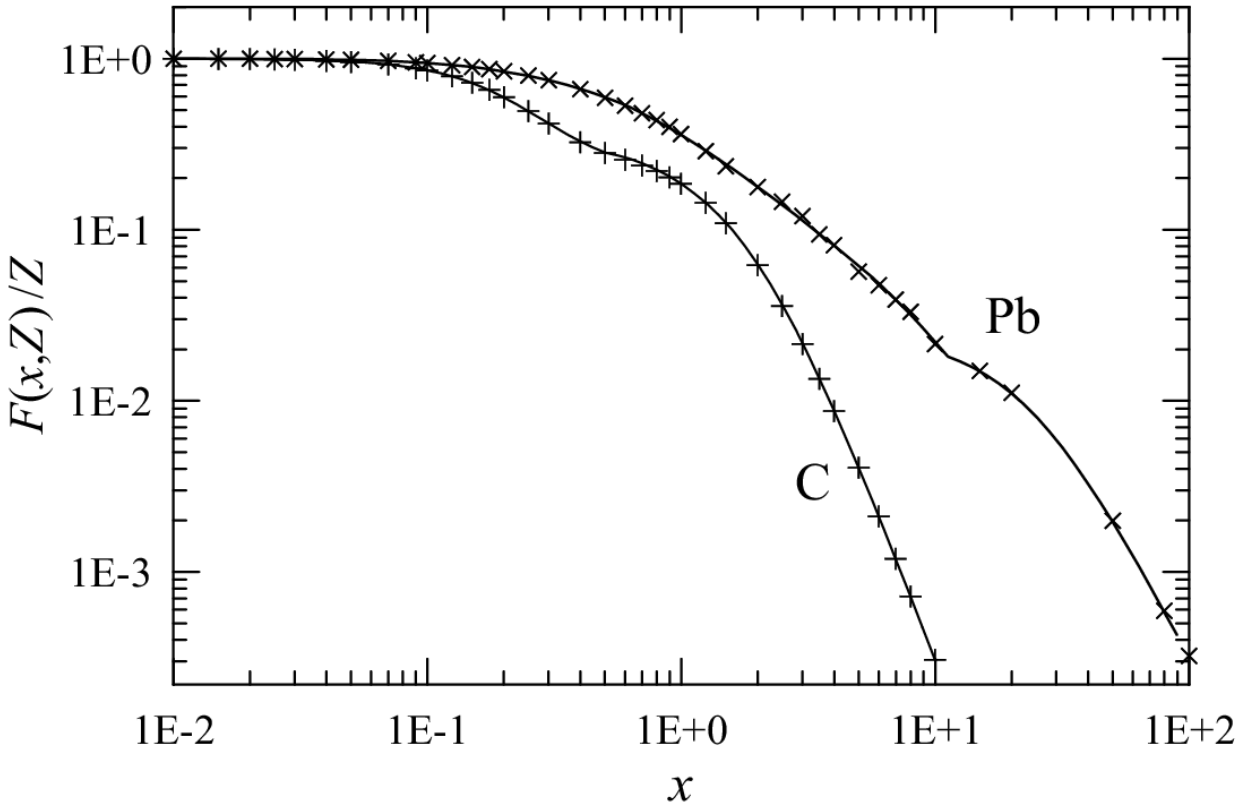

Photoelectric effect

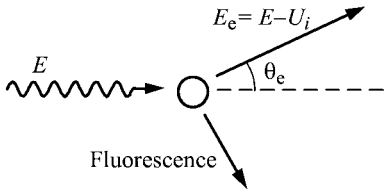

- CS from LLNL EPDL (Cullen et al 1997):
  Scofield's calculation of $\sigma_{ph,shell}$, shell = K,L,M
  Hubbell's total σ_{ph}
- U_{shell} from Lederer & Shirley (1978)
- θ_e (e^- direction) from Sauter (1931) PDF for K shell

Compton scattering

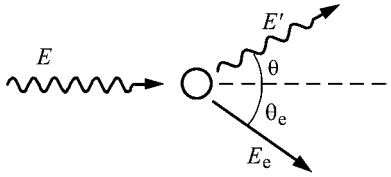

- Waller-Hartree: (Klein-Nishina) × (incoh. scattering function)

$$\frac{\mathrm{d}\sigma_{\mathrm{co}}}{\mathrm{d}\Omega} = \frac{r_{\mathrm{e}}^2}{2}\left(\frac{E_{\mathrm{C}}}{E}\right)^2\left(\frac{E_{\mathrm{C}}}{E}+\frac{E}{E_{\mathrm{C}}}-\sin^2\theta\right)\ S(E,\theta)$$

- Relativistic impulse approx (Ribberfors 1983)
  Includes **Doppler broadening + binding effects**

$$\frac{\mathrm{d}^2\sigma_{\mathrm{co}}}{\mathrm{d}E'\mathrm{d}\Omega} = \frac{\mathrm{d}\sigma_{\mathrm{KN}}}{\mathrm{d}\Omega}\times$$

$$\times\left(\sum_{\mathrm{shells}} f_i\, J_i(p)\ \Theta(E-E'-U_i)\right) F(p)\,\frac{\mathrm{d}p}{\mathrm{d}E'}$$

IA vs Klein-Nishina

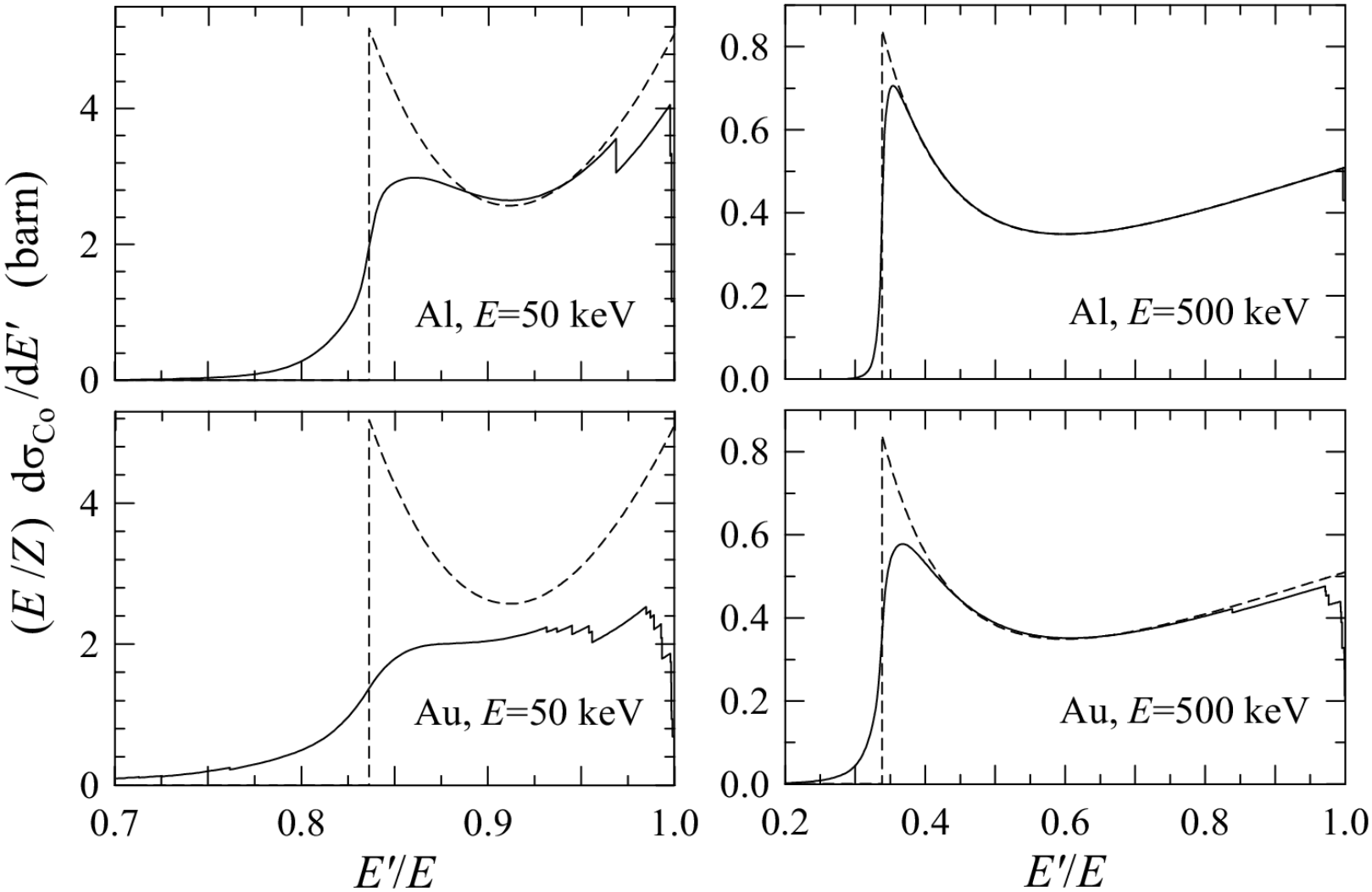

Pair production

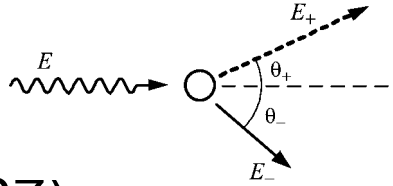

- Total CS from XCOM (Berger & Hubbell 1987)
- Bether-Heitler Born approx for DCS:

$$\frac{\mathrm{d}\sigma_{\mathrm{pp}}}{\mathrm{d}\epsilon} = r_{\mathrm{e}}^2 \alpha Z[Z+\eta]\left\{\left[\epsilon^2+(1-\epsilon)^2\right](\Phi_1 - 4f_{\mathrm{C}}) + \frac{2}{3}\epsilon(1-\epsilon)(\Phi_2 - 4f_{\mathrm{C}})\right\}$$

$$p(\cos\theta_\pm) \sim (1-\beta_\pm\cos\theta_\pm)^{-2}$$

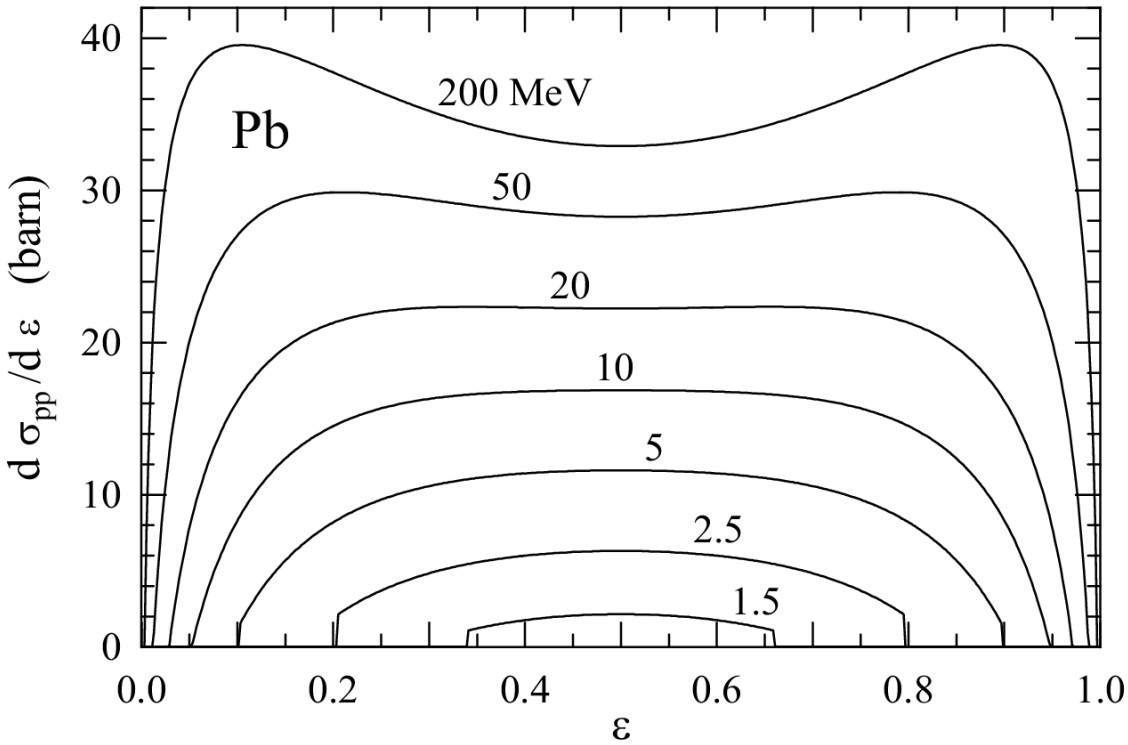

Atomic relaxation

- Ionization of inner shells (K, L, M):

$$E(\text{secondary } e^-) = E(\text{primary}) - U_{\text{shell}}$$

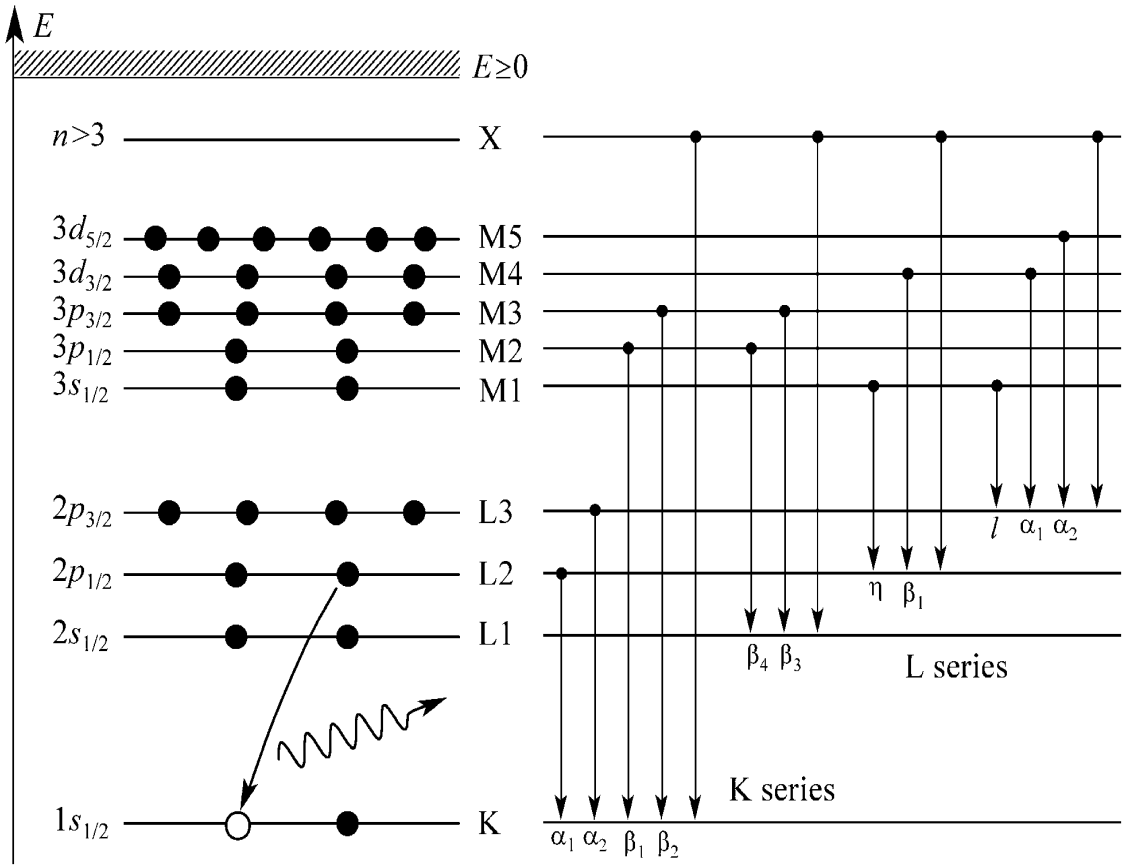

X-rays and Auger electrons

- Transitions probabilities from LLNL EADL (Perkins et al 1991)

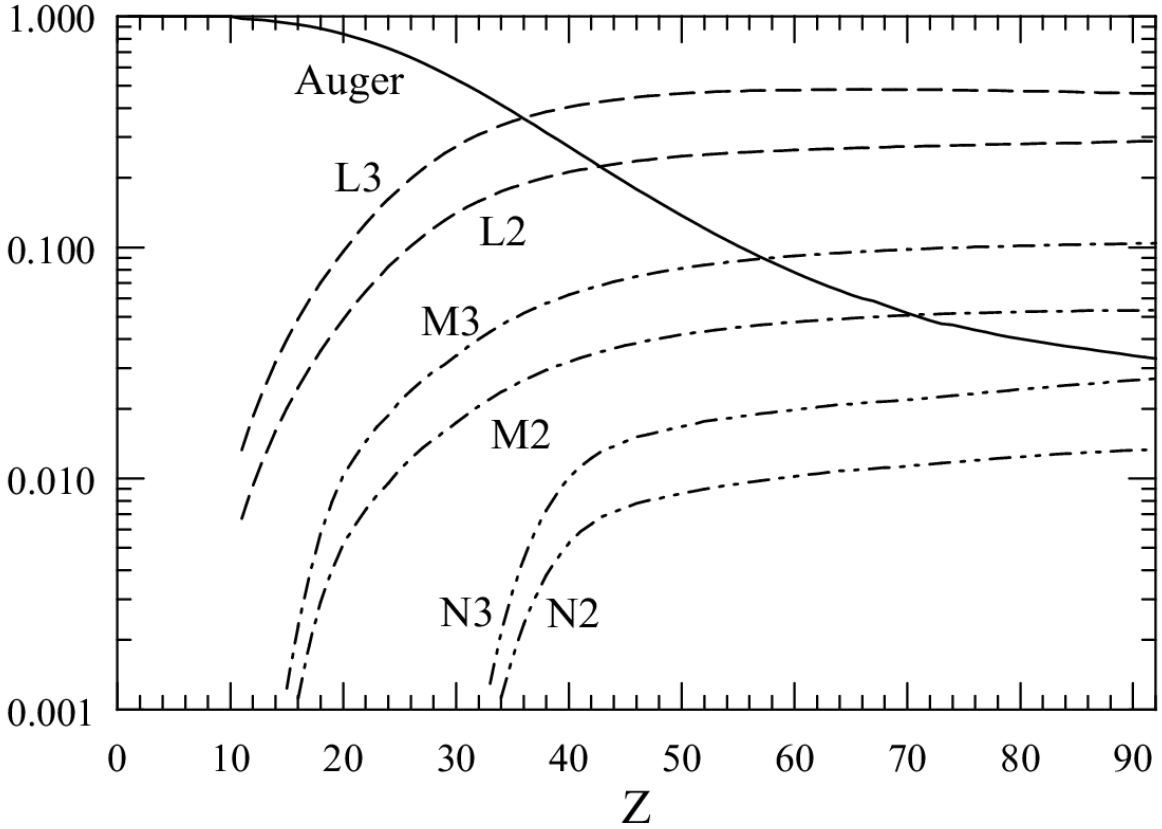

Electron interactions

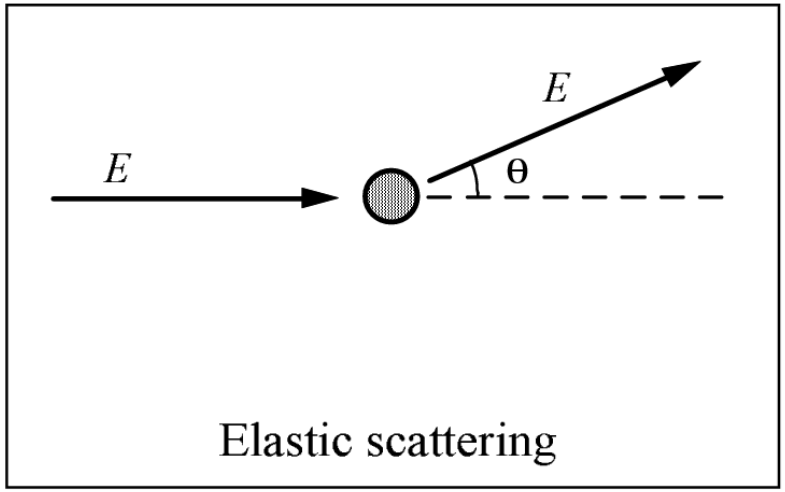

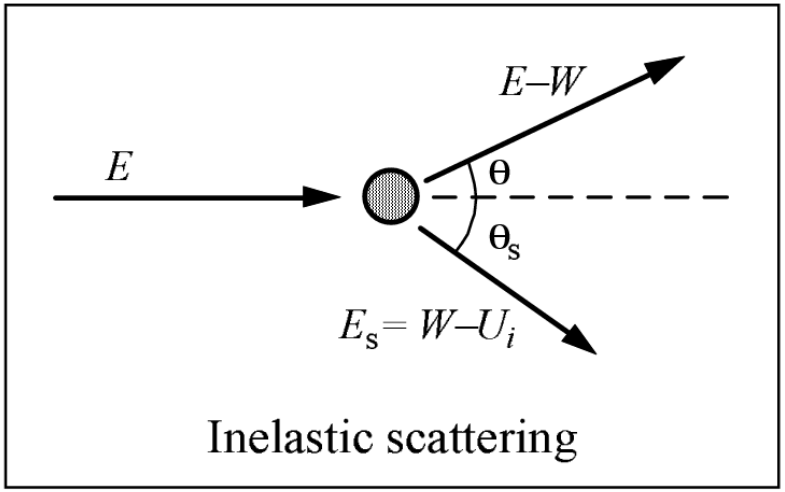

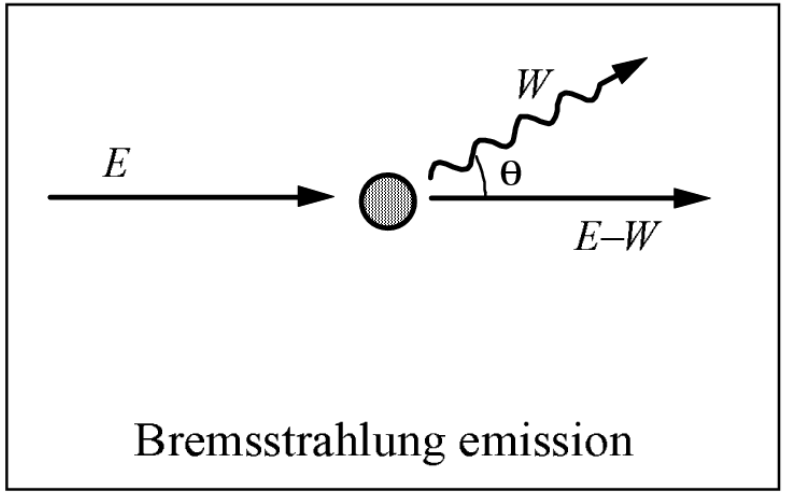

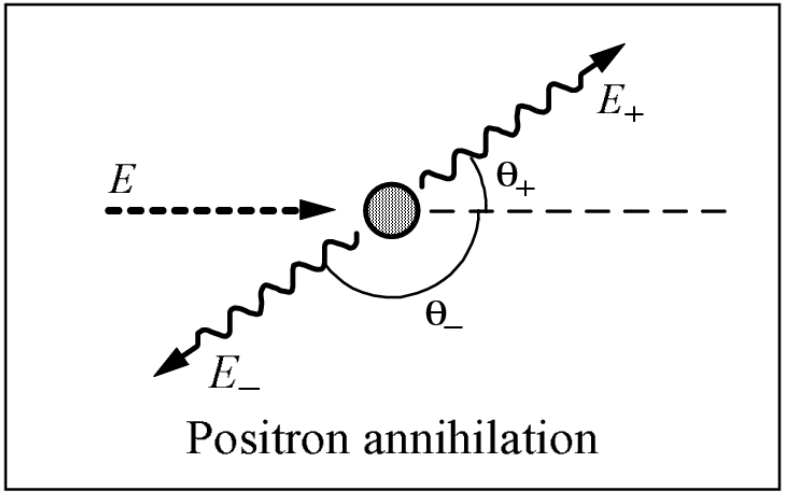

Elastic scattering

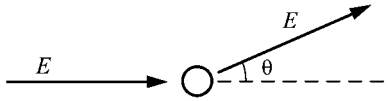

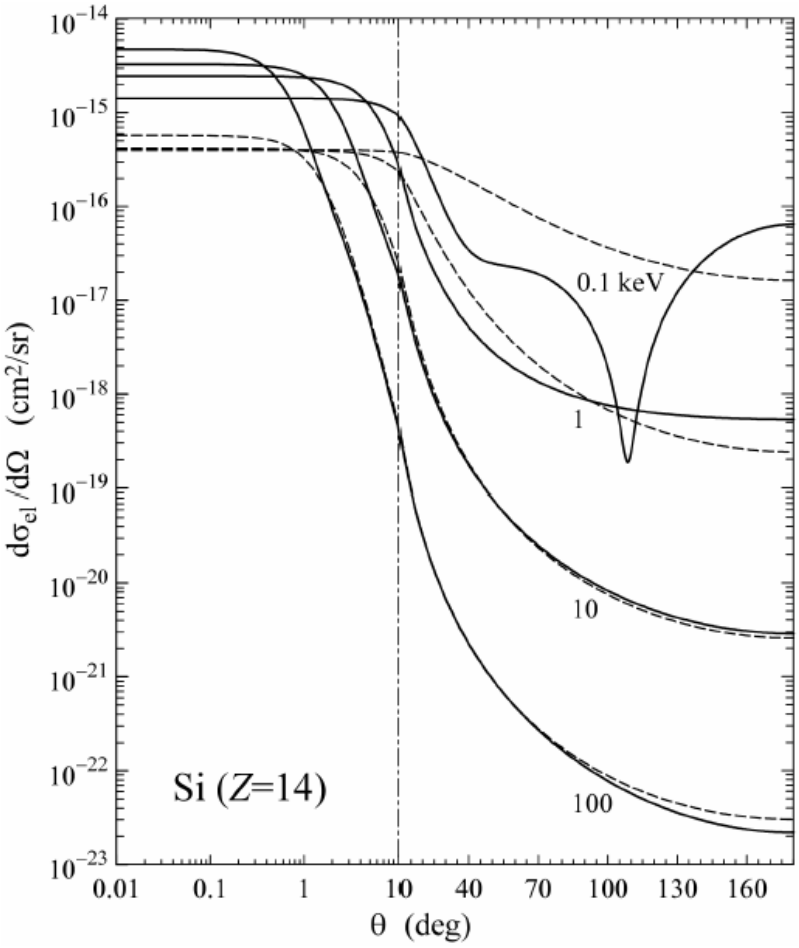

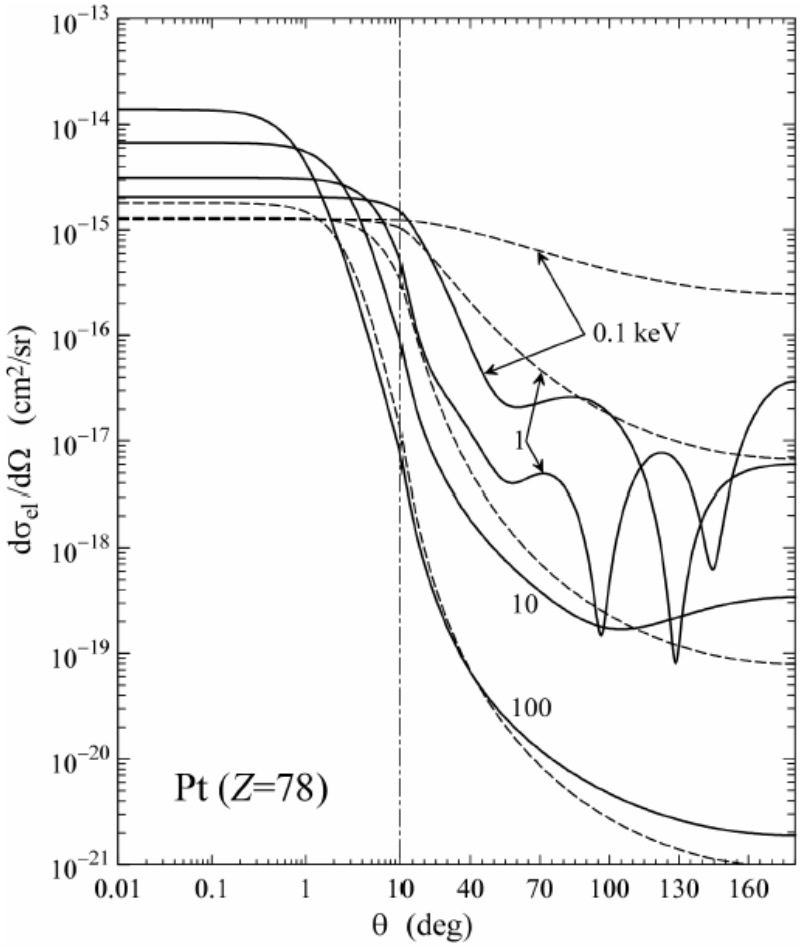

——— Partial wave

- - - - - - Screened Rutherford

Aggregation effects

Independent atom approx (coherent *vs.* incoherent scattering)

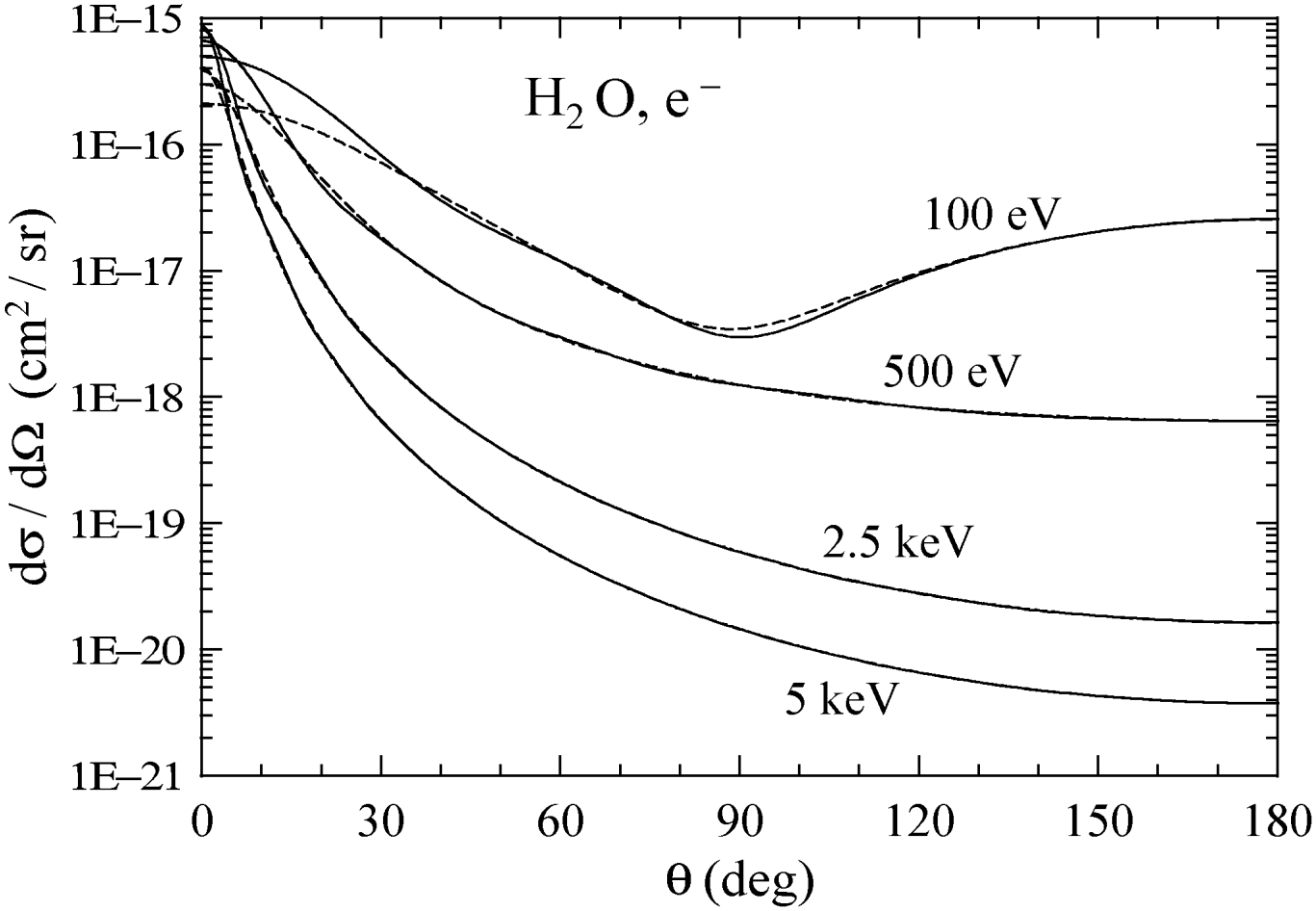

Inelastic scattering

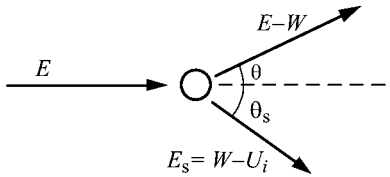

- Binary collisions with free e^- (e^+) at rest can be described by the Møller (Bhabha) DCS

- Collisions with atomic electrons, however, require a different approach (Bethe, 30's): using the plane-wave Born approx the (non-relativistic) DCS can be factorised as

$$\frac{\mathrm{d}^2\sigma_{\mathrm{in}}}{\mathrm{d}W\,\mathrm{d}Q} = \frac{2\pi e^4}{mv^2}\frac{1}{WQ}\frac{\mathrm{d}f(Q,W)}{\mathrm{d}W}$$

- Extended to condensed media (Fano 1963)

Analytical GOS vs ICRU37/experiment

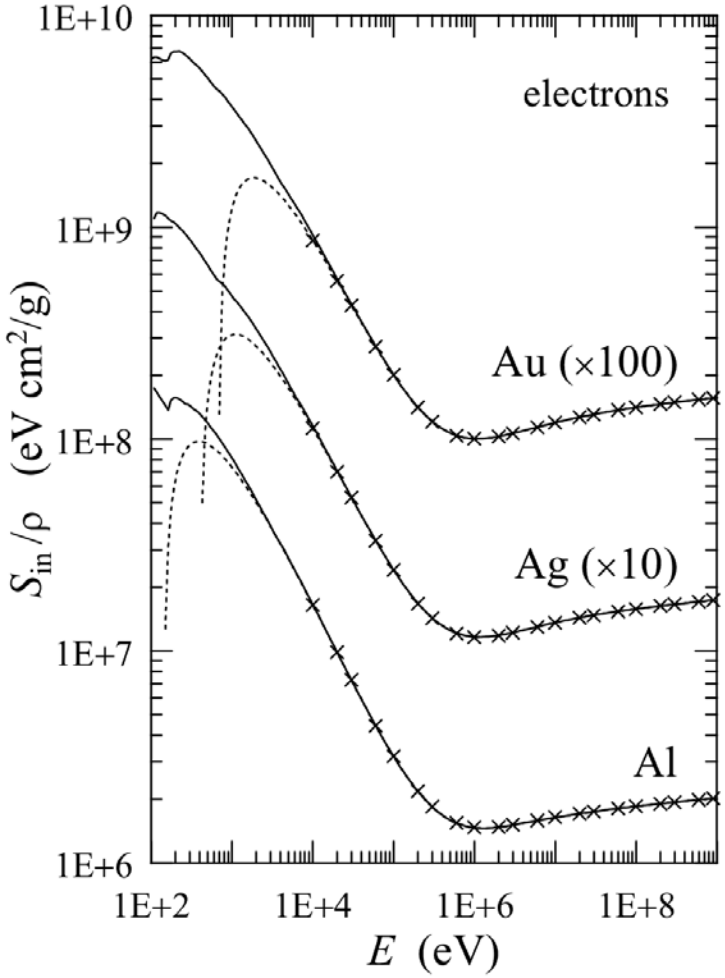

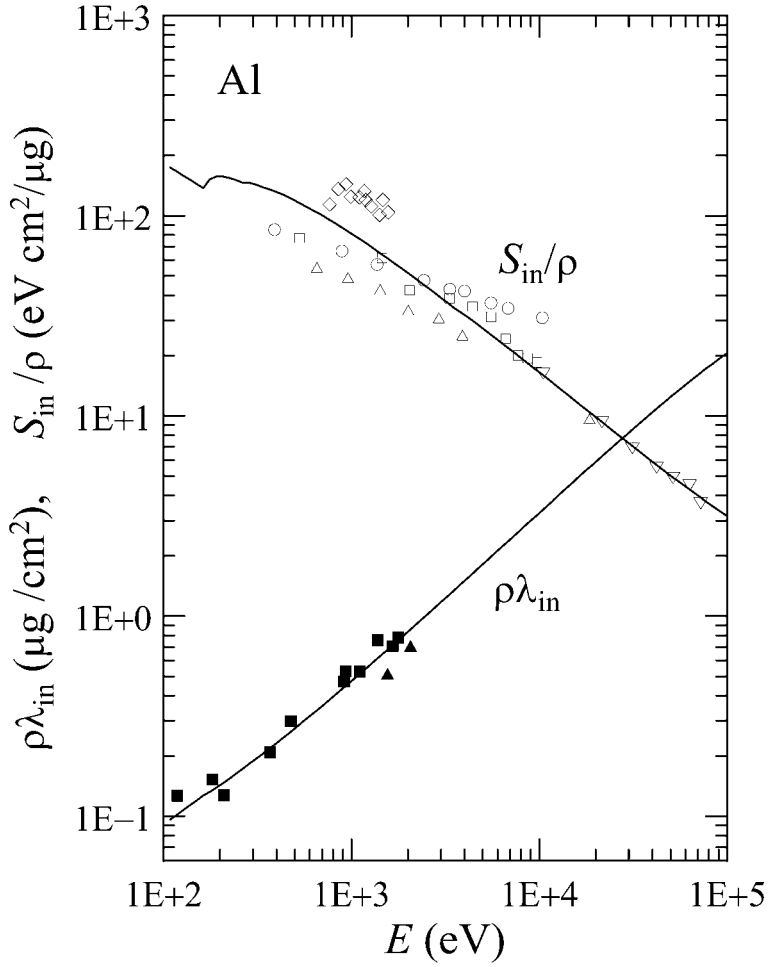

Bremsstrahlung emission

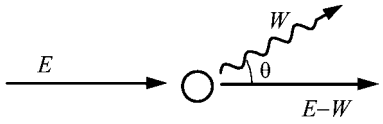

$$\frac{\mathrm{d}^2\sigma_{\mathrm{br}}}{\mathrm{d}W\,\mathrm{d}\cos\theta} = \frac{Z^2}{\beta^2}\,\frac{1}{W}\,\chi(Z,E,W)\,p(\cos\theta;Z,E,W)$$

- $\chi\,(Z,E,W)$: scaled bremsstrahlung DCS
  interpolation in Seltzer and Berger's (1986) database
- $p(\cos\,\theta;Z,E,W)$: shape function
  analytical fit to PW calculations by Kissel et al (1983)
  preserves the correlation between $\cos\theta$ and W
- DCS renormalized to ICRU 37 radiative stopping power

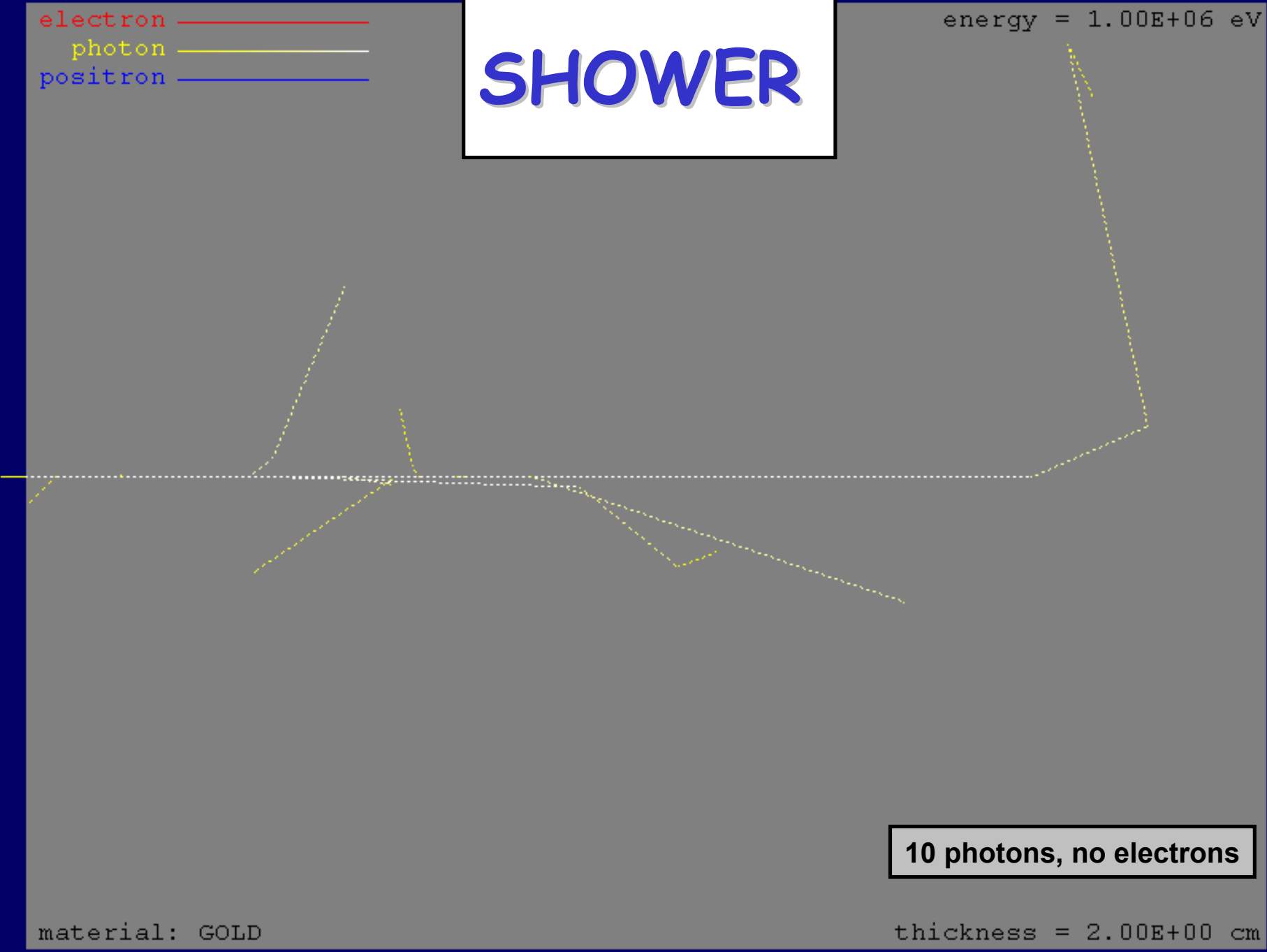
electron
photon
positron
SHOWER
energy = 1.00E+06 eV
10 photons, no electrons
material: GOLD
thickness = 2.00E+00 cm

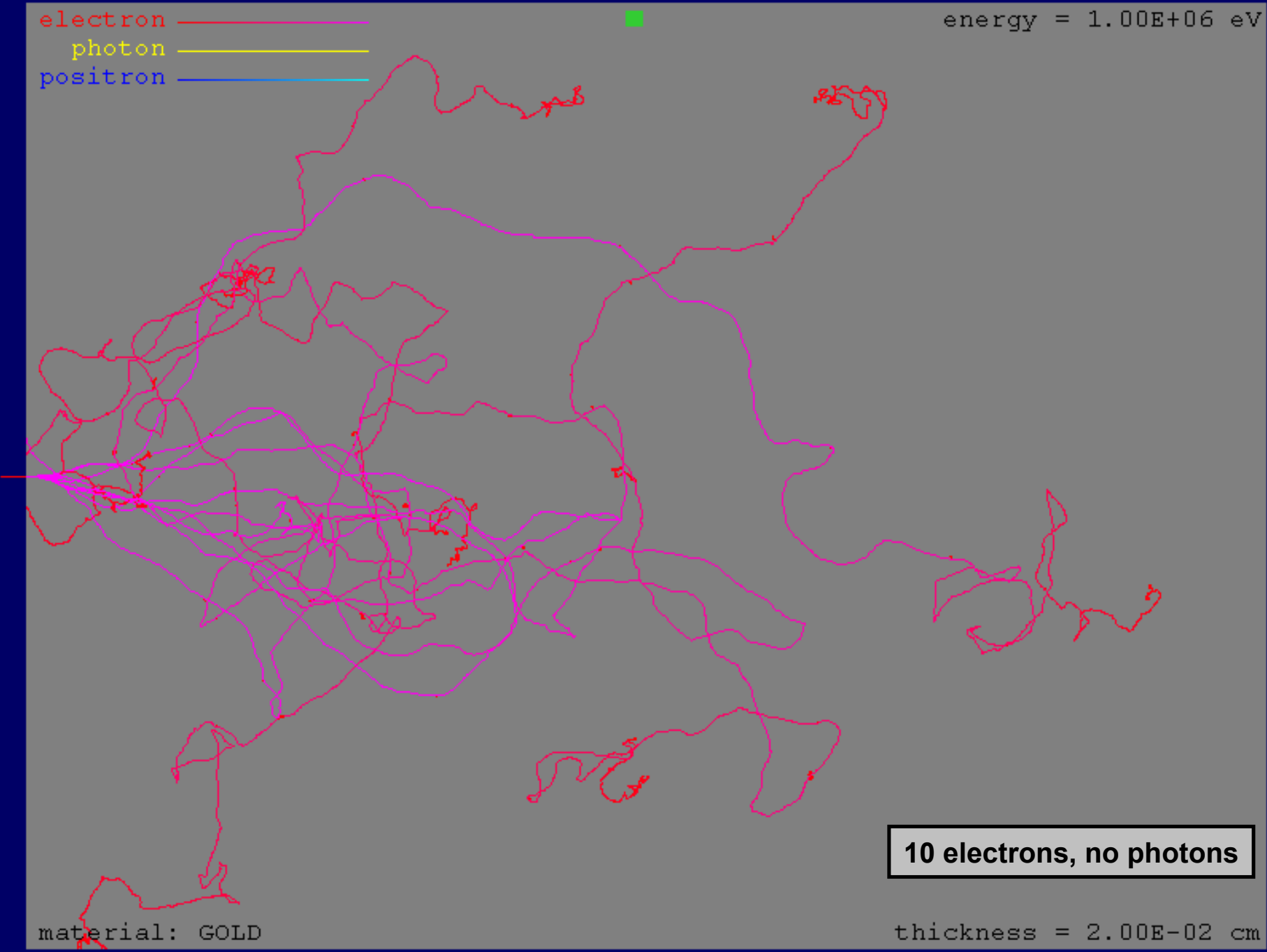
electron
photon
positron
energy = 1.00E+06 eV
10 electrons, no photons
material: GOLD
thickness = 2.00E-02 cm

Mixed simulation

Hard ($\theta > \theta_c$, $W > W_c$)

detailed (interaction-by-interaction), Poisson process

Soft ($\theta < \theta_c$, $W < W_c$)

condensed, in a single simulation step

Random-hinge method

$$s = -\lambda_{\text{hard}} \ln \xi_1$$

$$\tau = s\xi_2$$

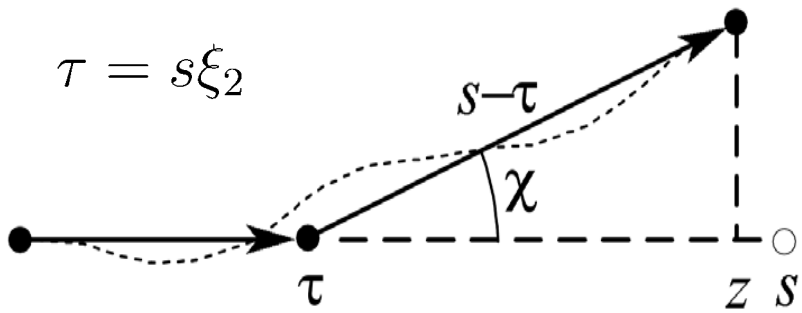

- Accurate spatial moments
- "Natural" interface crossing
- Artificial soft events preserve 1st & 2nd ΔE_{soft} moments (**no CSDA!**)

Geometry package: PENGEOM

Quadric surfaces

$$F(x,y,z) = A_{xx}x^2 + A_{xy}xy + A_{xz}xz + A_{yy}y^2 + A_{yz}yz + A_{zz}z^2 + A_x x + A_y y + A_z z + A_0 = 0,$$

… or

$$F_r(x,y,z) = I_1x^2 + I_2y^2 + I_3z^2 + I_4z + I_5 = 0$$

+ anisotropic scaling
+ rotation
+ translation

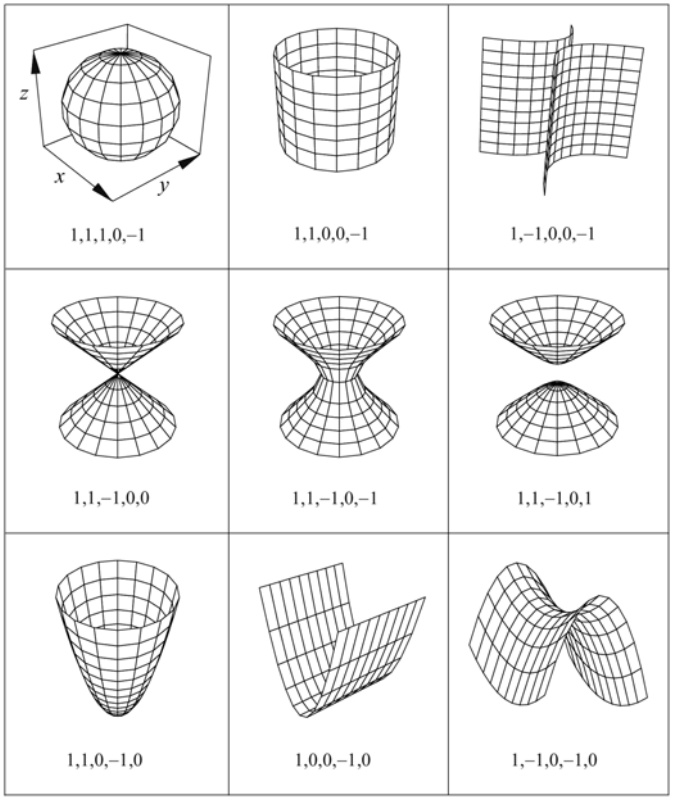

Non-planar reduced quadrics

Geometry viewers

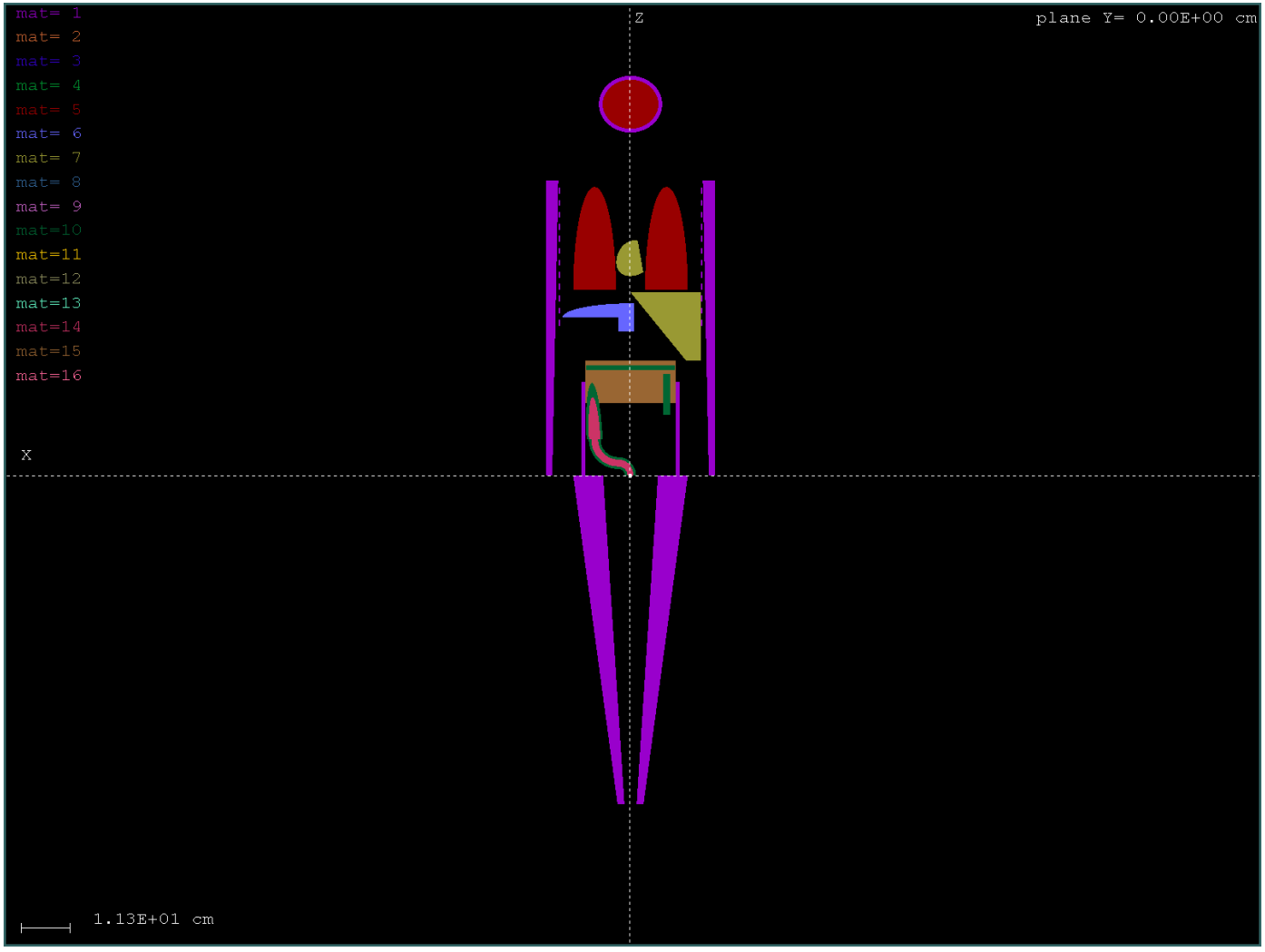

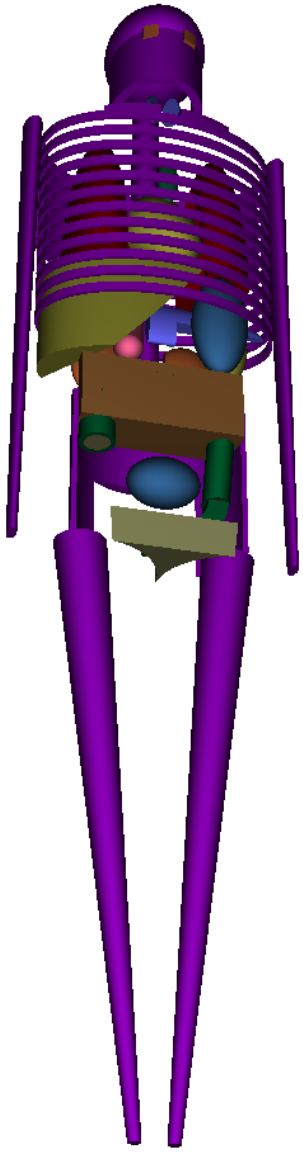

Operation

To be provided by the user

```
program main
call init
n = 0
history: do
  n = n+1
  call CLEANS
  call source
  particle: do
    call SECPAR(left)
    if (left.eq.0) exit particle ! Stack empty
    call START
    interact: do
      call JUMP(dsmax(mat),ds)
      call STEP(ds,dsef,ncross)
      if (ncross.ne.0) then
        if (mat.eq.0) exit interact ! Gone
        call START
        cycle interact
      endif
      call KNOCK(de,icol)
      if (e.lt.eabs(kpar,mat)) exit interact ! Absorbed
    enddo interact
  enddo particle
  if (n.ge.nhist) exit history ! Simulation done
enddo history
stop
```

```
COMMON/TRACK/E,X,Y,Z,U,V,W,WGHT,KPAR,IBODY,MAT,ILB(5)
```

Variance reduction techniques

As a result of a **low scoring probability**, some ill-conditioned problems require very large computing times. VR techniques are intended to reduce the time required to achieve a certain uncertainty.

These situations are frequently a consequence of

- A low interaction probability in the "detector" → ion chambers in linacs
- Deep penetration to reach the "detector" → shielding
- Highly unfavourable geometry → environmental radioactivity

Two convenient figures of merit to measure the performance of an MC algorithm are:

Efficiency: $\epsilon = \dfrac{1}{\Delta^2 t}$, $\Delta = \dfrac{u(Q)}{Q}$ which is independent of t

Intrinsic efficiency: $\epsilon_N = \dfrac{1}{\Delta^2 N}$ Note that $\epsilon = \underbrace{\epsilon_N}_{\text{algorithm}} \underbrace{\dfrac{N}{t}}_{\text{algthm+CPU+compiler}}$

Formal approach

In a formal sense, all MC simulations are equivalent to an integral

$$I = \int \mathrm{d}x \; p(x) q(x) \quad \Rightarrow \quad I \equiv \langle q \rangle \approx \; \overline{q} = \frac{1}{N} \sum_{i=1}^{N} q(x_i)$$

$$\langle q^2 \rangle = \int \mathrm{d}x \; p(x) q^2(x) \quad \Rightarrow \quad \langle q^2 \rangle \approx \frac{1}{N} \sum_{i=1}^{N} q^2(x_i)$$

$$I = \int \mathrm{d}x \; p' \underbrace{\left[\frac{p}{p'} \right]}_{\text{statistical weight}} q \equiv \int \mathrm{d}x \; p' \, q' \quad \Rightarrow \quad \langle q \rangle \approx \overline{q'} = \frac{1}{N} \sum_{i=1}^{N} q'(x_i)$$

$$\langle q'^2 \rangle = \int \mathrm{d}x \; p' q'^2 = \int \mathrm{d}x \; p' \left[\frac{p}{p'} \right]^2 q^2 = \int \mathrm{d}x \left[\frac{p}{p'} \right] p q^2 \; \neq \langle q^2 \rangle$$

Particle splitting

A particle is split into S identical particles with weight w/S

Should be used when a particle approaches the region of interest, to increase the likelihood of having a contribution

Russian roulette

A particle is killed with probability K and, if it survives, its weight is replaced by $w(p/p') = w/(1-K)$

Should be used when a particle goes away from the region of interest, to avoid simulating particles that are likely to not contribute

Splitting and Russian Roulette are complementary and frequently used in conjunction with **weight windows**

Benchmark simulations

J Sempau et al, Nucl. Instr. and Meth. B 207 (2003)

Backscattering coefficients

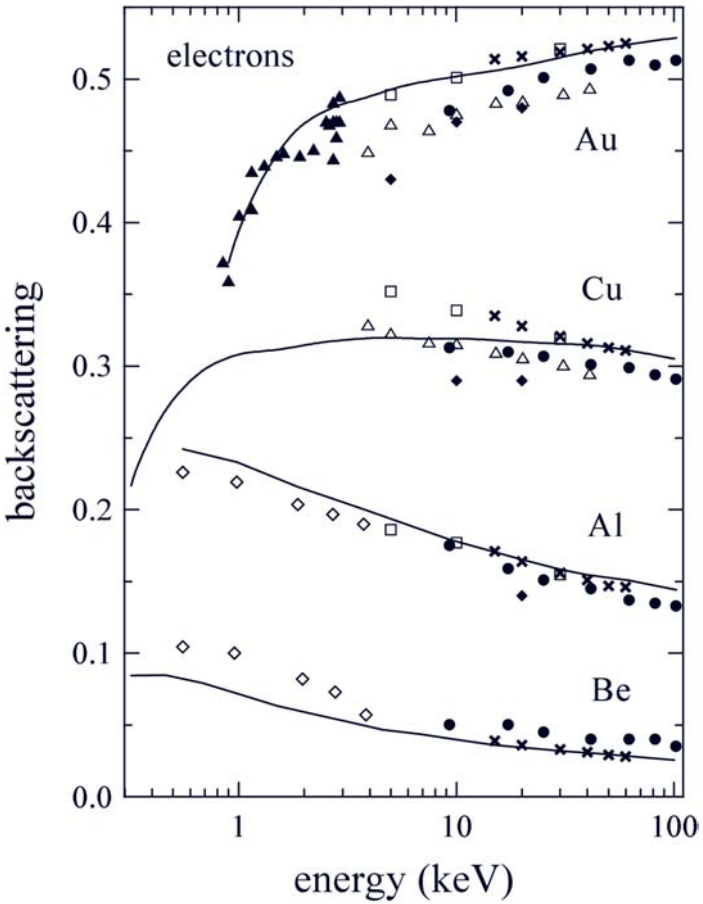

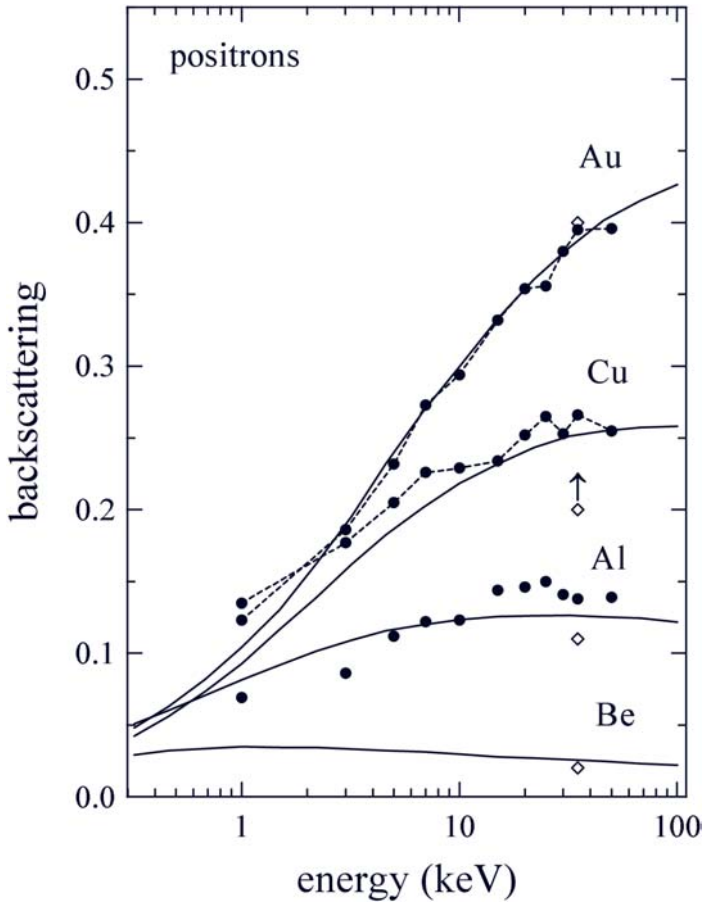

Transmission coefficients

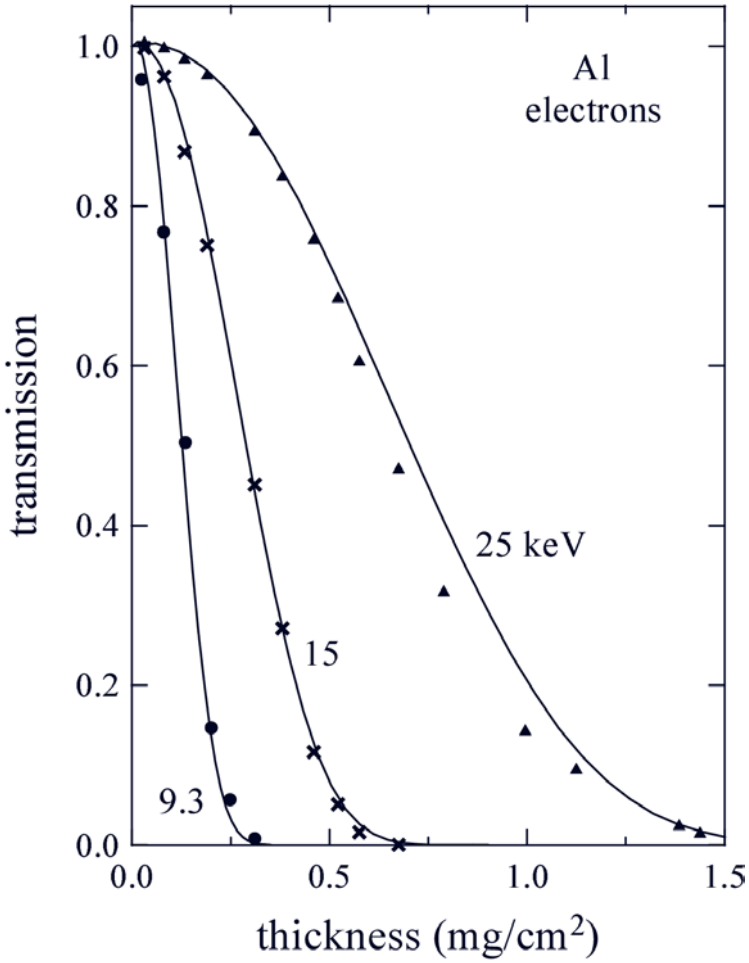

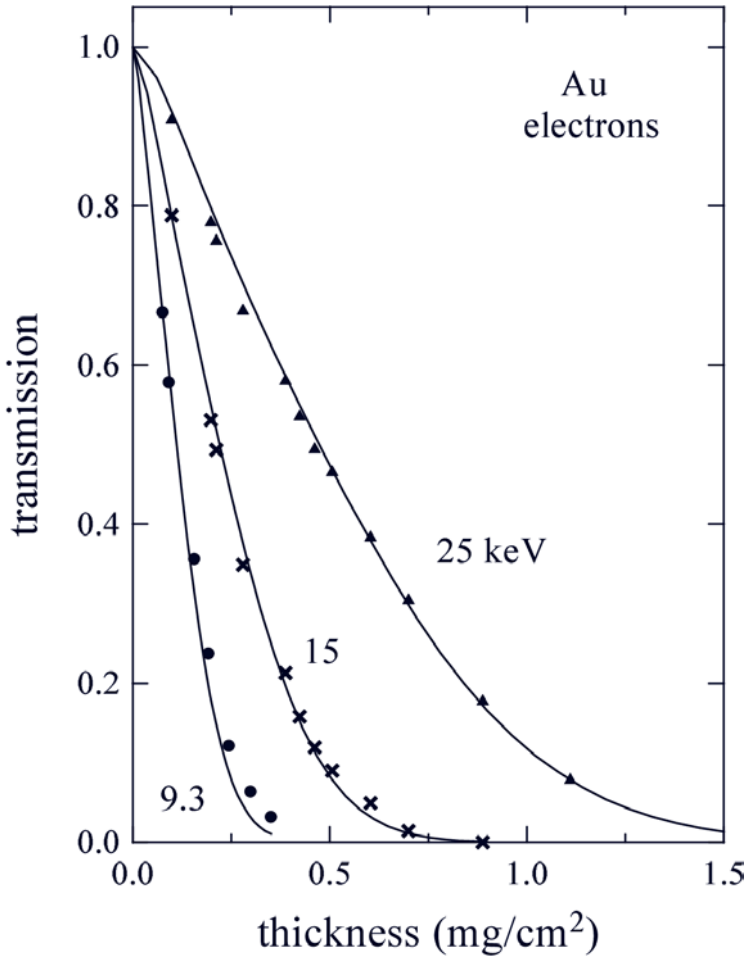

X-ray spectra in EPMA

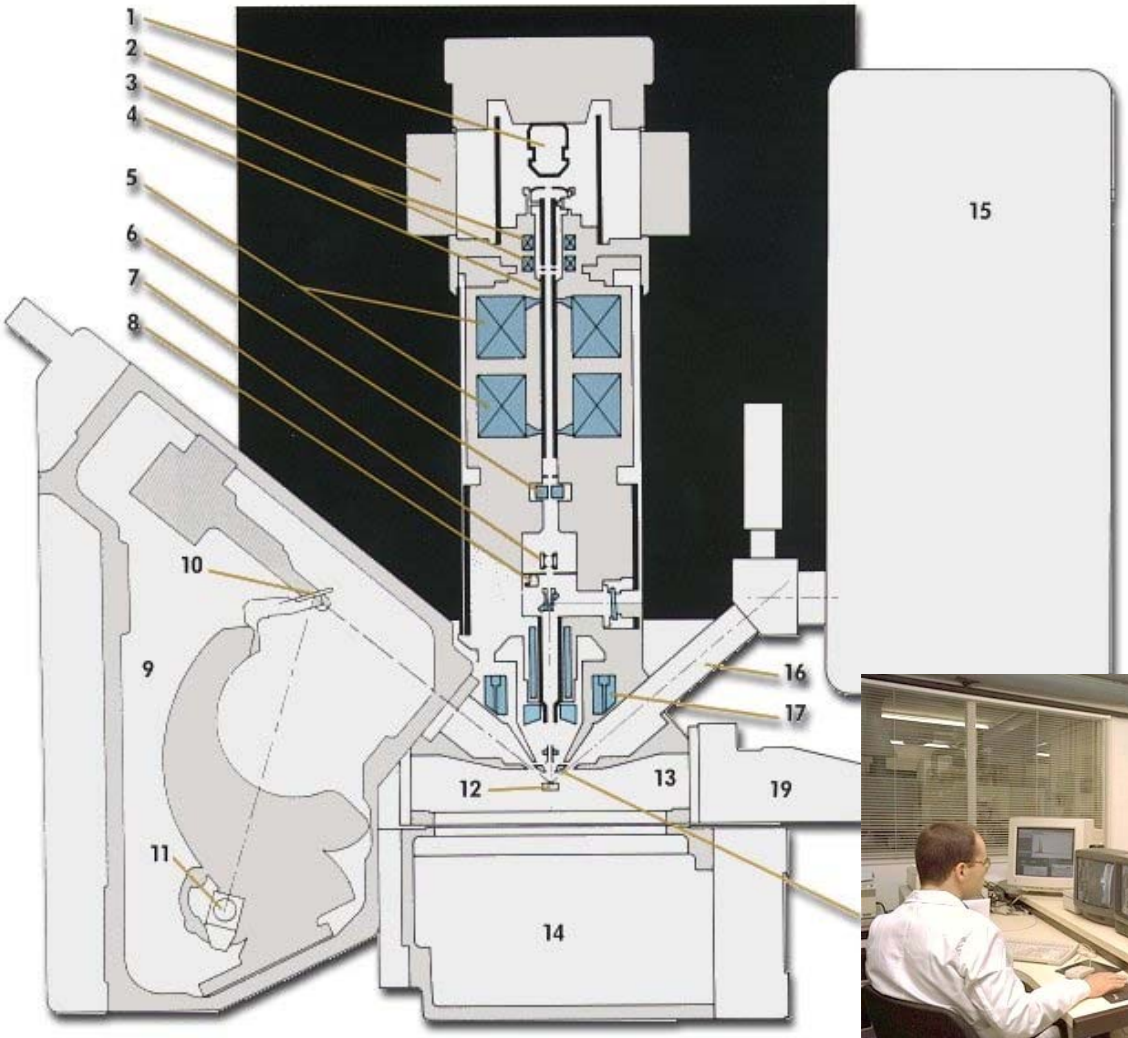

X Llovet et al, J. Appl. Phys. 93 (2003)

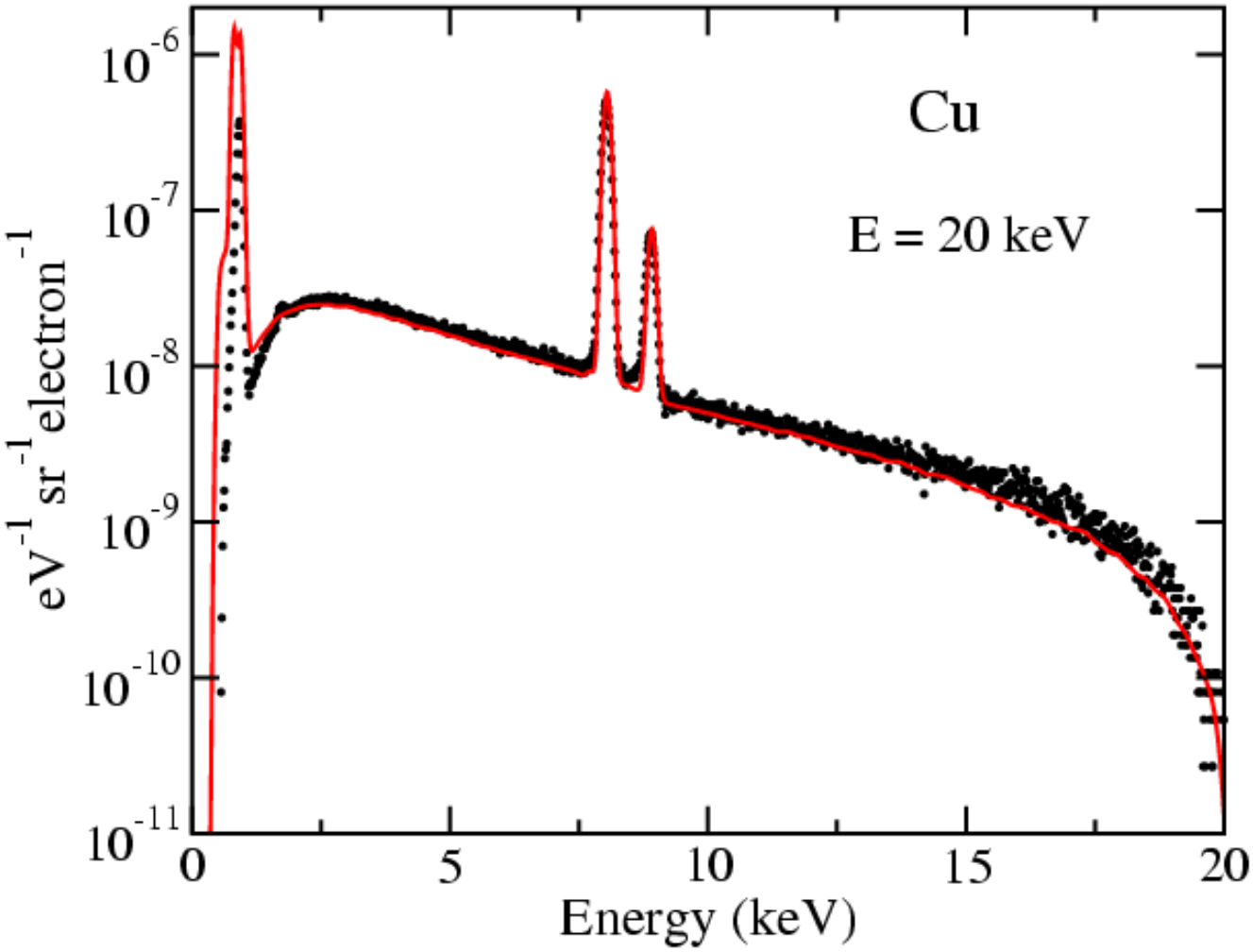

Ionization chambers

J Sempau et al,
Phys. Med. Biol. 49 (2004)

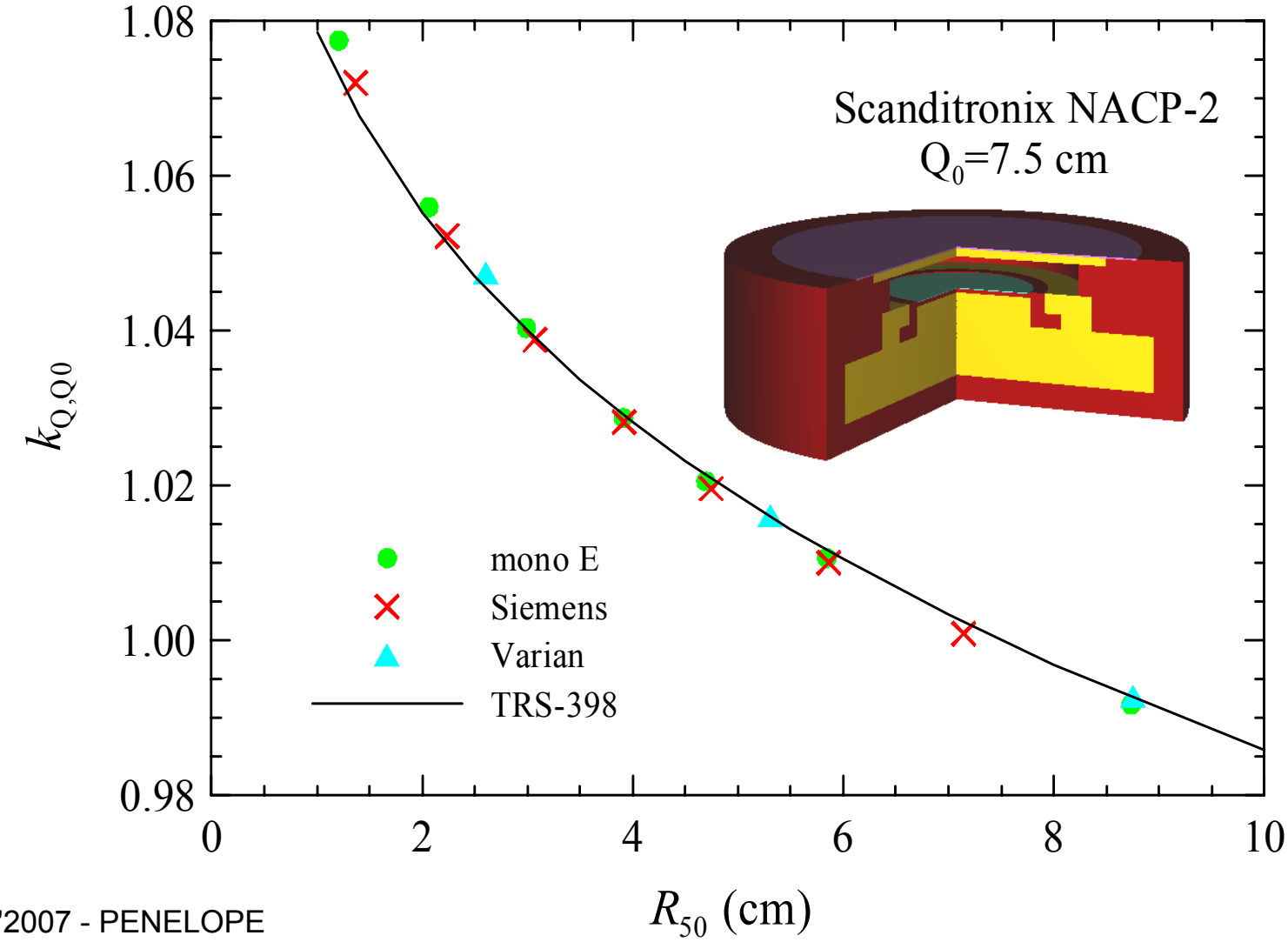

SPECT imaging

A Cot et al,
Phys. Med. Biol. 49 (2004)

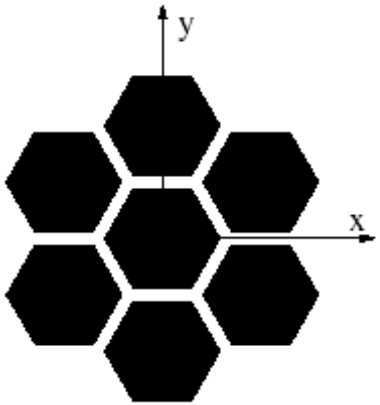

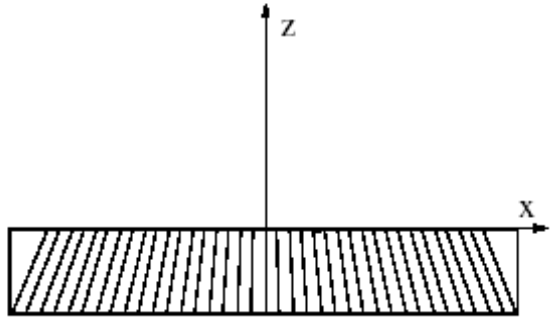

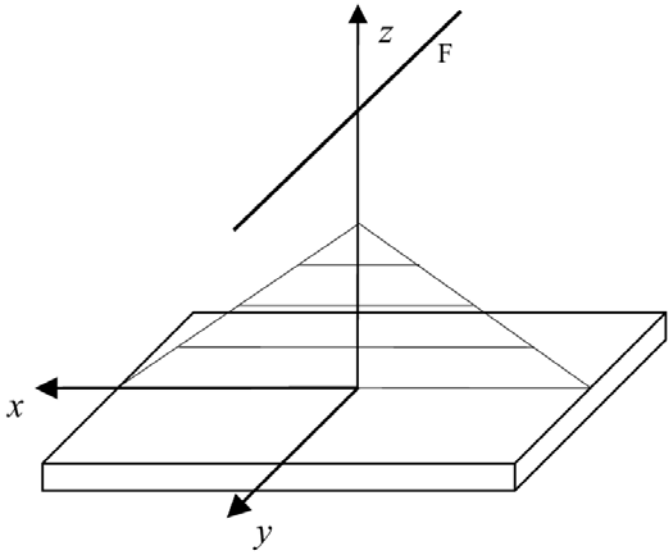

^{123}I gamma lines

159 keV (96.5%)

529 (1.62%)

440 (0.50%)

538 (0.44%)

505 (0.37%)

346 (0.15%)

624 (0.10%)

PENVOX

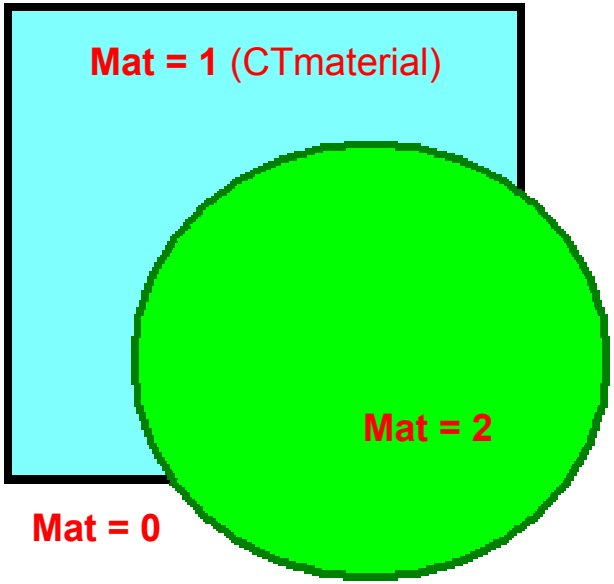

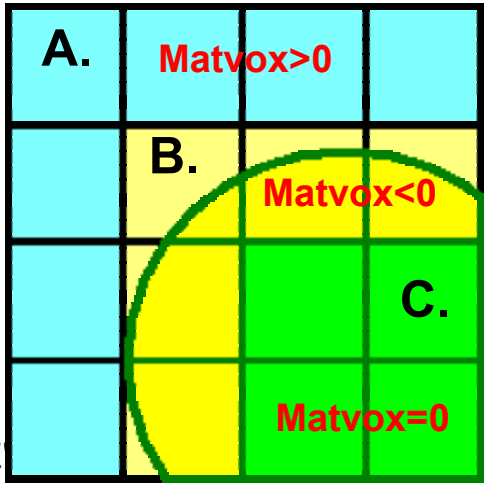

Combination of PENGEOM and voxels

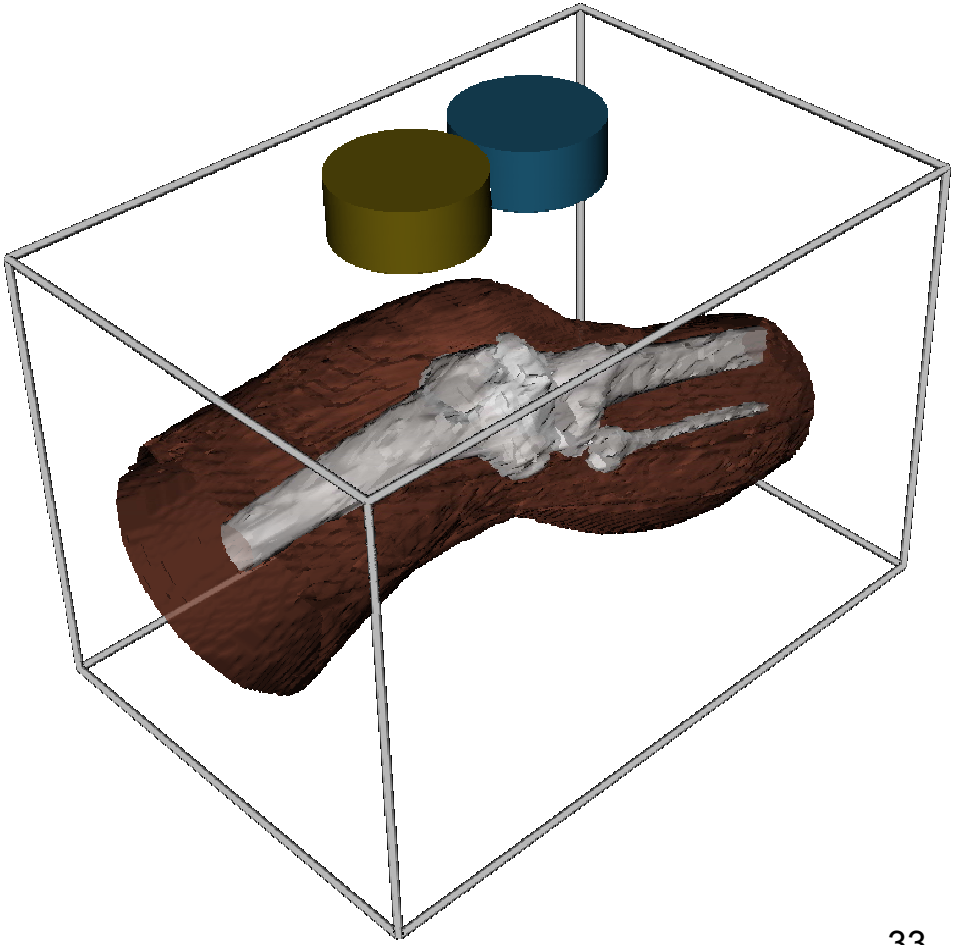

Other tools

In the distribution package

- Variance-reduction techniques
- Simulation in static EMFs

penEasy

- Modular main-program. Ready-made sources and tallies
- Coming soon: penvox, combination of voxels and quadrics
- **http://www.upc.es/inte/downloads/penEasy.htm**

clonEasy + seedsMLCG

- Parallelization using only Linux scripts
- Non-overlapping sequences of an MLCG
- **http://www.upc.es/inte/downloads/clonEasy.htm**
  ./seedsMLCG.htm

Distribution

- PENELOPE is open, free software available through the OECD Nuclear Energy Agency (NEA) Data Bank (+500 copies)
- The NEA organises a PENELOPE course anually
- Listserver: http://www.nea.fr/lists/penelope.html
- Citations:

  F. Salvat, J. M. Fernández-Varea and J. Sempau, *PENELOPE, A Code System for Monte Carlo Simulation of Electron and Photon Transport,* OECD Nuclear Energy Agency, Issy-les-Moulineaux, France, 2006

  J. Sempau, E. Acosta, J. Baró, J. M. Fernández-Varea and F. Salvat *An algorithm for Monte Carlo simulation of coupled electron-photon transport*, Nucl. Instrum. Meth. B 132 (1997) pp 377-390

The “yellow book”

http://www.nea.fr/html/science/pubs/2006/nea6222-penelope.pdf

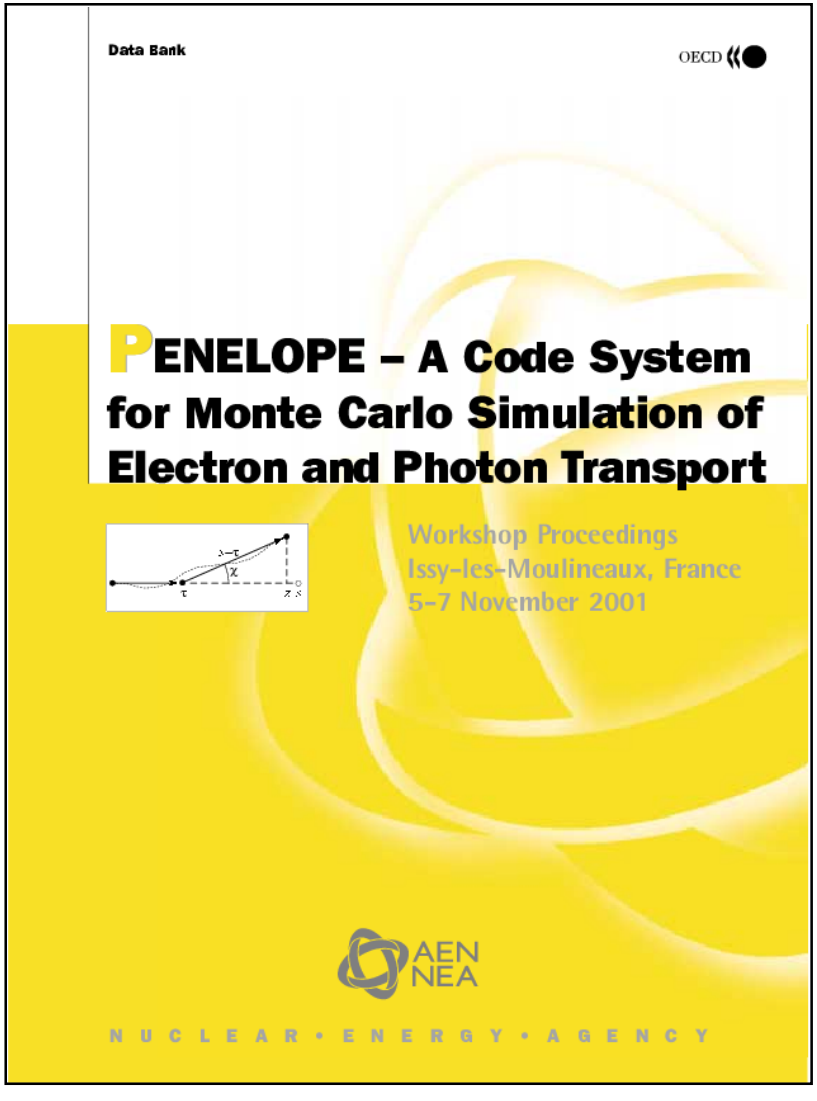

End. Thank you.

Outline

1. Fundamentals of Monte Carlo (40 min, AB)
   - Experiments, theory and numerical modeling
   - Components of the Monte Carlo method
   - The Monte Carlo method
   - Transport coefficients and cross sections
   - Random number generators
   - Variance reduction
2. PENELOPE (70 min, JS), *10-min break*
3. MANTIS **(70 min, AB)**
   - Introduction to MANTIS
   - Optical transport methods
   - Validation and examples
   - Applications in indirect x-ray imaging
   - Applications in display devices
   - Other applications
4. Imaging simulation using XSPECT (45, MJF)
5. File list and description for the companion CD
6. Hands-on demonstrations (afternoon session, AB/JS/MJF)

MANTIS - from the Greek *prophet* or *oracle*

Project goal and description

- An efficient[ab] and flexible[cd] simulation tool for R&D and optimization of radiation imaging systems that includes realistic source, object, and detector modules, and can be used for γ, x rays, $e^{\pm}$ and optical modalities.
- MANTIS features [3]:
  - PENELOPE (x ray and $e^{\pm}$) + DETECT-II (optical)
  - Particle energy range 100 eV - 1 GeV
  - All x-ray scattering included, analog or condensed transport
  - 3D optical blur with realistic columnar model
  - List-mode operation at interaction level, with simultaneous scoring of dose and imaging performance

[a] Detail of simulation can be tailored to the demands of the study.
[b] No added user interphase for efficient calculations in parallel environments.
[c] Free, open source, modular programming.
[d] Ability to model different key geometric scenarios involved in volumetric imaging.

What is MANTIS?

Components

- Requires full PENELOPE2005 distribution[a].
- Requires additional subroutines unique to MANTIS[b].
- Main program structure based on PENEASY package, a general-purpose main program for configuring and running PENELOPE.[c]
- Requires a current FORTRAN compiler.[d]

[a] Available from OECD Nuclear Energy Agency Data Bank (`http://www.nea.fr`).
[b] MANTIS is free, open source software. Requests should be sent to `aldo.badano@fda.hhs.gov`.
[c] Available free from `http://www.upc.es/inte`.
[d] A free compiler successfully used for MANTIS is G95 (`http://www.g95.org`).

Useful components (not required)

- GNUPLOT, a command-driven interactive plotting program.[a]

[a] Available multi-platform, free from `http://www.gnuplot.info`.

MANTIS tutorial

Tutorial for MANTIS

Aldo Badano and Josep Sempau

I. Introduction

MANTIS is an efficient and flexible simulation tool for R&D and optimization of radiation imaging systems that use x-ray, γ, $e^{\pm}$ and optical photons. The physics models in MANTIS are described in Ref. [1]. This tutorial describes the contents of the Monte Carlo code MANTIS distribution (version 1.0) and guides first-time users through the demonstration examples.[1] Please read the entire document before starting to use the package. Since MANTIS is an extension to PENELOPE [2], familiarity with the PENELOPE2005 package is needed.

II. Distribution package

The files included in this distribution of MANTIS are listed below.

- \. FORTRAN source:
  MANTIS.F
  DETECT2.F90
  PENELOPE.F
  PENAUX.F
  PENGEOM.F
  PENVARED.F
  SOURCEBOXISOTROPICGAUSSSPECTRUM.F
  SOURCEPHASESPACEFILE.F
  TALLYDETECT2.F
  TALLYENERGYDEPOSITION ...
  ...PULSEHEIGHTSPECTRUM.F
  TALLYPARTICLECURRENTSPECTRUM.F
  TALLYPHASESPACEFILE.F
  TALLYSPATIALDOSEDISTRIB.F
  TALLYSPATIALDOSEDISTRIB_C1.F
  TALLYSPATIALDOSEDISTRIB_C2.F
  TALLYSPATIALDOSEDISTRIB_C3.F
  TIMING.F
  This directory also includes a workspace and project file associated with Visual Studio:
  MANTIS.DSW
  MANTIS.DSP
  not needed if you don't use that software package.
- \demo Files needed to run the demo example described in Section V. More information about the input files can be found in the file header.
  Optical transport material properties:
  abs-vacuum.dm2
  backing.dm2
  csi.dm2
  diode.dm2
  gas.dm2
  pseudo-vacuum.dm2
  substrate.dm2
  Configuration for demonstration examples with wild character ? stands for R or L (see Section V for details):
  mantis_demo_CsI_H?.d2c contains general optical Monte Carlo configuration parameters
  mantis_demo_CsI_H?.d2d contains detector spectral sensitivity
  mantis_demo_CsI_H?.d2m contains material list
  mantis_demo_CsI_H?.d2s contains surface definitions
  mantis_demo_CsI_H?.d2x contains emission spectrum for scintillator
  mantis_demo_CsI_H?.pen contains general Monte Carlo configuration parameters for ionizing radiation transport (see PENELOPE documentation)
  Material file (for particle transport): dixid.mat
  Geometry file: dixid00.level4.geo
  Jobname file: mantis.job
  Output files (you can generate the same output files by running the example cases; useful to compare results): *.out, *.dat.
- \doc This tutorial, TUTORIAL_mantis.pdf.
- \gnuplot_scripts A few Gnuplot scripts for MANTIS output.
- \release Intermediate compilation files obtained

AB is from the CDRH/NIBIB Laboratory for the Assessment of Medical Imaging Systems, Division of Imaging and Applied Mathematics, Office of Science and Engineering Laboratories, Center for Devices and Radiological Health, U.S. Food and Drug Administration. 12720 Twinbrook Parkway, Rockville, MD 20857, telephone (301) 443-5020, fax (301) 443-9101, email aldo.badano@fda.hhs.gov. The mention of commercial products herein is not to be construed as either an actual or implied endorsement of such products by the Department of Health and Human Services. This is a contribution of the U.S. Food and Drug Administration, and is not subject to copyright. JS is with the Universitat Politècnica de Catalunya, Barcelona, Spain, email josep.sempau@upc.es.

[1] MANTIS is free, open source software. Requests for the version 1.0 package should be sent to aldo.badano@fda.hhs.gov.

MANTIS TUTORIAL, VERSION 1.0, JANUARY 30, 2006 1

Tutorial for MANTIS

Aldo Badano and Josep Sempau

I. Introduction

MANTIS is an efficient and flexible simulation tool for R&D and optimization of radiation imaging systems that use x-ray, γ, $e^{\pm}$ and optical photons. The physics models in MANTIS are described in Ref. [1]. This tutorial describes the contents of the Monte Carlo code MANTIS distribution (version 1.0) and guides first-time users through the demonstration examples.[1] Please read the entire document before starting to use the package. Since MANTIS is an extension to PENELOPE [2], familiarity with the PENELOPE2005 package is needed.

II. Distribution package

The files included in this distribution of MANTIS are listed below.

- \. FORTRAN source:
  MANTIS.F
  DETECT2.F90
  PENELOPE.F
  PENAUX.F
  PENGEOM.F
  PENVARED.F
  SOURCEBOXISOTROPICGAUSSSPECTRUM.F
  SOURCEPHASESPACEFILE.F
  TALLYDETECT2.F
  TALLYENERGYDEPOSITION ...
  ...PULSEHEIGHTSPECTRUM.F
  TALLYPARTICLECURRENTSPECTRUM.F
  TALLYPHASESPACEFILE.F
  TALLYSPATIALDOSEDISTRIB.F
  TALLYSPATIALDOSEDISTRIB_C1.F
  TALLYSPATIALDOSEDISTRIB_C2.F
  TALLYSPATIALDOSEDISTRIB_C3.F
  TIMING.F
  This directory also includes a workspace and project file associated with Visual Studio:
  MANTIS.DSW
  MANTIS.DSP
  not needed if you don't use that software package.
- \demo Files needed to run the demo example described in Section V. More information about the input files can be found in the file header.
  Optical transport material properties:
  abs-vacuum.dm2
  backing.dm2
  csi.dm2
  diode.dm2
  gas.dm2
  pseudo-vacuum.dm2
  substrate.dm2
  Configuration for demonstration examples with wild character ? stands for R or L (see Section V for details):
  mantis_demo_CsI_H?.d2c contains general optical Monte Carlo configuration parameters
  mantis_demo_CsI_H?.d2d contains detector spectral sensitivity
  mantis_demo_CsI_H?.d2m contains material list
  mantis_demo_CsI_H?.d2s contains surface definitions
  mantis_demo_CsI_H?.d2x contains emission spectrum for scintillator
  mantis_demo_CsI_H?.pen contains general Monte Carlo configuration parameters for ionizing radiation transport (see PENELOPE documentation)
  Material file (for particle transport): dixid.mat
  Geometry file: dixid00.level4.geo
  Jobname file: mantis.job
  Output files (you can generate the same output files by running the example cases; useful to compare results): *.out, *.dat.
- \doc This tutorial, TUTORIAL_mantis.pdf.
- \gnuplot_scripts A few Gnuplot scripts for MANTIS output.
- \release Intermediate compilation files obtained

AB is from the CDRH/NIBIB Laboratory for the Assessment of Medical Imaging Systems, Division of Imaging and Applied Mathematics, Office of Science and Engineering Laboratories, Center for Devices and Radiological Health, U.S. Food and Drug Administration. 12720 Twinbrook Parkway, Rockville, MD 20857, telephone (301) 443-5020, fax (301) 443-9101, email aldo.badano@fda.hhs.gov. The mention of commercial products herein is not to be construed as either an actual or implied endorsement of such products by the Department of Health and Human Services. This is a contribution of the U.S. Food and Drug Administration, and is not subject to copyright. JS is with the Universitat Politècnica de Catalunya, Barcelona, Spain, email josep.sempau@upc.es.

[1] MANTIS is free, open source software. Requests for the version 1.0 package should be sent to aldo.badano@fda.hhs.gov.

Optical transport methods in MANTIS

Assumptions

- Geometrical optics treatment neglects effect of finite wavelength.
- Light ray is assumed to carry one single quanta (reflection coefficients interpreted as probabilities)
- Materials considered optically isotropic.
- Light emission in scintillators considered isotropic.

Refraction

- Snell's law: $n_1 \sin\theta_1 = n_2 \sin\theta_2$.
- Transmission and reflection probabilities:

$$P_{\parallel,trans} = \frac{\sin(2\theta_1)\sin(2\theta_2)}{\sin^2(\theta_1+\theta_2)\cos^2(\theta_1-\theta_2)} \qquad P_{\perp,trans} = \frac{\sin(2\theta_1)\sin(2\theta_2)}{\sin^2(\theta_1+\theta_2)}$$

$$P_{\parallel,refl} = \frac{\tan^2(\theta_1-\theta_2)}{\tan^2(\theta_1+\theta_2)} = 1 - P_{\parallel,trans} \qquad P_{\perp,refl} = \frac{\sin^2(\theta_1-\theta_2)}{\sin^2(\theta_1+\theta_2)} = 1 - P_{\perp,trans}$$

Skip optical physics details

Polarization

Polarization-dependent coefficients

If $\omega_\perp$ and $\omega_\parallel$ are the polarization components with respect to a surface ($\omega_\perp^2 + \omega_\parallel^2 = 1$), the reflection probabilities [8] is

$$P_{refl} = \frac{\omega_\perp^2 P_{\perp,refl} + \omega_\parallel^2 P_{\parallel,refl}}{\omega_\perp^2 + \omega_\parallel^2}$$

with $P_{trans} = 1 - P_{refl}$.

Polarization after a boundary crossing

After reflection: $\omega_\parallel^{'} = \omega_\parallel P_{\parallel,refl}$, and $\omega_\perp^{'} = \omega_\perp P_{\perp,refl}$.

Similarly, after refraction, $\omega_\parallel^{'} = \omega_\parallel P_{\parallel,trans}$, and $\omega_\perp^{'} = \omega_\perp P_{\perp,trans}$.

A final normalization is computed $\omega_\parallel^{'\,2} + \omega_\perp^{'\,2} = 1$.

Surface models

Surface types

Smooth (optically flat), rough, partially absorber/rough reflector, partially absorber/specular reflector, perfect absorber, partially absorber/diffuse reflector, optically thin film, or transparent.

Surface definition

- Explicit: assigned reflection coefficient and angular distribution.
- Implicit: determined by physics models.

Roughness algorithm

- Tilting of the normal vector **n** using isotropic unit vector **v**
- Modified normal direction given by $\mathbf{n} + a\mathbf{v}$.

Rayleigh scattering (at crystalline defects)

- Limiting case of Mie theory for small spheres: $\mu_{sca} \propto \lambda^{-4}$ [8, 9].

Coupling particle and optical transport

From energy deposited in scintillator to light emission

1. When energy e is deposited in a scintillator, the code generates a number of optical photons q given by $q = e\mathcal{P}(\Gamma)$ where Γ is the optical gain in #/eV. $\mathcal{P}(x)$ is Poisson with mean x.
2. Photons generated randomly from emission spectrum.
3. Photons that reach the photodiode are detected according to the spectral sensitivity at optical energy (E).
4. If detected, the signal is $s = \mathcal{P}(E/\epsilon)$ where ϵ is energy for a e-h pair (for a-Si:H, $\epsilon = 3.6$ eV).
5. s binned in space for point-response functions, and in pulse-height mode, for pulse-height spectra.

Validation strategy I

Parameters for validation (*ad hoc* approach)

- **Information factor**:

$$I = \frac{M_1^2(q)}{M_0(q)M_2(q)}$$

where $M_i(q)$ is i^{th} moment of the pulse-height spectrum. If $M(q)$ is Poisson, $I > 0.9$. For $\overline{q} = 200$, $I = 0.995$. I is related to the Fano factor

$$M_1(q)/\sigma^2(q)$$

$F = 1$ for Poisson and $F << 1$ for most scintillators [10].

- **Light output**
- **Point-response function**

See Badano *et al.*, Mon 1:40pm, "Validation of simulated point-response functions in columnar phosphor screens", Badano *et al.* [6510-33].

Validation strategy II

Model parameters

- Optical properties of CsI: $0 < \mu_{\text{abs}} < 10\ \text{cm}^{-1}$, $0 < \mu_{\text{sca}} < 10\ \text{cm}^{-1}$
- Surface roughness of column walls
- Reflectivity of backing and sensor layer: $0.90 < r_{\text{backing}} < 1.00$ for HL, $0.00 < r_{\text{backing}} < 0.20$ for HR, and $0 < r_{\text{sensor}} < 0.25$

Validation procedure for information factor

- **Model development at 18.5 keV**
  - Initial guess for the screen model including optical properties and geometry, from the literature (whenever possible)
  - Compute parameters from MANTIS output (I, light output, PRF)
  - Adjust parameters within range to satisfy all three parameters
  - Repeat until consistency with experimental measurements
- **Model validation**: Check validity of model for x-ray energies covering diagnostic range.

Validation strategy III

Model development

Parameter	Measured	MANTIS
18.5 keV		
Swank factor [11]	0.9	0.99
Light output(ζ)	$\sim$0.80	0.77

Model validation

40.5 keV		
Swank factor	0.75	0.73
Light output (ζ)	$\sim$0.80	0.77
60.5 keV		
Swank factor	0.87	0.88
Light output (ζ)	$\sim$0.80	0.77

Validation of pulse-height spectra

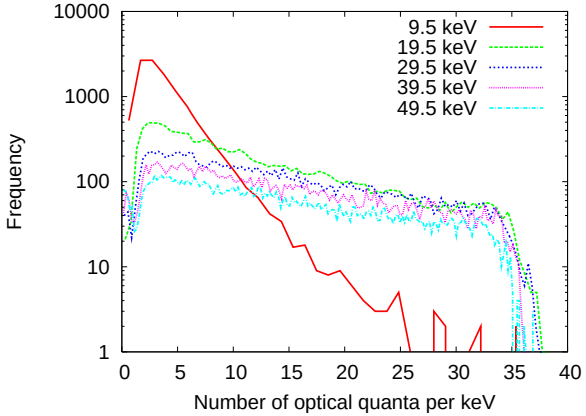

Gd_2O_2S:Tb, front-screen

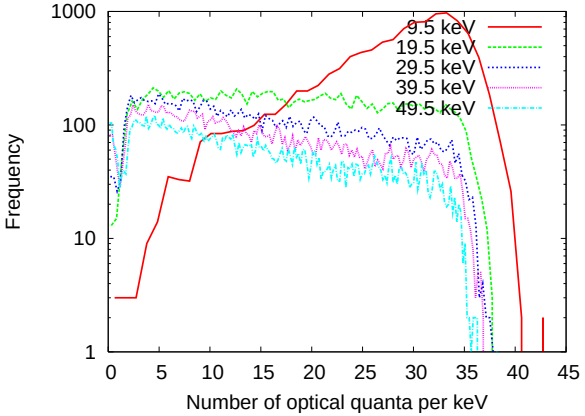

Gd_2O_2S:Tb, back-screen

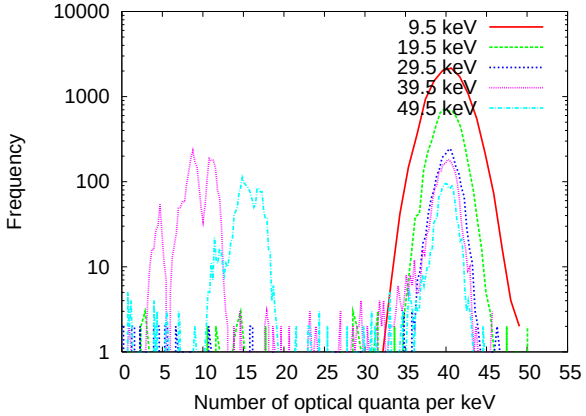

CsI, front-screen, 100 μm

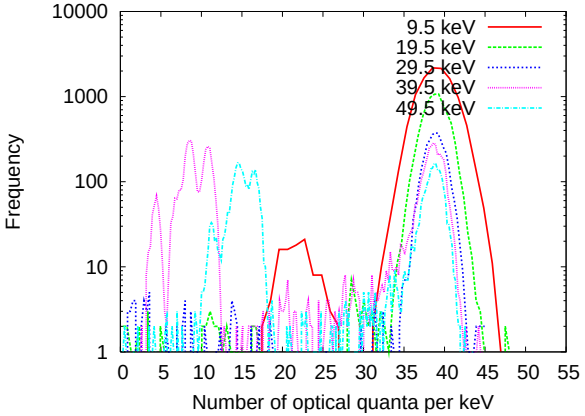

CsI, front-screen, 150 μm

Validation of information factors

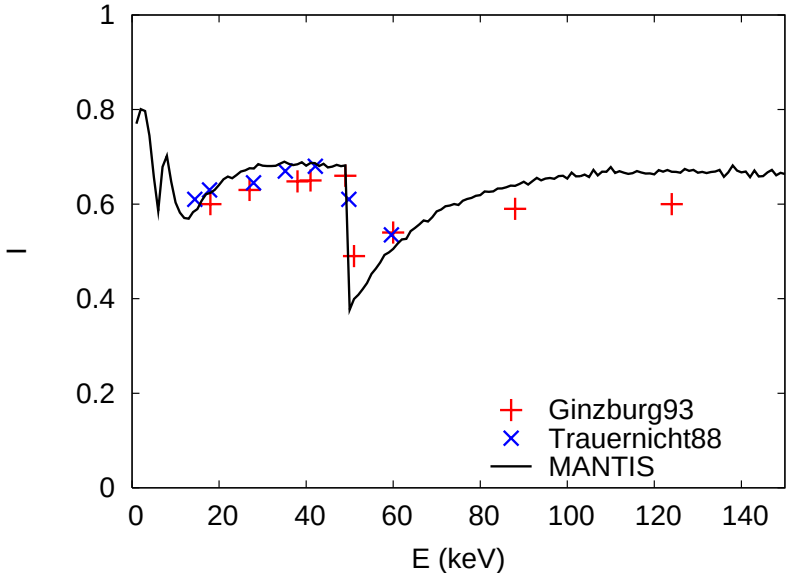

Gd_2O_2S:Tb

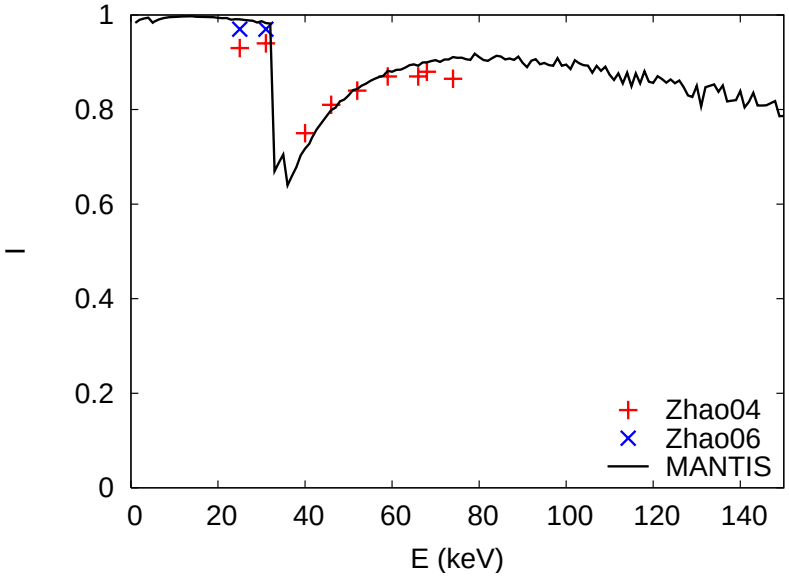

CsI:Tl

3D columnar phosphor model

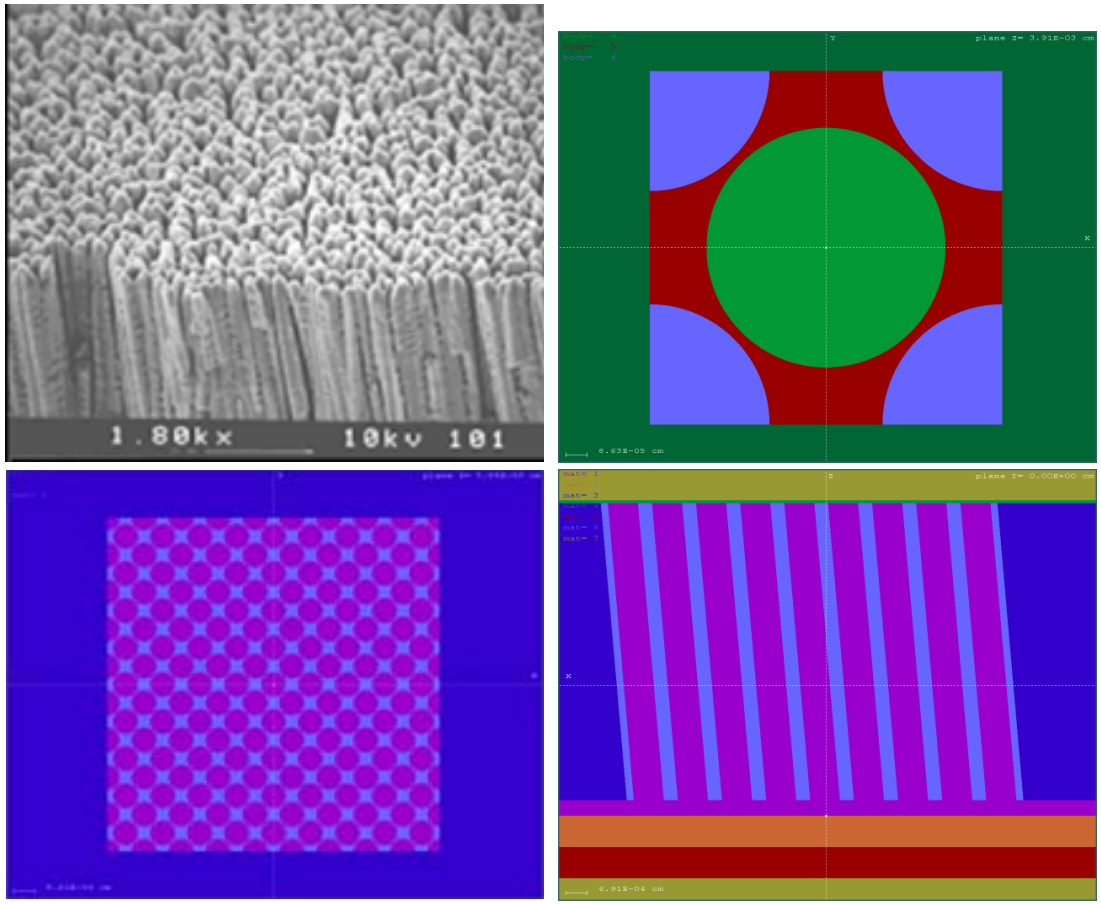

Top-left: typical structure for CsI:Tl needle-like crystals (courtesy of V Nagarkar, RMD Inc). Top-right: basic cell for columnar array. Bottom-left: top-view of perpendicular column array. Bottom-right: array of 5°-tilted columns. Figures obtained with GVIEW.

Particle paths in 3D columnar CsI

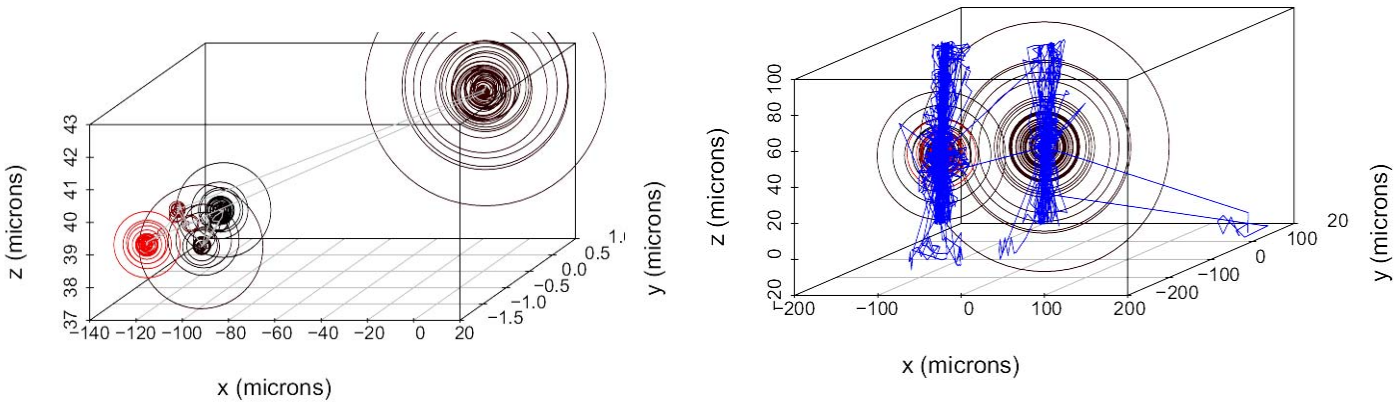

- Energy deposition (left) and optical photon trajectories (right, in blue) for a 39.5 keV x ray (only first 5 optical histories for clarity).
- The diameter of the circles centered on energy deposition locations is proportional to the deposited energy.
- Energy deposited in 2 columns via fluorescence or Compton scattering.
- Column outlines deduced from the multiple reflections.

Is imaging performance isotropic?

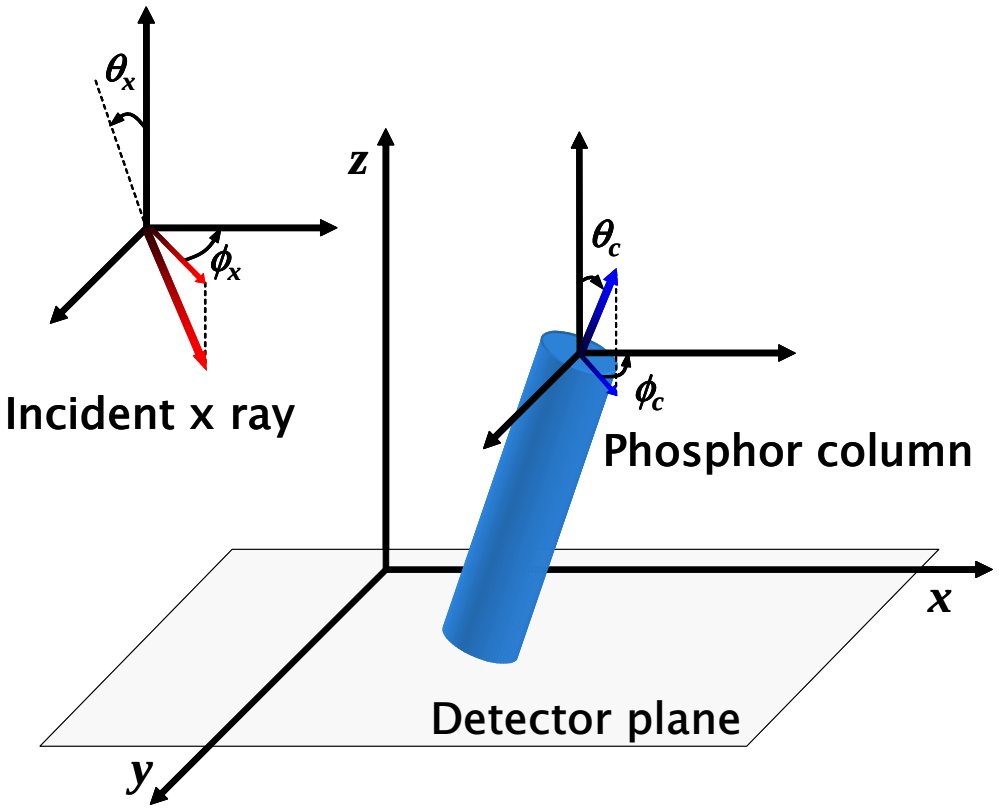

Geometry and angles for the definition of the columnar tilt in the phosphor and for the obliqueness of the x-ray beam.

Asymmetries in the point-response functions

Energy deposition for 10° and 15° x-rays (500-μm CsI:Tl, 5°-tilt columns).

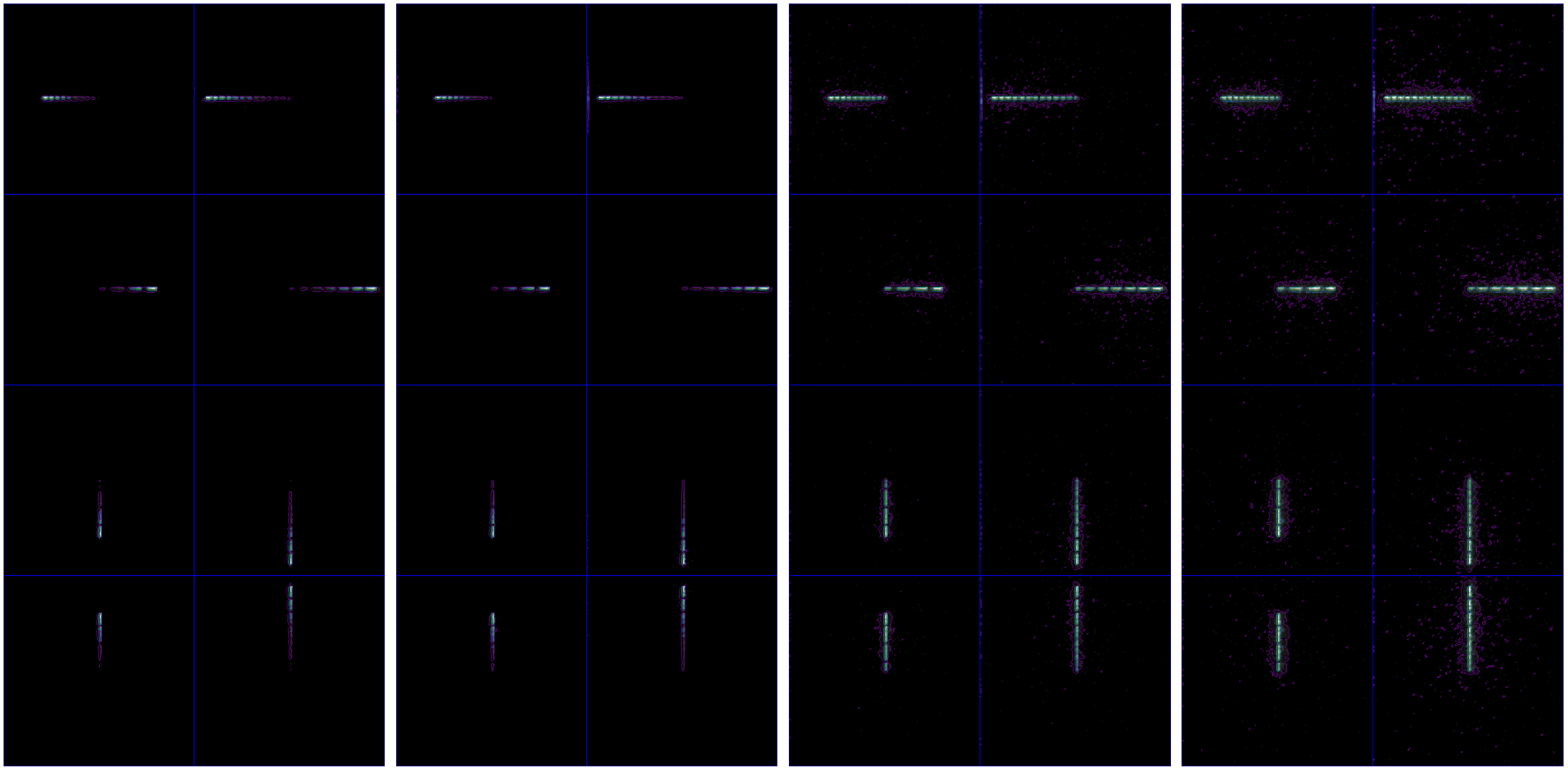

P^{xe}, 19 keV P^{xe}, 39 keV P^{xe}, 59 keV P^{xe}, 79 keV

Contour lines for 0.25, 0.1, and 0.01.

Asymmetries in the point-response functions

PRFs for 10° and 15° x-ray incidence angle (500-μm CsI:Tl, 5°-tilt columns).

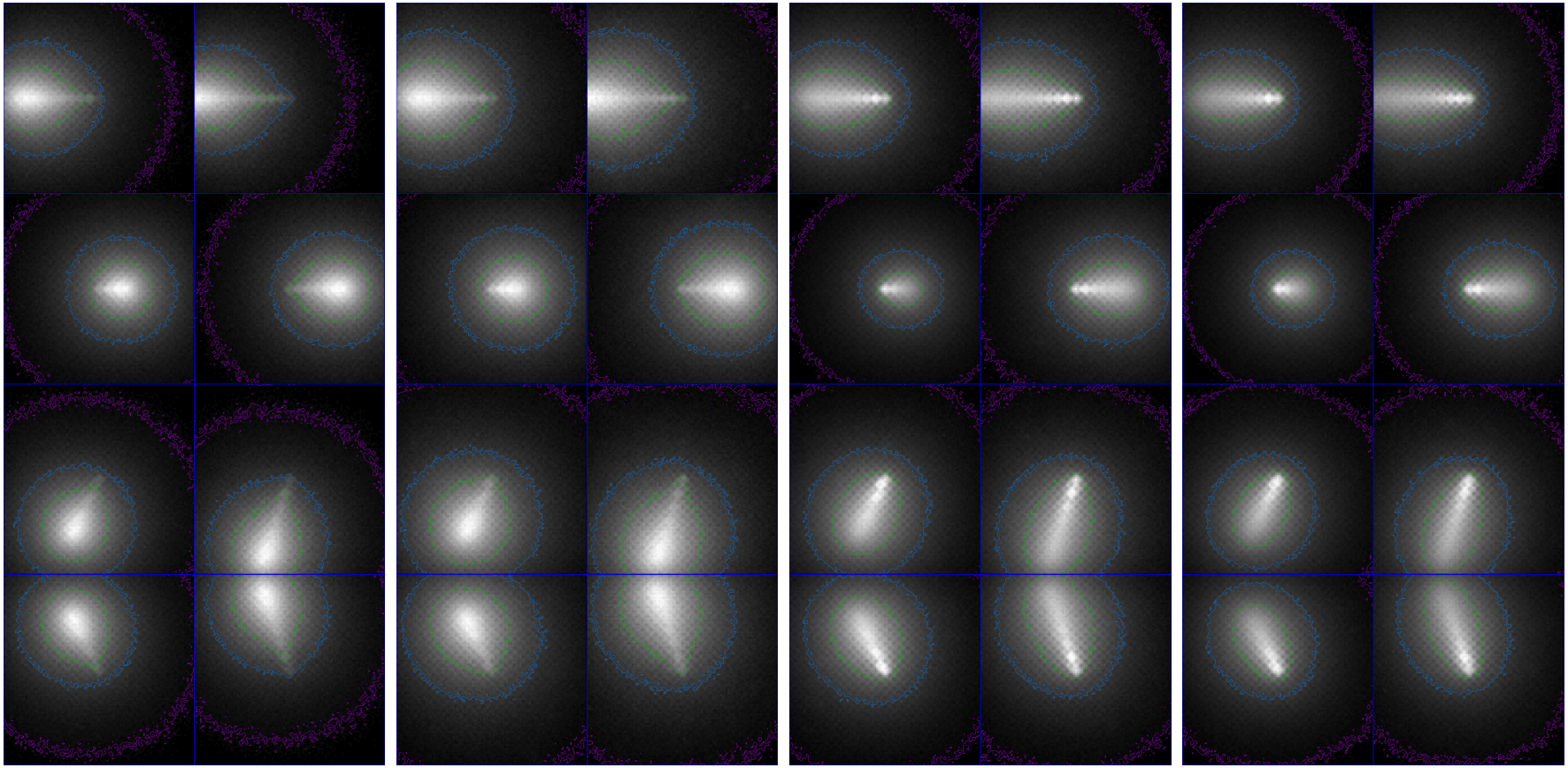

P^{xeo}, 19 keV P^{xeo}, 39 keV P^{xeo}, 59 keV P^{xeo}, 79 keV

Contour lines for 0.25, 0.1, and 0.01.

HR vs HL screen designs - PRF

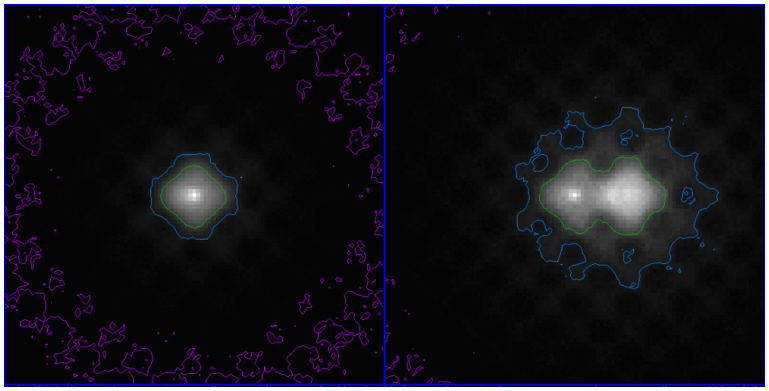

100 μm HL, 19 keV

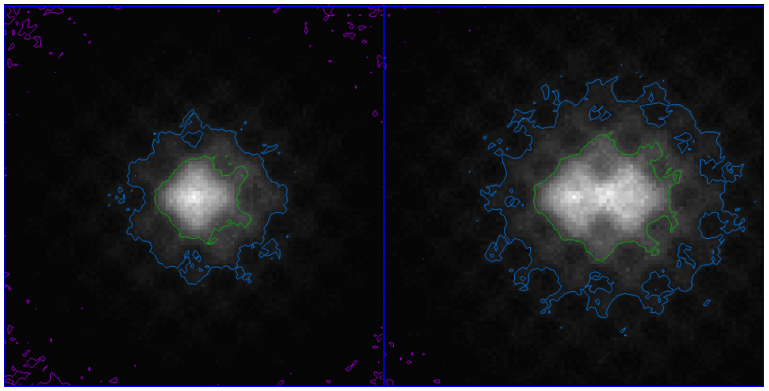

100 μm HL, 79 keV

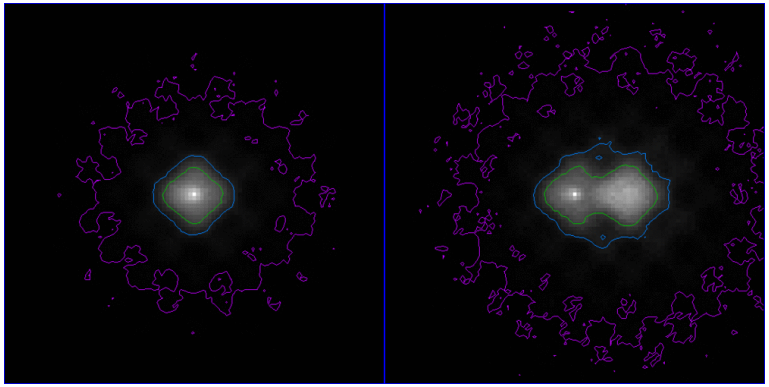

100 μm HR, 19 keV

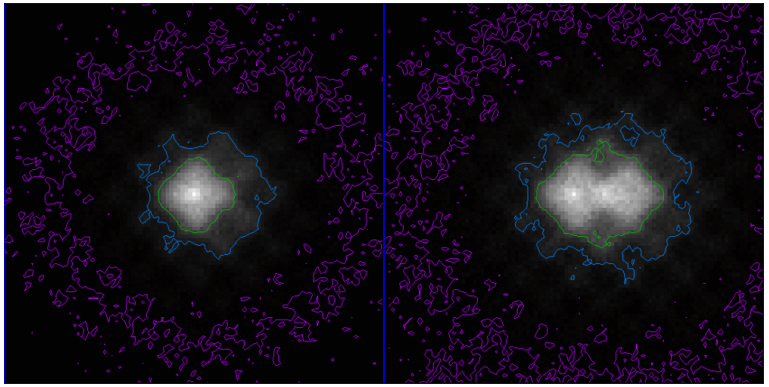

100 μm HR, 79 keV

Each image is 100$\times$100 μm with $\theta_x = 10^\circ$ (first sub-figure), and $\theta_x = 15^\circ$ (second sub-figure) x-ray incidence angle with $\phi_c = 0^\circ$.

HR vs HL screen designs - PRF

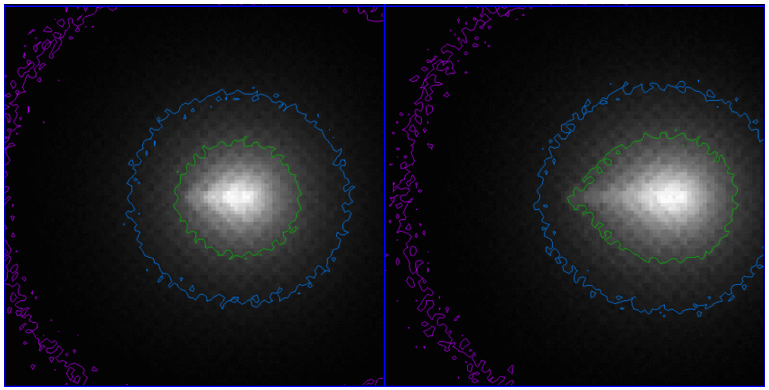

500 μm HL, 19 keV

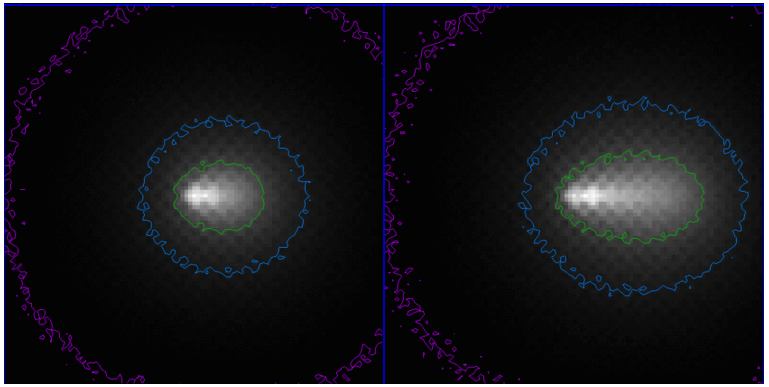

500 μm HL, 79 keV

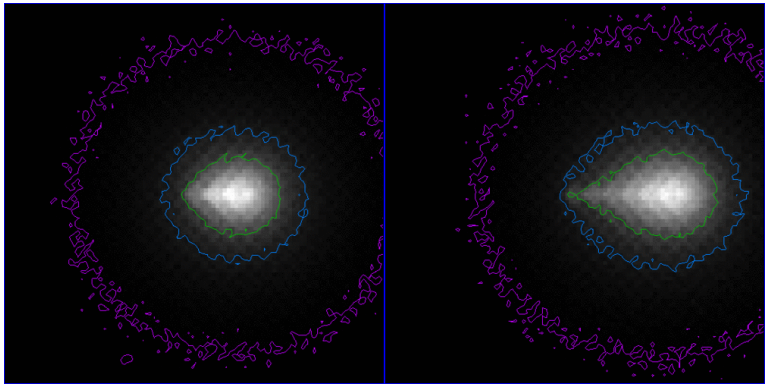

500 μm HR, 19 keV

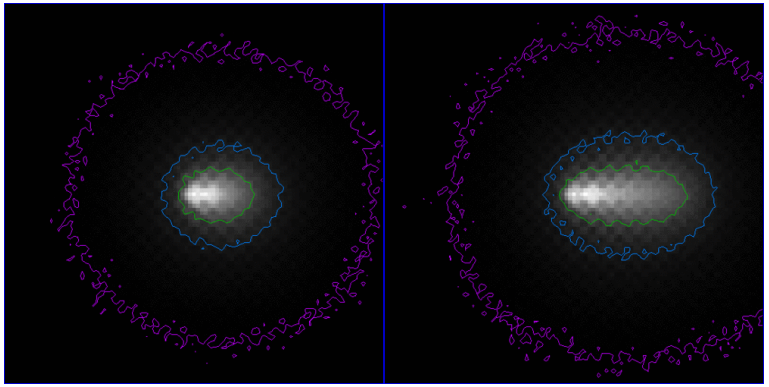

500 μm HR, 79 keV

Each image is 300$\times$300 μm with $\theta_x = 10^\circ$ (first sub-figure), and $\theta_x = 15^\circ$ (second sub-figure) x-ray incidence angle with $\phi_c = 0^\circ$.

HR vs HL screen designs (pulse-height spectra)

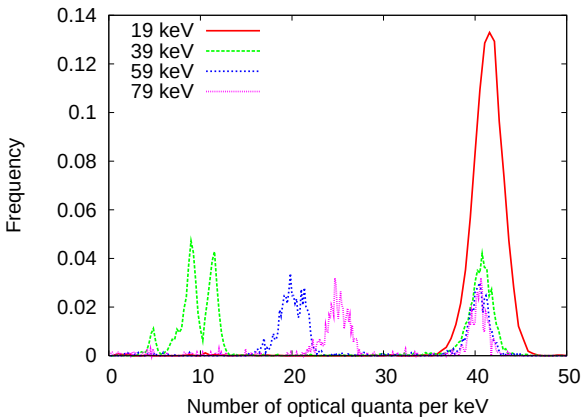

HL, 100 μm

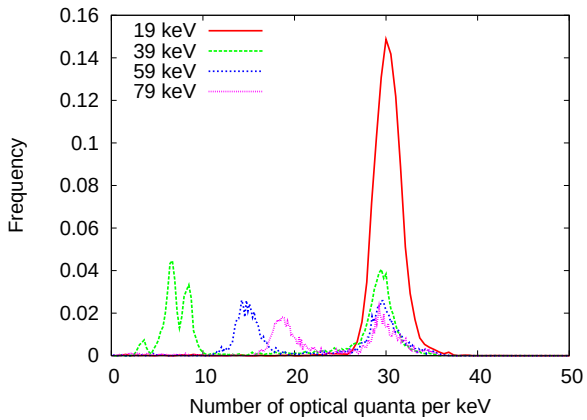

HL, 500 μm

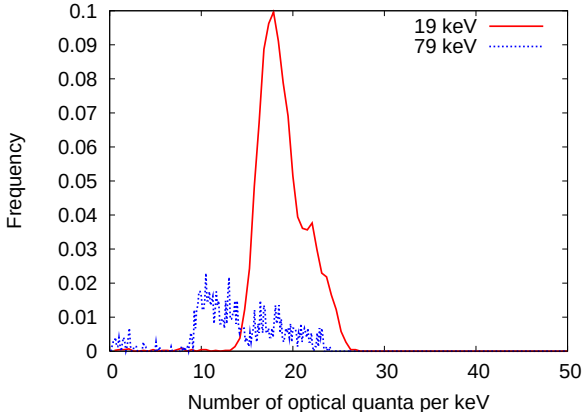

HR, 100 μm

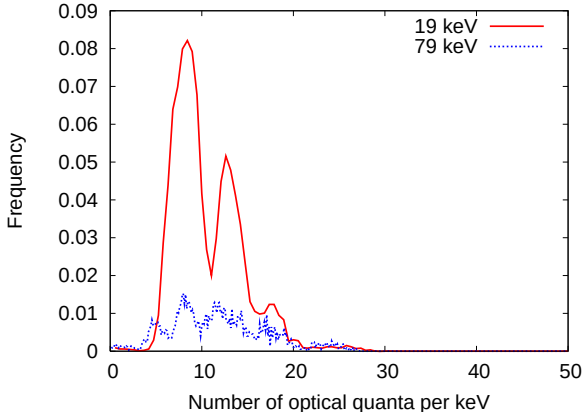

HR, 500 μm

Applications in display devices

Cathodoluminescent displays displays

- Veiling glare in field-emission displays [12]
- Monte Carlo modeling of glare in cathode-ray tubes for medical imaging [13, 14]

Organic light-emitting devices

- Monte Carlo analysis of the spectral photon emission and extraction efficiency of organic light-emitting devices [15]

Other devices

- Fingerprint imager based on a Si:H active-matrix photo-diode arrays [16]

Other applications

✓X-ray imaging grids

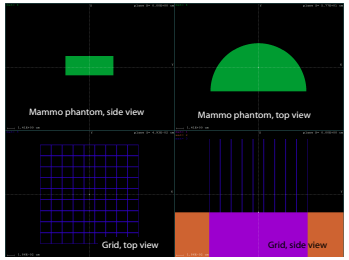

✓Realistic computational phantoms for volumetric imaging

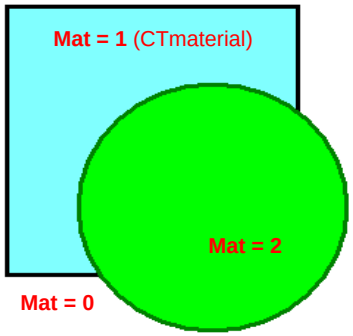

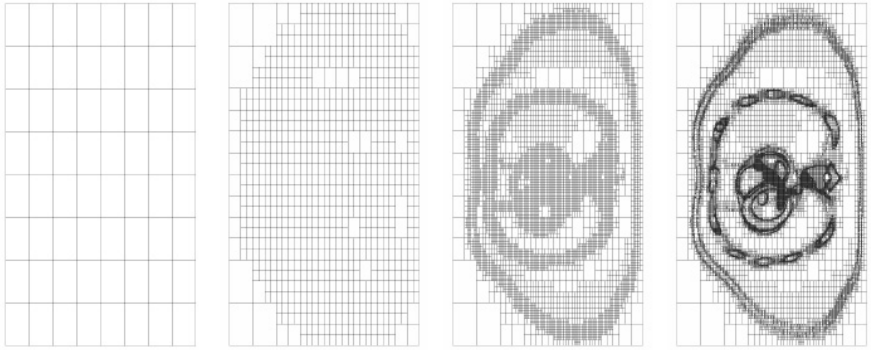
(a) 3 subdivisions (b) 5 subdivisions (c) 7 subdivisions (d) 9 subdivisions

Octree structures and triangular meshes. See Badal *et al.*, Mon 2pm, “Monte Carlo package for simulating radiographic images of realistic anthropomorphic phantoms described by triangle meshes” [6510-34].

✓Multi-modality imaging: breast tomosynthesis and CT, PET, SPECT, optical imaging, and imaging in radiation therapy beams.

References I

B. D. Gallas, J. S. Boswell, A. Badano, R. M. Gagne, and K. J. Myers.

An energy- and depth-dependent model for x-ray imaging.

Medical Physics, 31(11):3132–3149, 2004.

A. Badano, R. M. Gagne, B. D. Gallas, R. J. Jennings, J. S. Boswell, and K. J. Myers.

Lubberts effects in columnar phosphors.

Medical Physics, 31(11):3122–3131, 2004.

A. Badano and J. Sempau.

Combined x-ray, electron, and optical Monte Carlo simulations of indirect radiation imaging systems.

Phys. Med. Biol., 51:1545–1561, 2006.

G. Marsaglia, A. Zaman, and W.W. Tsang.

Toward a universal random number generator.

Statistics and Probability Letters, 8:35–39, 1990.

M. Matsumoto and T. Nishimura.

Mersenne twister: a 623-dimensionally equidistributed uniform pseudorandom number generator.

ACM Trans. on Modeling and Computer Simulation, 8(1):3–30, 1998.

M. Matsumoto and T. Nishimura.

Monte Carlo and Quasi-Monte Carlo Methods 1998, chapter Dynamic Creation of Pseudorandom Number Generators, pages 56–69.

Springer, 2000.

References II

H. P. Smith and J. C. Wagner.
Nuclear Mathematical and Computational Sciences: A Century in Review, A Century Anew.
American Nuclear Society, LaGrange Park, IL, 2003.

M. Born and E. Wolf.
Principles of Optics.
Pergamon Press, third revised edition, 1965.

M. Kerker.
The scattering of light.
Academic Press, 1969.

W. W. Moses.
Current trends in scintillator detectors and materials.
Nuclear Instruments and Methods in Physics Research A, 487:123–128, 2002.

W. Zhao, G. Ristic, and J. A. Rowlands.
X-ray imaging performance of structured cesium iodide scintillators.
Medical Physics, 31(9):2594–2605, 2004.

A. Badano and M. J. Flynn.
Monte Carlo modeling of the luminance spread function in flat panel displays.
Proc. International Display Research Conference, 21:382–385, 1997.

References III

A. Badano and M. J. Flynn.

Monte Carlo modeling of glare in cathode-ray tubes for medical imaging.

Proc. SID, pages 495–498, 1998.

A. Badano.

Image Quality Degradation by Light Scattering Processes in High Performance Display Devices for Medical Imaging.

PhD thesis, University of Michigan, 1999.

A. Badano and J. Kanicki.

Monte Carlo analysis of the spectral photon emission and extraction efficiency of organic light-emitting devices.

Journal of Applied Physics, 90(4):1827–1830, 2001.

J. Lan, A. Cole, J. VanZandt, A. Dickinson, F. Van de Ven, N. Bird, A. Badano, and J. Kanicki.

Fingerprint imager based on a si:h active-matrix photo-diode arays.

Proc. of the International Electron Device Meeting, 2000.

Outline

1. Fundamentals of Monte Carlo (40 min, AB)
   - Experiments, theory and numerical modeling
   - Components of the Monte Carlo method
   - The Monte Carlo method
   - Transport coefficients and cross sections
   - Random number generators
   - Variance reduction
2. PENELOPE (70 min, JS), *10-min break*
3. MANTIS (70 min, AB)
   - Introduction to MANTIS
   - Optical transport methods
   - Validation and examples
   - Applications in indirect x-ray imaging
   - Applications in display devices
   - Other applications
4. **Imaging simulation using XSPECT (45, MJF)**
5. File list and description for the companion CD
6. Hands-on demonstrations (afternoon session, AB/JS/MJF)

Health System

RADIOLOGY RESEARCH

Computational Simulation of Radiation Imaging Systems using XSPECT*

Michael Flynn
Dept. of Radiology
mikef@rad.hfh.edu

Henry Ford Health System

*copyright HFHS 2007

Part 4 - OBJECTIVE

"Introduction to XSPECT and the use of Monte Carlo methods for determining detector signal, detector noise, radiation dose, and x-ray spectra in cascaded models of imaging system"

XSPECT

XSPECT is a collection of programs that simulate the production, attenuation, and detection of x-rays in order to describe the performance of radiation imaging systems.

- **X-ray Spectrum:** The spectral distribution of the source is generated using computer models for electron target tubes or can be input from previously stored tabular data.
- **Material Attenuation:** Energy dependant spectral attenuation is computed from libraries having data on material composition and x-ray interaction coefficients.
- **Exposure:** Utility programs allow the spectra to be integrated or the determination of exposure(i.e. air ionization).
- **Dose:** Evaluation of absorbed dose from pre-computed tabulated data specific to a particular object geometry.
- **Contrast and Noise:** From pre-computed tables of signal and noise detection efficiency, the response of a particular detector system can be computed.

XSPECT BACKGROUND:

- The programs for XSPECT version 3.5 have evolved from software developments begun in 1983 in the X-ray Imaging Research Laboratory at HFHS.
- Contributions to this effort have come from Michael Flynn, Scott Wilderman, Zhiheng Ge, James Pipe, Sean Hames, Charles Dodge.
- XSPECT is now used at the core software for a Computational Laboratory course at the University of Michgan (NERS-580/BIOE-580).
- Particular recognition must be given to the efforts of Scott Wilderman who wrote the majority of the original code, assembled the initial database of interaction cross sections, and modified his Monte Carlo code, SKEPTIC, to deduce detector and dose tables.
- A major revision, version 4.0, is now in beta test.

Computational Simulation of Radiation Imaging Systems using XSPECT*

A) X-ray Energy Spectrum.

i. Introduction (pg 6)

ii. Experimental spectral data (pg 9)

iii. Analytic spectral models (pg 12)

iv. Xspect 3.5/4.0 spectral estimates (pg 16)

B) Cross section & material composition.

C) xSpect: Exposure, Contrast, Noise, & Dose

X-ray fluence rate (ICRU), #/m^2/s

differential energy spectrum, #/(m2-s-keV)

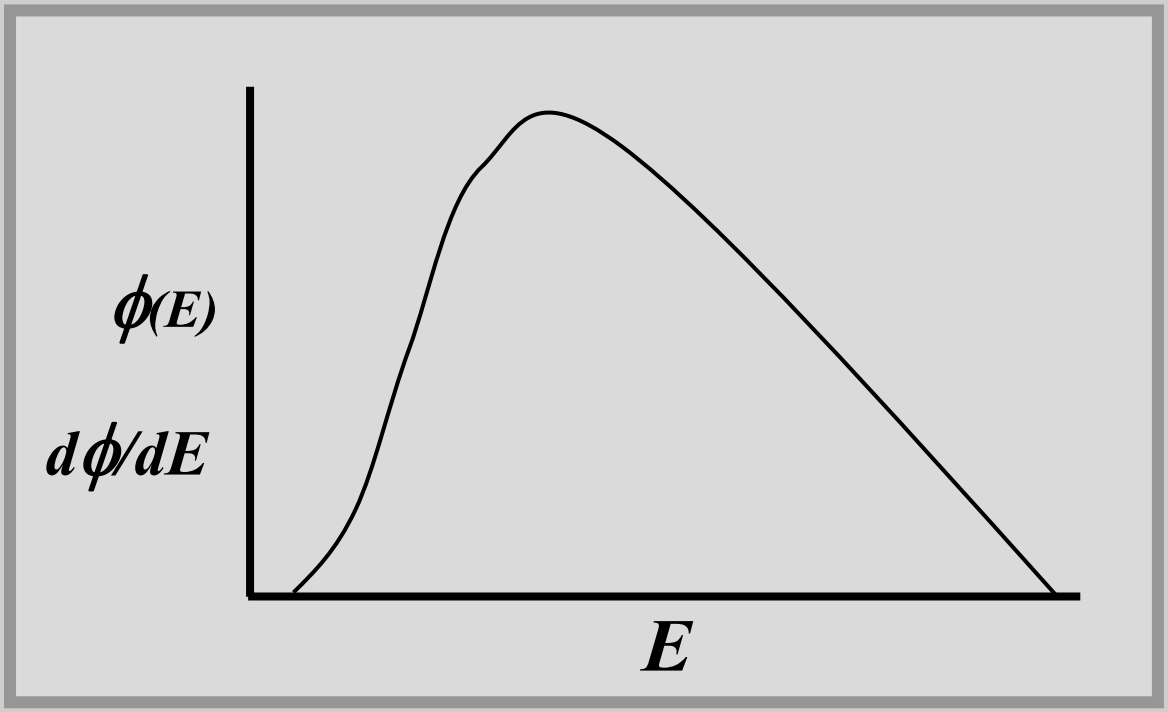

By convention, we will refer to the differential energy spectrum of xray quantities by writing the symbol as a function of energy,

$$\phi(E) = {d\phi}/{dE}$$

4.A.i – per mA-S units

Electron Impact X-ray Source

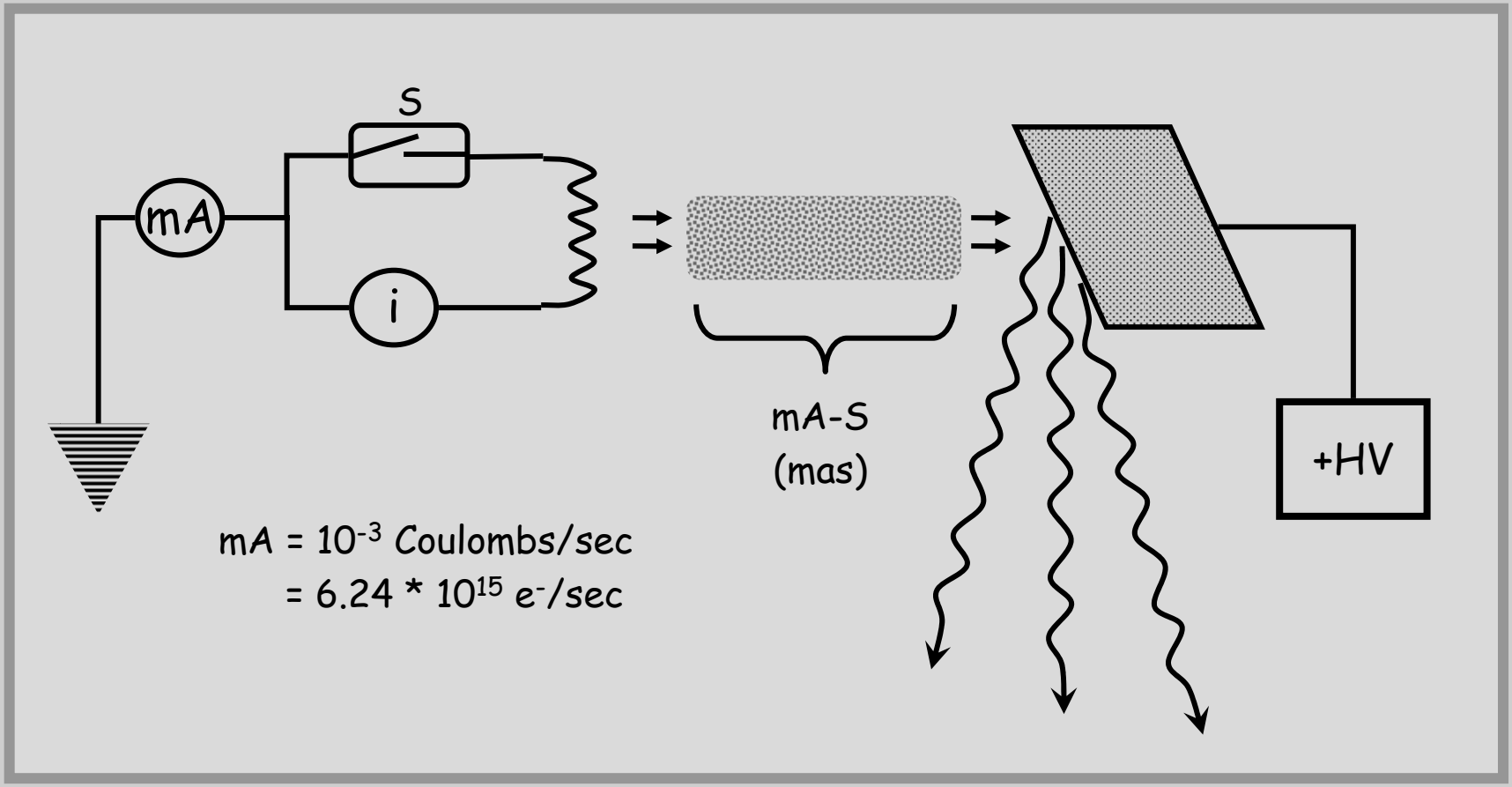

- The production of x-rays is proportional to the number of electrons that strike the target and therefore the mA-S.
- It is thus common to normalize the emission fluence rate as <u>photons/m^2/mA-S</u> or alternatively as <u>photons/steradian/mA-S</u>.

4.A.i – per solid angle units

Xray fluence can either be expressed in terms of xrays/steradian or xrays/mm^2. It is often more convenient to describe the fluence from a source in photons/steradian since it is independent of the distance (i.e. radius) from the emission point. To convert from xrays/steradian to xrays/mm^2, simply divide by r^2.

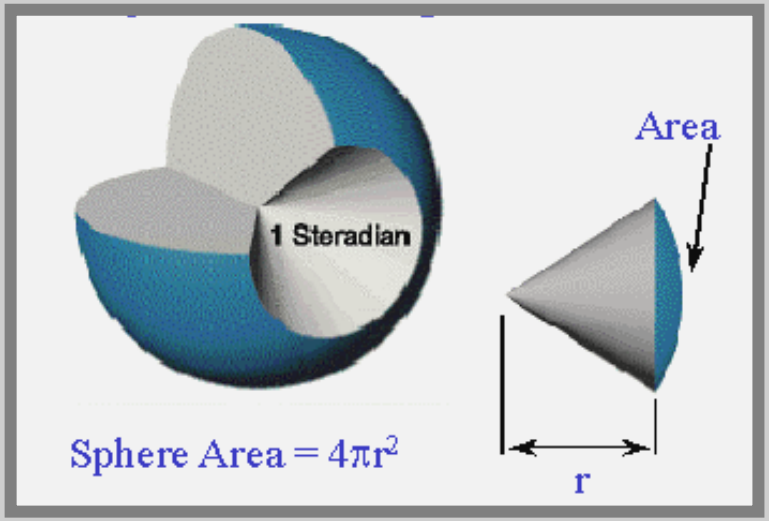

The steradian is the unit used to describe the "solid angle" associated with a portion of the unit sphere.

photons/mm^2 = (photons/steradian) / r^2, for r in mm

4.A.ii - Experimental Spectral Data

- Limited data available for specific targets, takeoff angle, and tube filtration
- Difficult to accurately measure.
  - Complicated detector response corrections.
  - Absolute intensity determined from exposure
  - Actual intrinsic filtration uncertainty.
  - Target surface roughness effects.

4.A.ii - X-ray Spectra – Experimental Data

--- US FDA ---

- Fewell & Shuping, FDA 81-8162 (1981)
  Tungsten, glass, 70-140 kV
- Fewell & Shuping, FDA 79-8071 (1978)
  Tungsten & Molybdenum, glass+, 20-60 kVp
- Fewell, Jennings & Quinn, BRH/CRDH (1991, 1994)
  Tungsten, Molybdenum & Rhodium
  18-42 (every 2) kV, ~.5mm Be
- Boone & Seibert
  Boone, Fewell & Jennings
  Med. Phys., 24(11&12),1997
  - Interpolated polynomials with experimental output normalization
  - TASMIP – tungsten
  - RASMIP – rhodium MASMIP - molybdenum

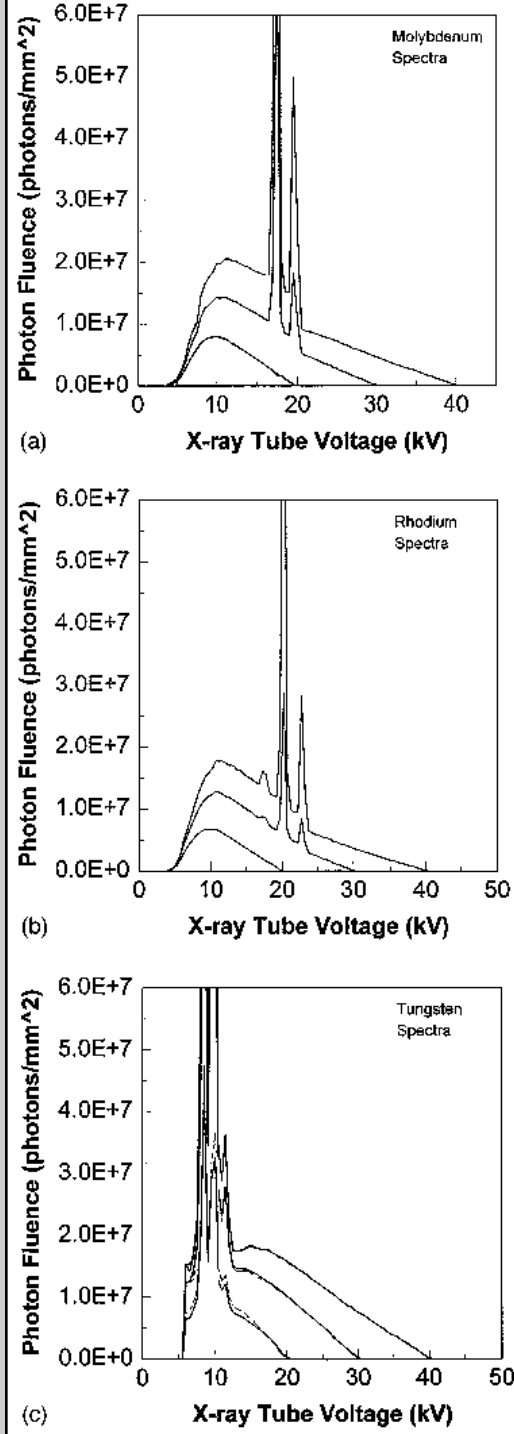

- Mercier, Radiation Research 154, 564–581 (2000)
  - Tungsten, 20°, 7 mm Be – 80, 90, 100, 120, 150 kV
  - Tungsten, 12°, Glass/oil/Al - 30, 50, 60, 70 kV

Tube μGy/mAs at 1 m EPPT (± 0.1 μm) keV	Isovolt[b] 336.4 1.4 μm 151.8 kVp	Isovolt[b] 264.3 1.3 μm 122.3 kVp	Isovolt[b] 215.1 1.2 μm 101.5 kVp	Isovolt[b] 206.2 1.15 μm 92.8 kVp	Isovolt[b] 177.5 1.1 μm 82.4 kVp
50.5	3.62×10^6	2.74×10^6	2.06×10^6	1.84×10^6	1.44×10^6
51.0	3.58×10^6	2.71×10^6	2.03×10^6	1.81×10^6	1.42×10^6
51.5	3.56×10^6	2.68×10^6	2.00×10^6	1.77×10^6	1.39×10^6
52.0	3.52×10^6	2.64×10^6	1.97×10^6	1.73×10^6	1.37×10^6
52.5	3.49×10^6	2.62×10^6	1.94×10^6	1.70×10^6	1.34×10^6
53.0	3.46×10^6	2.59×10^6	1.91×10^6	1.67×10^6	1.31×10^6
53.5	3.44×10^6	2.56×10^6	1.88×10^6	1.64×10^6	1.28×10^6
54.0	3.40×10^6	2.53×10^6	1.85×10^6	1.61×10^6	1.26×10^6
54.5	3.37×10^6	2.50×10^6	1.82×10^6	1.58×10^6	1.23×10^6
55.0	3.34×10^6	2.47×10^6	1.79×10^6	1.55×10^6	1.21×10^6
55.5	3.30×10^6	2.44×10^6	1.76×10^6	1.52×10^6	1.18×10^6
56.0	3.27×10^6	2.41×10^6	1.74×10^6	1.50×10^6	1.16×10^6

X rays/mAs·cm2 at 1 m in 0.5-keV energy bins

4.A.iii - Analytical Models

- Integration of x-ray production along the electron path under the continuous slowing down approximation (CSDA)
- Arbitrary targets and takeoff angle.
- Difficult to describe backscatter and self-absorption which is dependant on electron transport in the target.

4.A.iii –Brems. Differential Cross Section (DCS)

- The probability per atom that an electron traveling with energy T will produce an x-ray within the energy range from E to E+dE is known as the differential radiative cross section, $d\sigma_r/dE$.
- Theoretic expressions indicate that the bremsstrahlung DCS can be expressed as;

$$\frac{d\sigma_r}{dE} = f_r(T,E,Z)\frac{Z^2}{\beta^2}\frac{1}{E}$$

- Where β is the velocity of the electron in relation to the speed of light.
- The slowing varying function, $f_r(T,E,Z)$, is often tabulated as the scaled bremsstrahlung DCS.

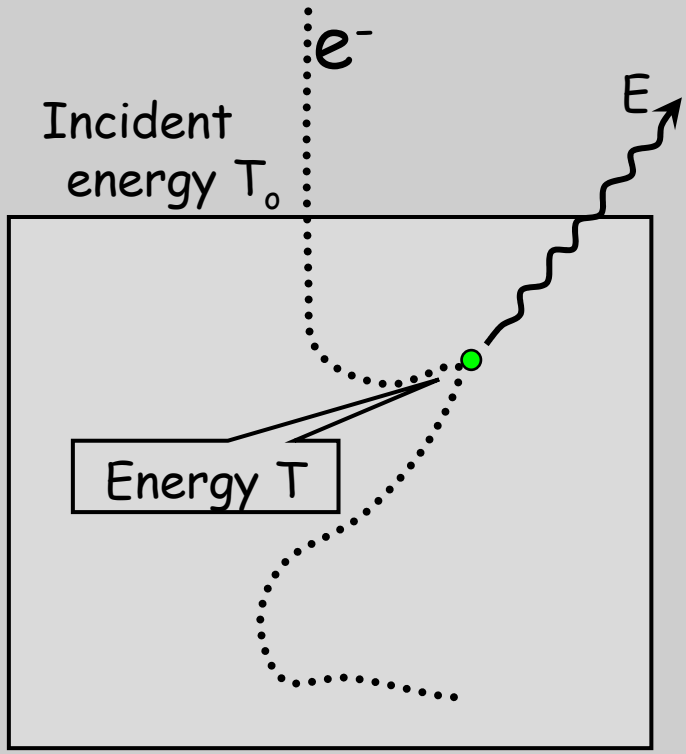

$$\beta^2 = 1 - \frac{1}{(1+\tau)^2}$$

$$\tau = T / m_e c^2$$

Seltzer SM & Berger MJ, Atomic Data & Nucl. Data Tables, 35, 345-418(1986).

4.Aiii –DCS pathlength integration

- The total radiative production of x-rays with energy in the range from E to E+dE can be found by integrating the production per unit pathlength over the path of the electron.

$$\sigma_{rs}(T,E) = N\sigma_r(T,E) = \frac{d\sigma_{rs}}{dEdS}$$

$$\sigma_{rs}(T,E) = 0, T \le E$$

Probability per cm per keV

$$\phi(E) = \frac{d\phi}{dE} = \int_0^{S(E)} \sigma_{rs}(T(S),E)dS$$

- Using the electron stopping power, dT/dS, this can be converted to an integration over the energy of the electron as it slows down.

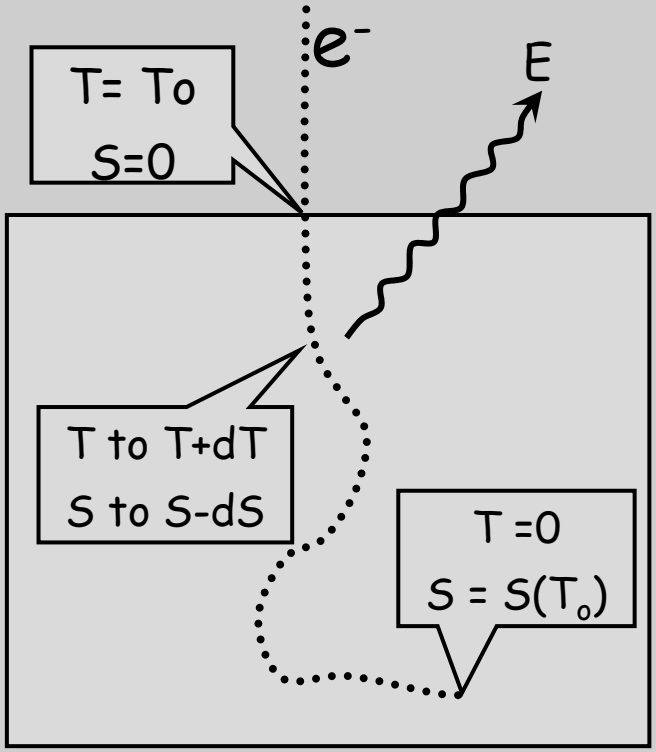

$$\phi(E) = \int_E^{T_o} \frac{\sigma_{rs}(T,E)}{dT/dS} dT$$

Xrays/electron/keV

4.Aiii - Classic integral bremsstrahlung models

- Kramers HA, Philos. Mag. 46(275) 1923.

  Semi-classical DCS, 1/T dT/dS, no absorbtion

- Storm E, Phys. Rev. A 5(6) 1972.

  Born/Sommerfield DCS, Berger&Seltzer dT/dS, fixed depth

- Birch & Marshall, Phys. Med. Biol. 24(3) 1979.

  polynomial DCS, Bethe dT/dS, T-W penetration

- Tucker et.al., Med. Phys., 18(2&3) 1991.

  Polynomial DCS, Berger&Seltzer dT/dS, T-W penetration

- These integral models have all been used in computational simulation software.
- However, the effects of electron transport in the target are not formally described.
- Transport effects (backscatter, absorption) are only approximated by very simplified expressions.

4.A.iv - Xspect 3.5/4.0 spectral estimates

- xSpect version 3.5 use the storm model for bremstrahlung radiation with a self absorption correction based on the tabata extrapolated range.
- Characteristic radiation is estimated from a power law expression dependant on overvoltage (Webster).
- xSpect version 4.0 uses electron distribution functions obtained from Penelope MC models to estimate the spectra from an integral model that fully describes the effects of electron transport

4.A.iv - XSPECT – spect_gen

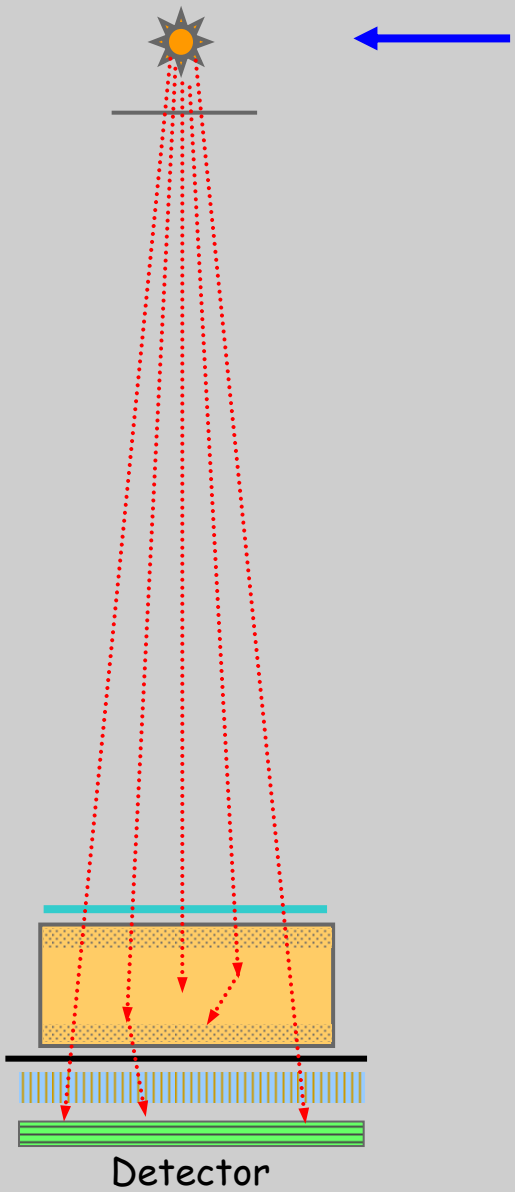

- xSpect 3.5 spect_gen script call
  - Storm bremsstrahlung model
  - Self abs. based on tabata range
  - Z dependant characteristic model
- Validation
  - Tungsten – Fewell
  - Molybdenum - Boone (Jennings)

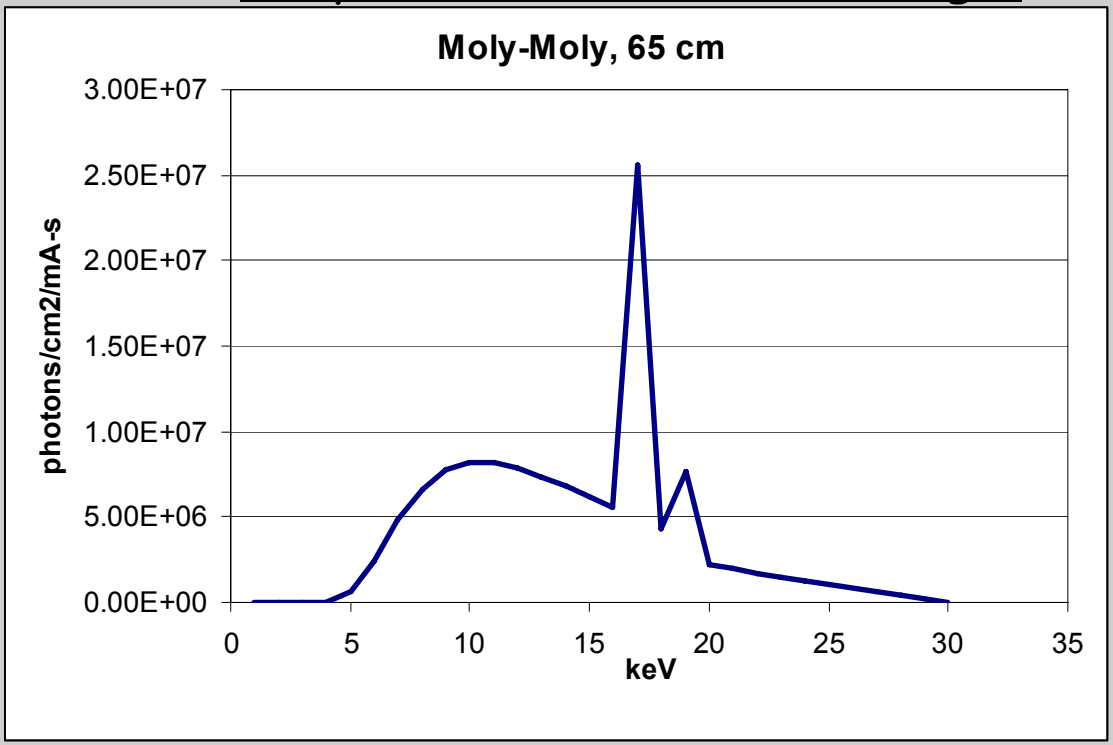

4.A.iv - Spect_gen Spectra Format

X-ray spectra are stored in a standard data structure that is read or modified by various program routines.

A text structure is used so that the spectrum can be passed to procedures as a script variable or plotted.

Z angle waveform kVp

Npts dkeV distance

Ergs:photons per sr:cm^2
1 1 - ergs/(mAs-sr-keV)
1 2 - ergs/(mAs-cm^2-keV)
2 1 - xrays/(mAs-sr-keV)
2 2 - xrays/(mAs-cm^2-keV)

```
# spect_gen: 42  12.000  1  50.00
#    99   0.5000      0.0000
#    2   1  (unit flags)
#  Energy      ergs/mAs-sr-keV
    1.000        0.0000E+00
    1.500        0.0000E+00
    2.000        1.4350E-09
    2.500        1.9378E-04
       .
       .
       .
    49.500        1.6423E+01
    50.000        0.0000E+00
```

Conversion Utilities:
sr2cm cm2sr
cm2cm
erg2no no2erg

Monte Carlo description of electron transport.

Three basic types of interaction influence electron transport and x-ray production.

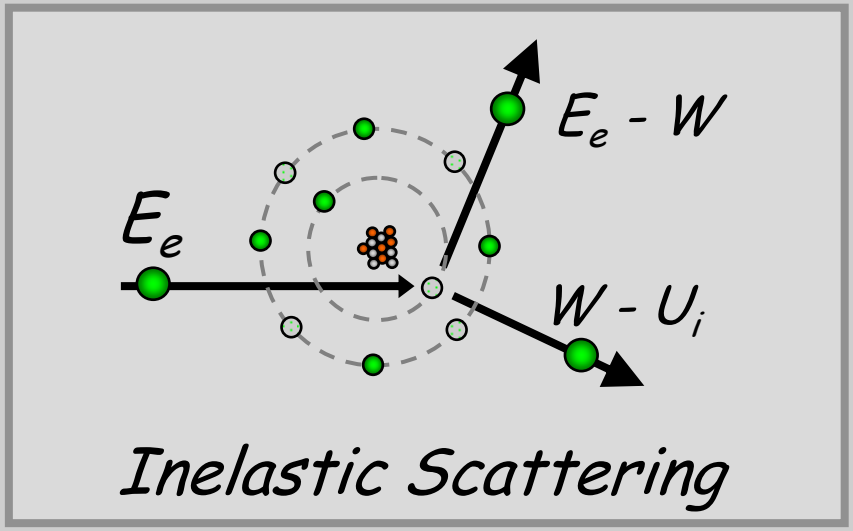

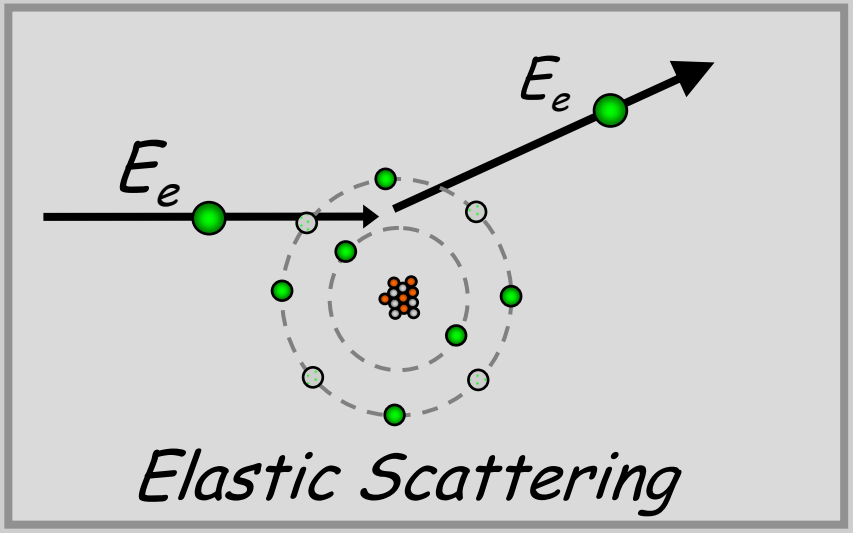

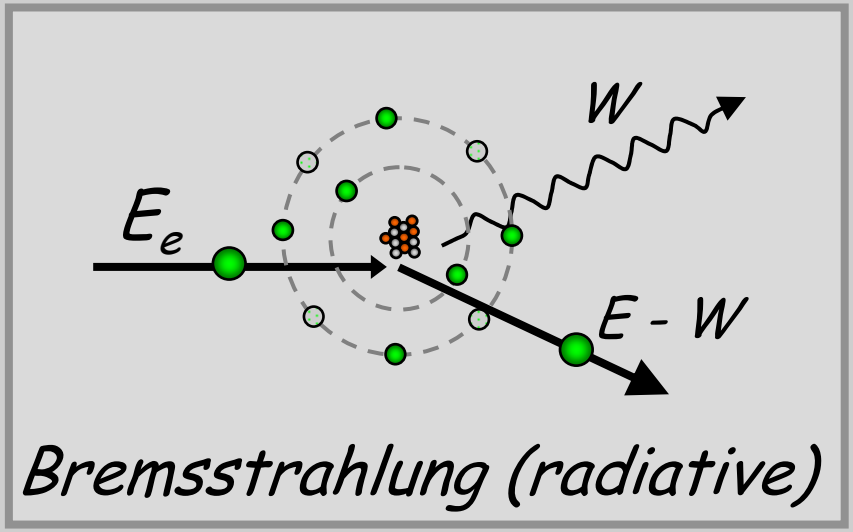

PENELOPE

- Tungsten
- 1μm x 1μm
- 100 keV

For take-off angles of
°-22.5°
0.0006 of the electrons produce an emitted x-ray of some energy.

4.A.iv – Electron number versus T.

As the incident electron slows down in the target, the average number of electrons as a function of slowing down energy, T, varies from 1.0 due to

- those electrons that escape the surface (backscatter) and
- to the production of energetic secondary electrons

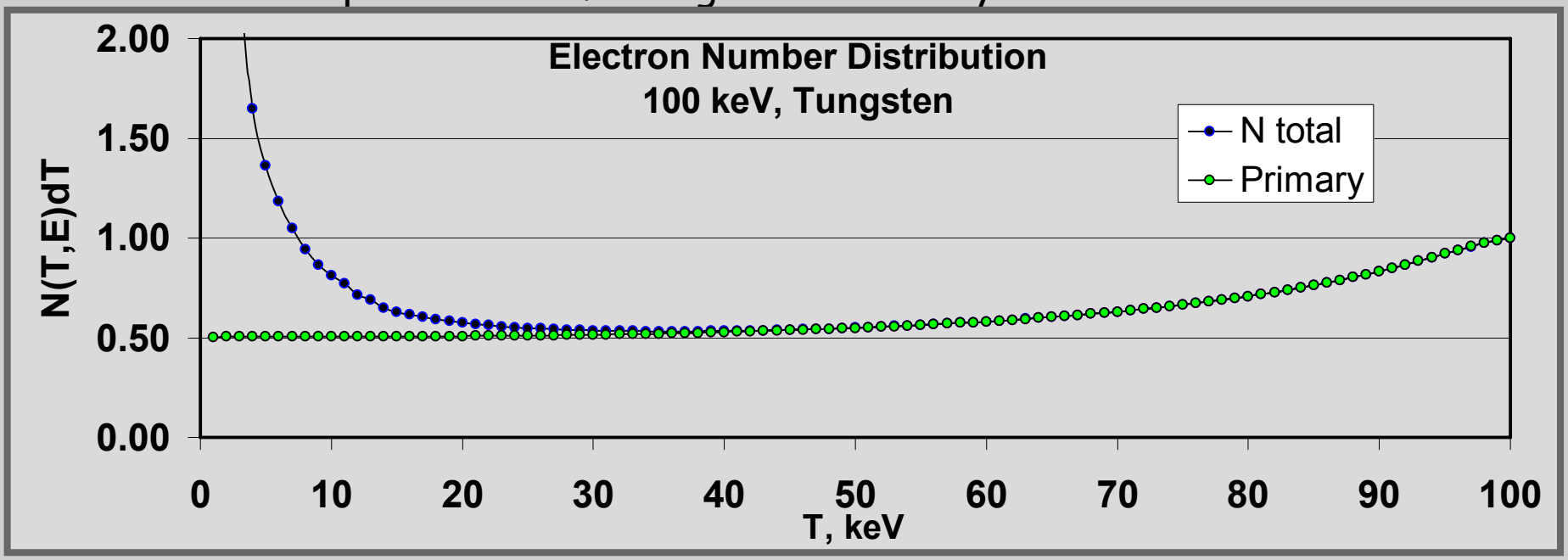

$$\phi(E) = \int_{E}^{T_o} N(T,T_o)\frac{\sigma_{rs}(T,E)}{dT/dS}dT$$

N(T,To) is the number of electrons still in the target as a function of the slowing down energy, *T*.

4.A.iv - Electron depth distribution vs T

- Electrons are broadly distributed in depth, Z, as they slow down due to extensive scattering.
- Most electrons tend to rapidly travel to the mean depth and diffuse from that depth.

$$\phi(E) = \int_E^{T_o} N(T,T_o) f_a(E,T) \frac{\sigma_{rs}(T,E)}{dT/dS} dT$$

$$f_a(E,T) = \int_0^{Z_{\max}} P_z(T,Z) e^{-\mu(E)Z/\sin(\alpha)} dZ$$

Pz(T,Z) is the differential probability (1/cm) of that an electron within the target is at depth Z

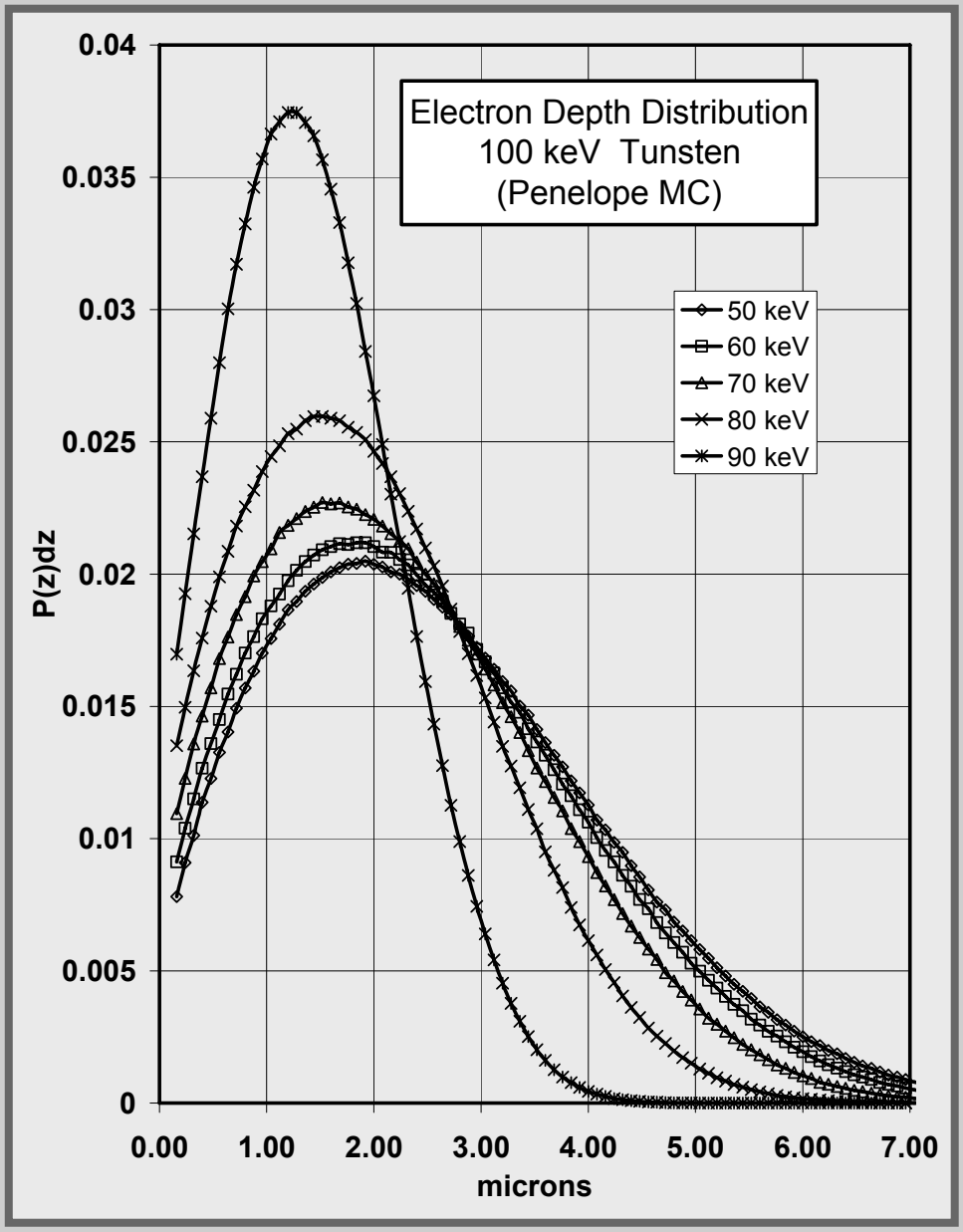

4.A.iv - angular dependence of DCS

The shape function for atomic-field bremsstrahlung is defined as the ratio of the cross section differential in photon energy and angle to the cross section differential only in energy.

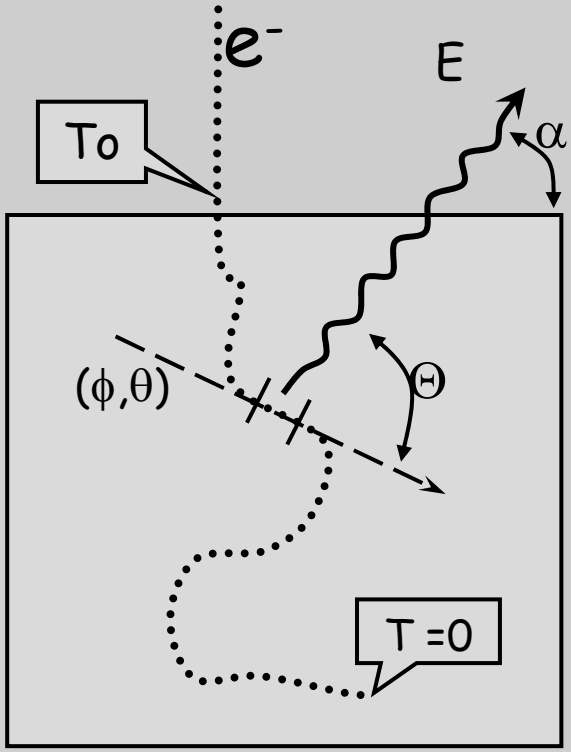

$$S(T,E,\Theta) = \frac{d^2\sigma_{r\Theta}/dEd\Omega}{d\sigma_r/dE}$$

$$\sigma_{r\Theta}(T,E,\Theta) \equiv d^2\sigma_{r\Theta}/dEd\Omega$$

$$\sigma_r(T,E) \equiv d\sigma_r/dE$$

$$\sigma_{r\Theta}(T,E,\Theta) = S(T,E,\Omega)\sigma_r(T,E)$$

σ_{rs} - Barns/nuclei/keV/sr

σ_{rs} - Barns/nuclei/keV

Θ - electron (ϕ,θ) – xray (α)

α - xray takeoff angle

(ϕ,θ) – electron vector direction

4.A.iv - Kissel shape function, S(T,E)

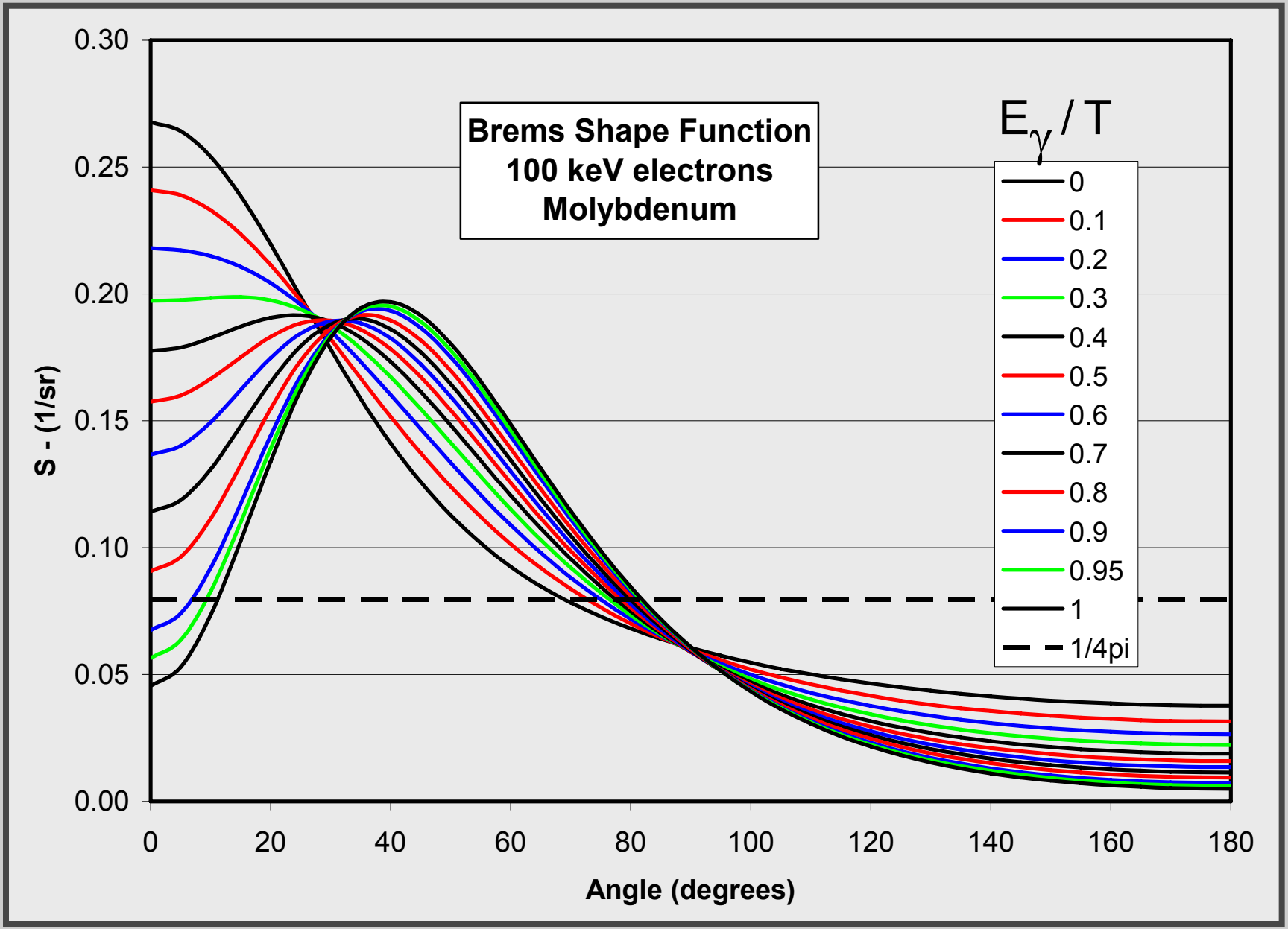

4.A.iv - Electron angular distribution vs T,Z

Angular distribution in relation to depth as a ratio of the extrapolated range.

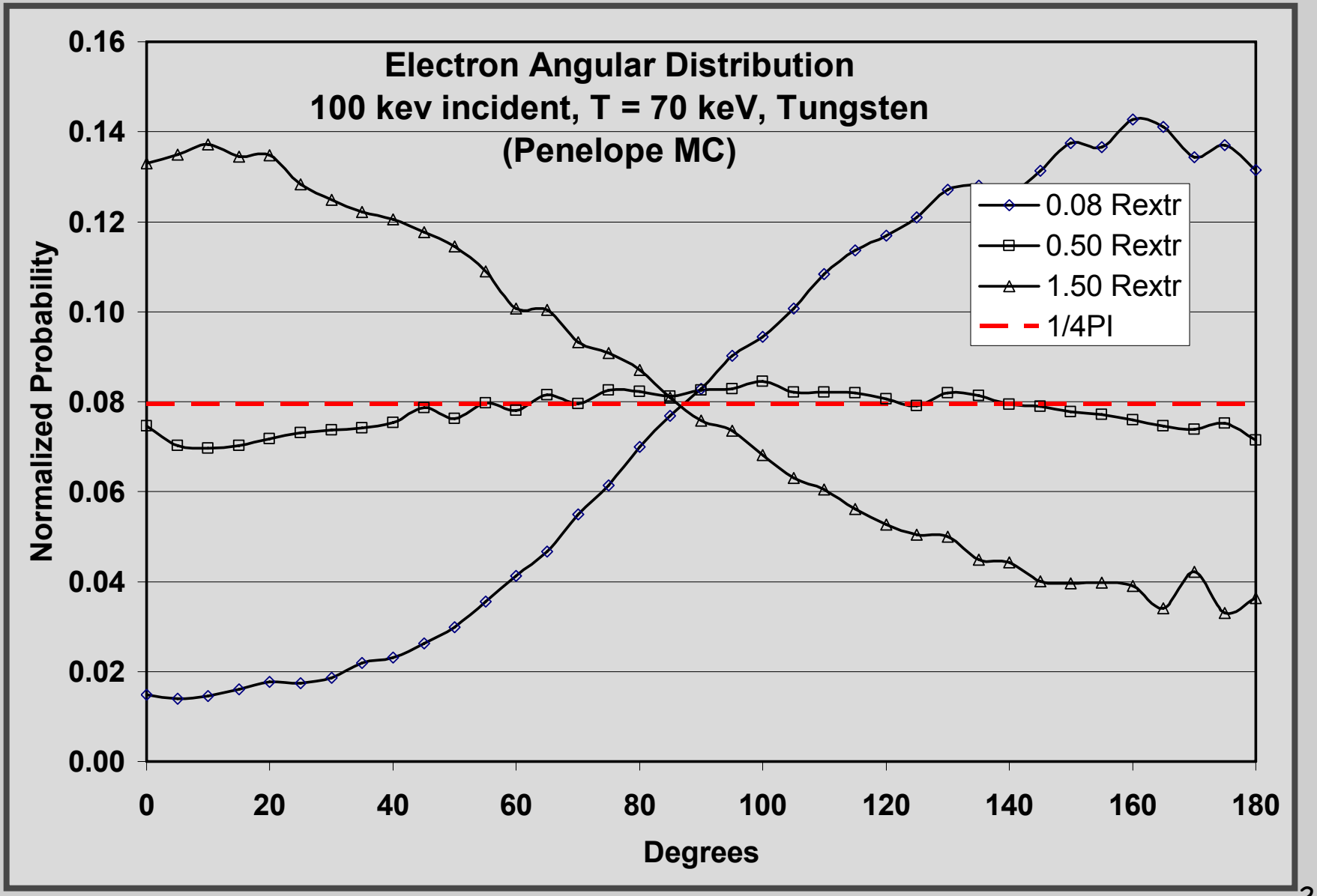

4.A.iv - Integral model with analytic e^- transport

- The effects of anisotropic electron angular distribution as a function of depth can be described by including an angular average of the shape function in the depth integration.
- For XSPECT 4.0, Q matrices are precomputed for various takeoff angles so that the spectrum can be determined as a function of To using numerical solution

$$\phi(E) = \int_E^{T_o} N(T,T_o) Q(E,T) \frac{\sigma_{rs}(T,E)}{dT/dS} dT$$

$$Q(E,T) = \int_0^{Z_{\max}} S_{\phi\theta}(T,E,Z) P_z(T,Z) e^{-\mu(E)Z/\sin(\alpha)} dZ$$

$$S_{\phi\theta} = \int_0^{\pi} P_\phi(\phi,T,Z) \left[\int_0^{2\pi} S(T,E,\Theta(\phi,\theta,\alpha) d\theta \right] \sin(\phi) d\phi$$

4.A.iv - XSPECT models vs experiment

xspect 3.5 and xspect 4.0 in relation to Mercier experimental

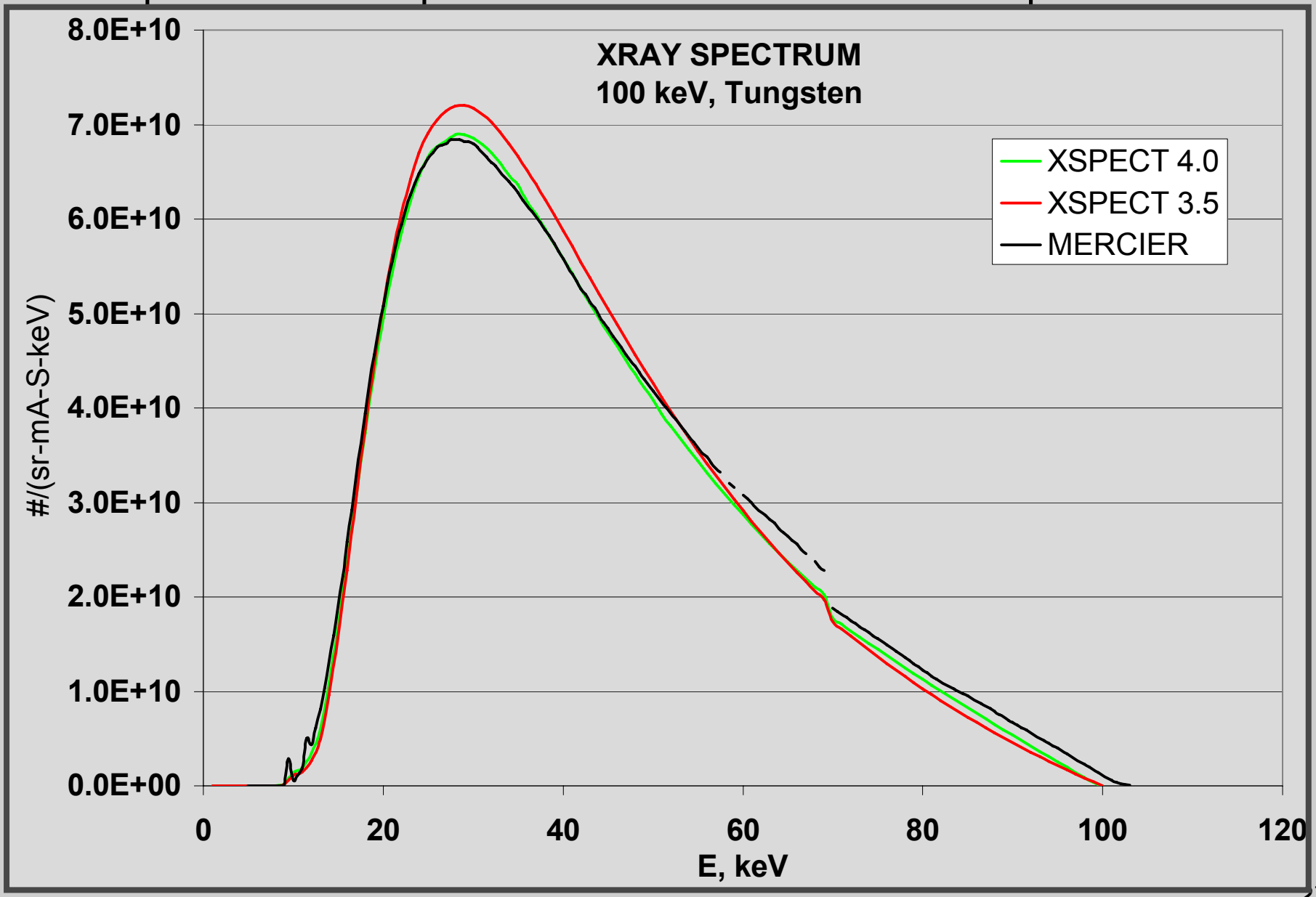

* XSPECT 4.0, normalized values

Computational Simulation of Radiation Imaging Systems using XSPECT*

A) X-ray Energy Spectrum.

B) Cross section & material composition.

i. X-ray interactions & attenuation (pg 29)

ii. Sources of cross section data (pg 32)

iii. Evaluated interaction data (pg 34)

iv. Xspect materials & attenuation (pg 39)

C) xSpect: Exposure, Contrast, Noise, & Dose

4.B.i - Xray Interactions

Attenuation is computed from Beer's law using the linear attenuation coefficient, μ, computed from cross sections and material composition.

$$\mu = N_1\sigma_{PE} + N_2\sigma_{PE} + N_3\sigma_{PE}$$

Where N_i is the number of atoms in species i and σ_i is the cross section for interaction i.

$$I = I_o e^{-\mu x}$$

$$\mu = \mu_{PE} + \mu_{INC} + \mu_{COH}$$

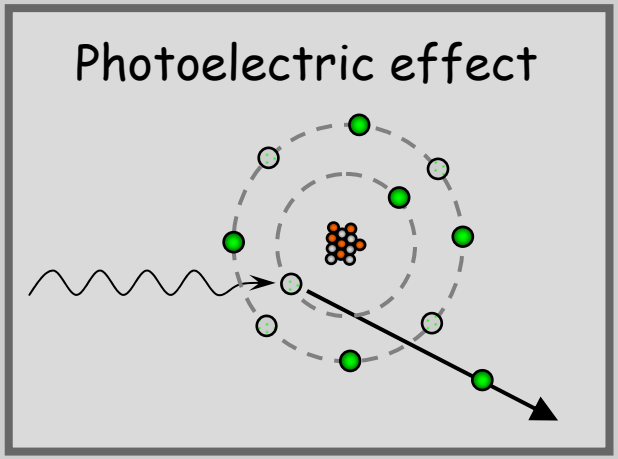

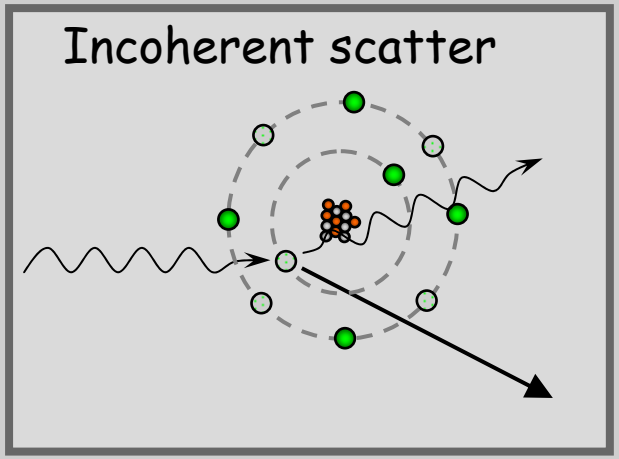

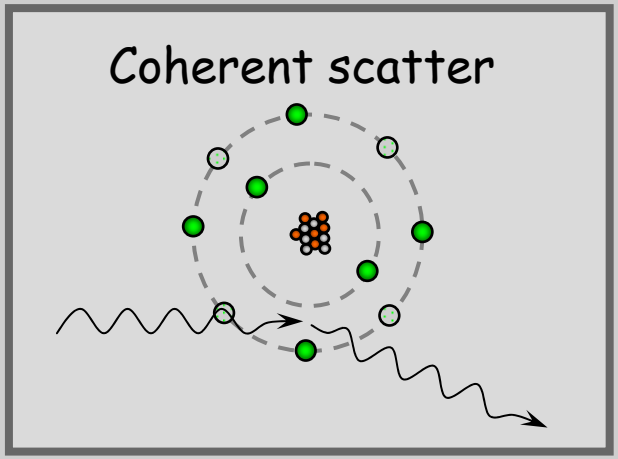

In the energy range of interest for diagnostic xray imaging, 10 – 250 keV, there are three interaction processes that contribute to attenuation.

4.B.i - Xray attenuation coefficients – H2O, Pb

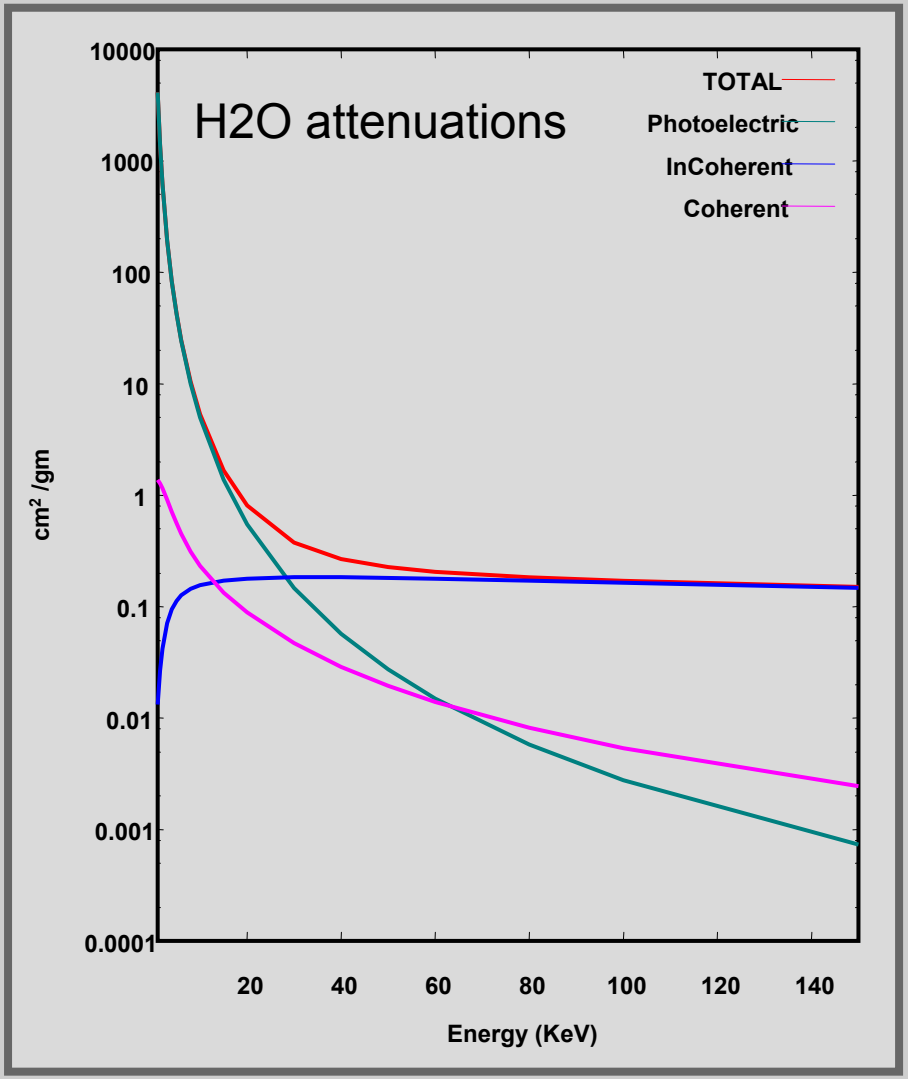

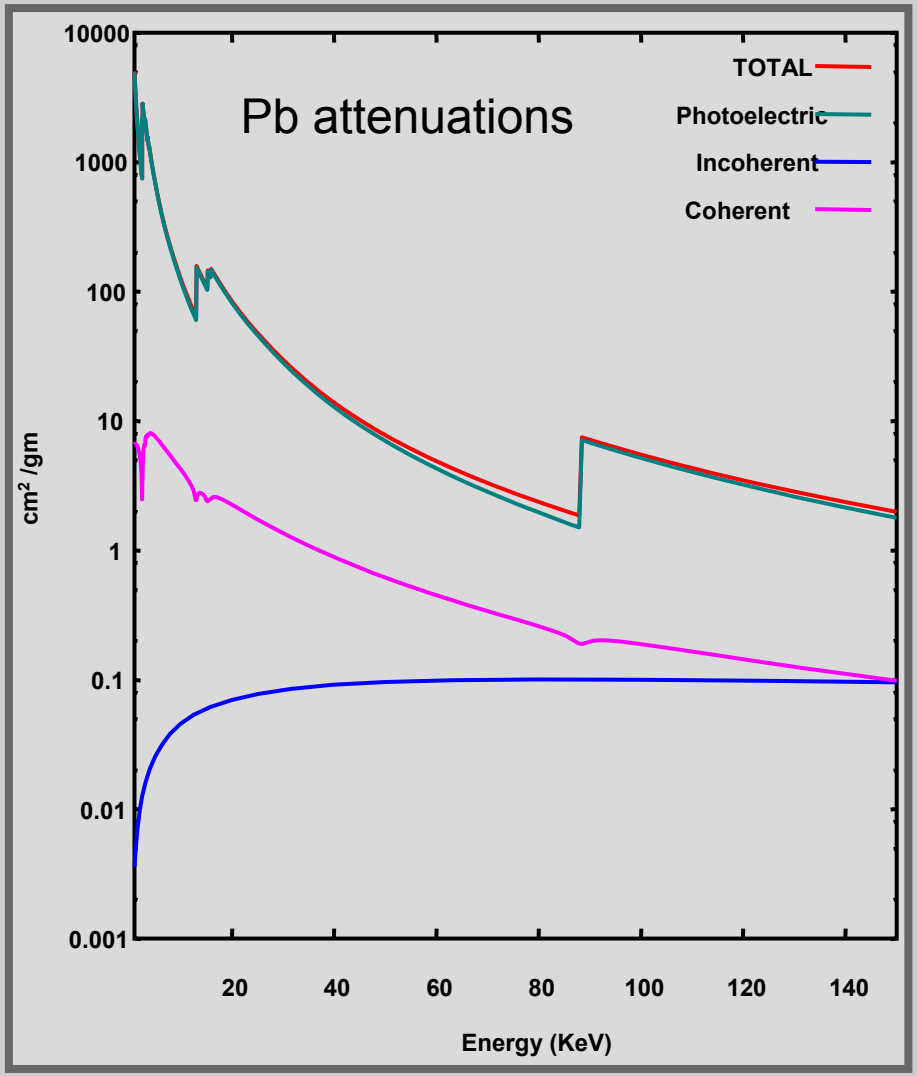

Coherent ~ 10% of total cross section

Measured vs. Computed

- Measured data is best, but μ data is not available for all energies and materials
- Current theory allows accurate computation of cross sections.
- Data from national labs is primarily computed and supplemented with measured data
- Data is generally presented either as tabulated data or as functional fits to data.
- Computations:
  - Derived from E-M theories
  - Form Factors, Klein-Nishina, S-Matrix
  - Photon / Atom Interactions - typified by Rayleigh scatter
  - Photon / Electron Interactions – typified by Thomson scatter

4.B.ii – Sources of cross section data

- **NIST:**
  - FFAST Chantler, Olsen, Dragoset, et.al. (2003)
    - PE, Coherent + Incoherent, f' and if''
    - K-N for Incoherent
    - Coherent RFF H-F - corrections by Chantler
    - PE RFF H-F - corrections by Chantler
  - XCOM Berger, Hubbell, Seltzer, Coursey, Zucker (1998)
    - All three cross section estimates
    - K-N and H-F estimates
    - Coherent RFF H-F relativistic Hartree-Fock atomic form factors
    - PE from Scofield's application of Hartree-Slater model
- **LBL:**
  - Atomic Data and Nucl. Data Tables, Henke, Gullikson, Davis (1993)
    - f' and if'' values available
    - Measurements supplemented with H-F NRFF of Henke

4.B.ii – Sources of cross section data (cont.)

- **LLNL:**
  - EPDL (evaluated photon data libr.) Cullen, Hubbell, Kissel (1997)
    - Estimates of Coh, Incoh, PE, PP, and neutron/electron data
    - PE - Scofield's H-F
    - Coherent NRFF from Hubbel
    - Incoherent K-N
  - RTAB Kissel (2000)
    - Rayleigh scatter database
    - multiple approaches MFF, RFF, NRFF etc..
  - McMaster, Del Grande (1969) (McBook)
    - All three cross section estimates - measured
    - Polynomial fits to each cross section
- **SANDIA:**
  - Biggs and Lighthill, ITS code(1990)
    - PE, Incoh, Coh – measured
    - Polynomial fits to data

4.B.iii – Evaluated interaction data

Dodge (SPIE 2004);

"Comparison of Photon Attenuation Coefficients (2-150 KeV) for Diagnostic Imaging Simulations"

- Data plotted in 3-D for total cross section, all elements, and energies 1-150 KeV at 1 KeV intervals
- 2-D plots for elements common to diagnostic imaging, and for areas identified on the 3-D plots.
- Each cross section type for each method was plotted simultaneously to qualitatively compare μ's

4.B.iii - 3D comparison example

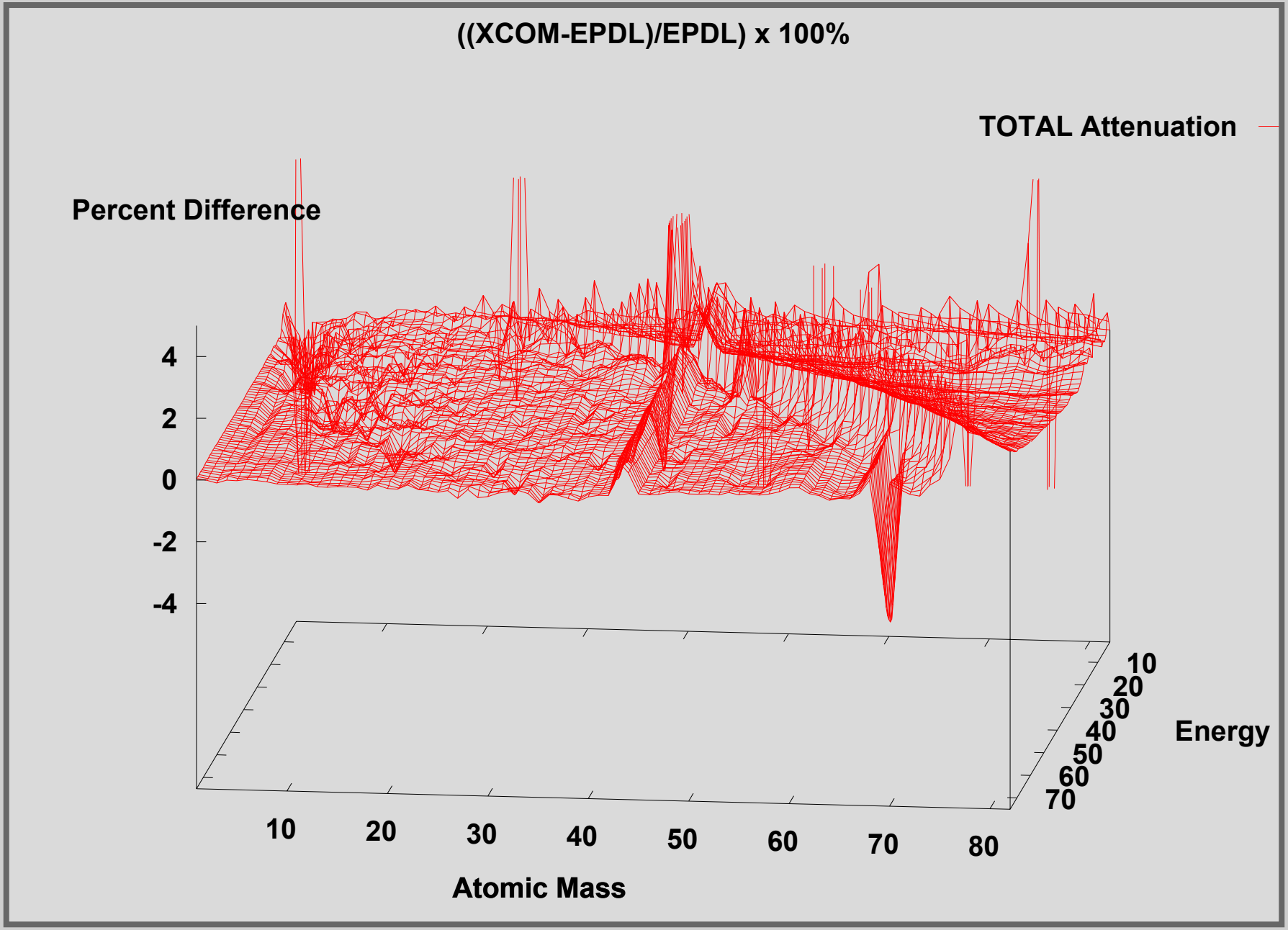

4.B.iii - 2D comparisons

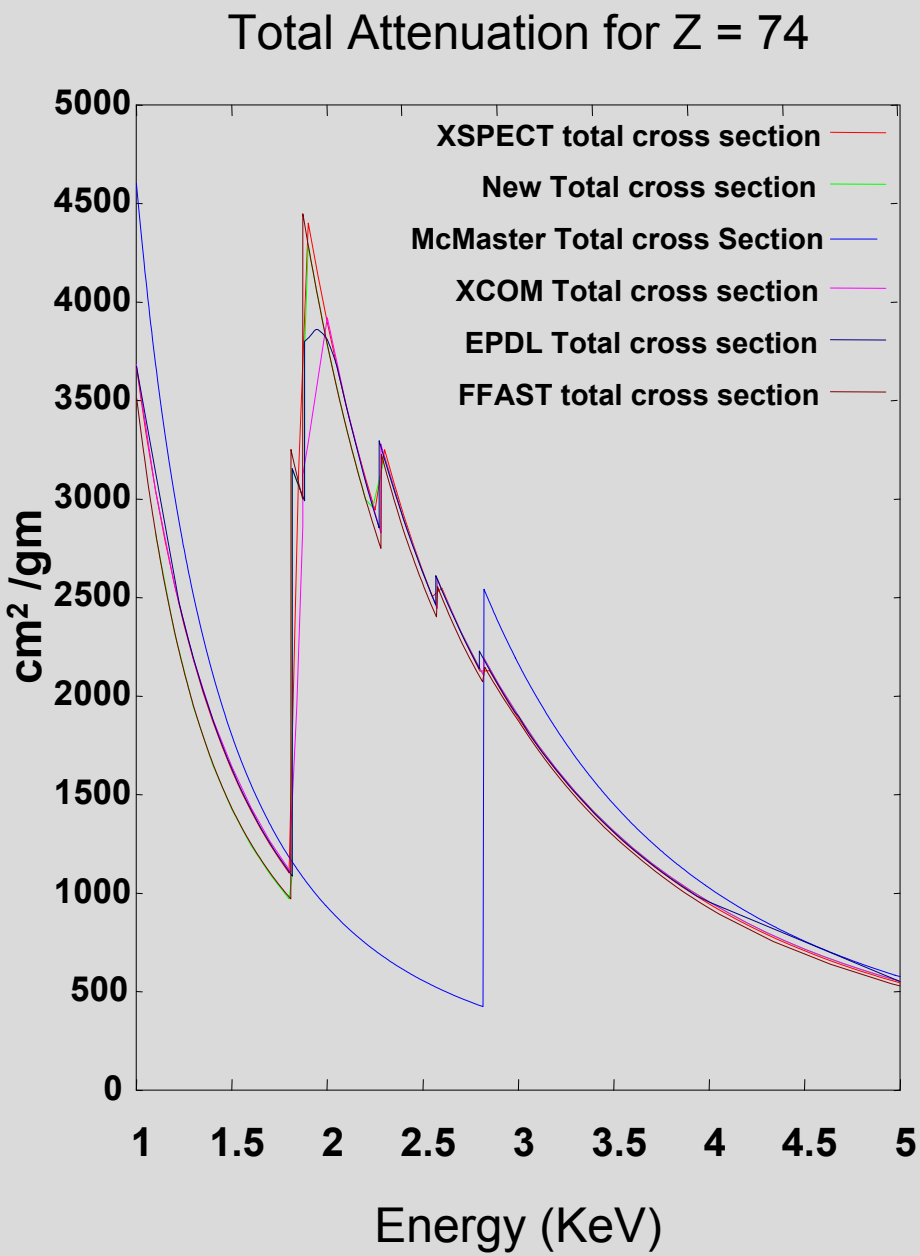

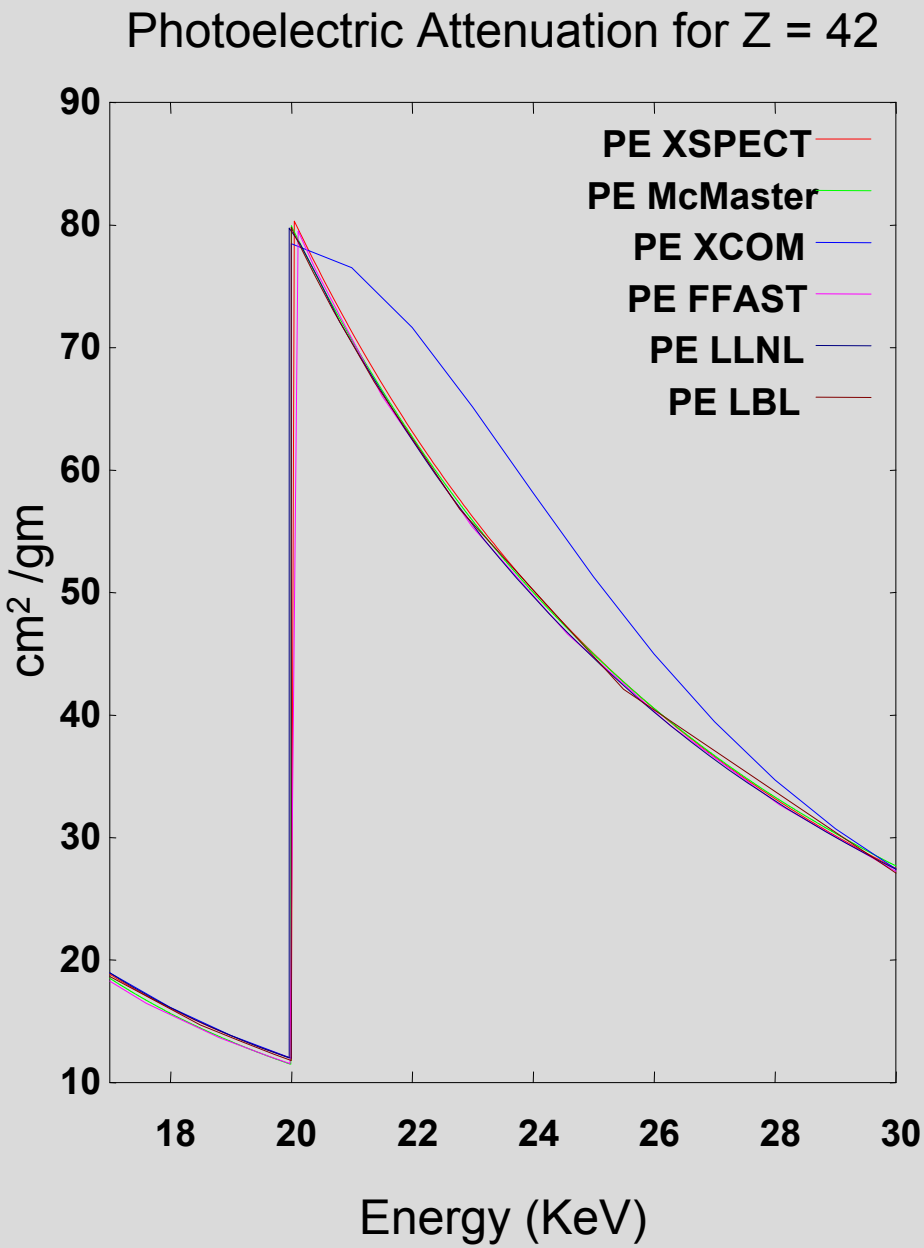

4.B.iii - Which is best ?

All methods work well - within >1% away from edges

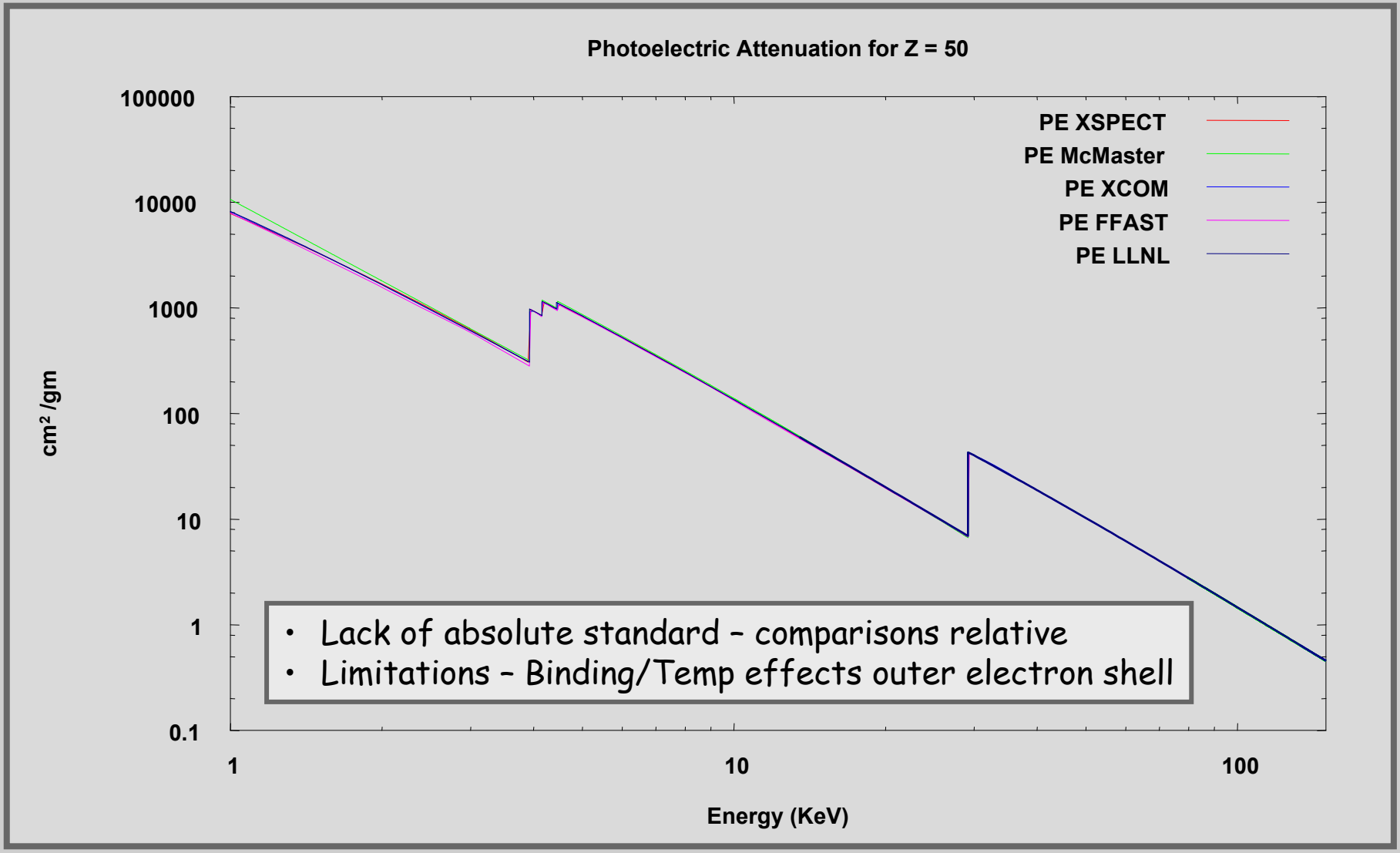

- Lack of absolute standard – comparisons relative
- Limitations – Binding/Temp effects outer electron shell

4.B Pros & Cons - the Good, the Bad and the Ugly

	PRO	CON
EPDL	• Tabular format, FTP server • Energies to 100 GeV • Resonances in coherent scatter	• Disagreement at shell edges • Data in EPDL format
FFAST	• Emphasis on low E estimates • Energies to 1 MeV	• Code/Data not readily available • web access only
XCOM	• Open Source code online • Energies to 100 GeV • Web access to individual data	• Anomalous data for some elements
RTAB	• Energies to 10 MeV • Data files for many methods • Web access to individual data	• Resonance spikes (electron bound transition states) • Smoothing of data required
McMaster	• Gold standard for many years • Polynomial expressions	• Outdated data • Much smoothing of outer shells
TIGER	• Data tables available	• Older data • some smoothing of outer shells
LBL	• Can Download tabulations • Measured data where available	• Energy up to 30 KeV

4.B.iv – xSpect Material & Attenuation

Cross Sections

- XSPECT 3.5
  - TIGER (Biggs & Lighthill) for PE
  - McMasters for Coherent
  - McMasters for Incoherent
- XSPECT 4.0
  - EPDL for Coherent
  - EPDL for Incoherent
  - FFAST for PE

4.B.iv – Primary spectrum attenuation

- XSPECT 'atten' script call
- Typically computed at object surface and detector surface.

$\Phi_{br}(E)$ and $\Phi_{det}(E)$, Photons/cm2/mA-s

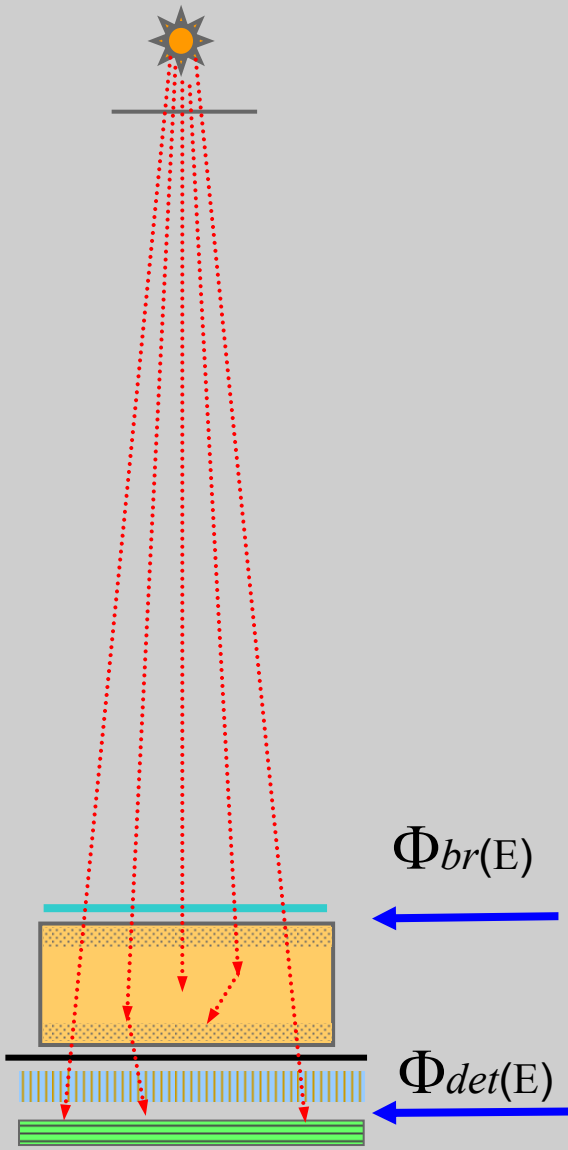

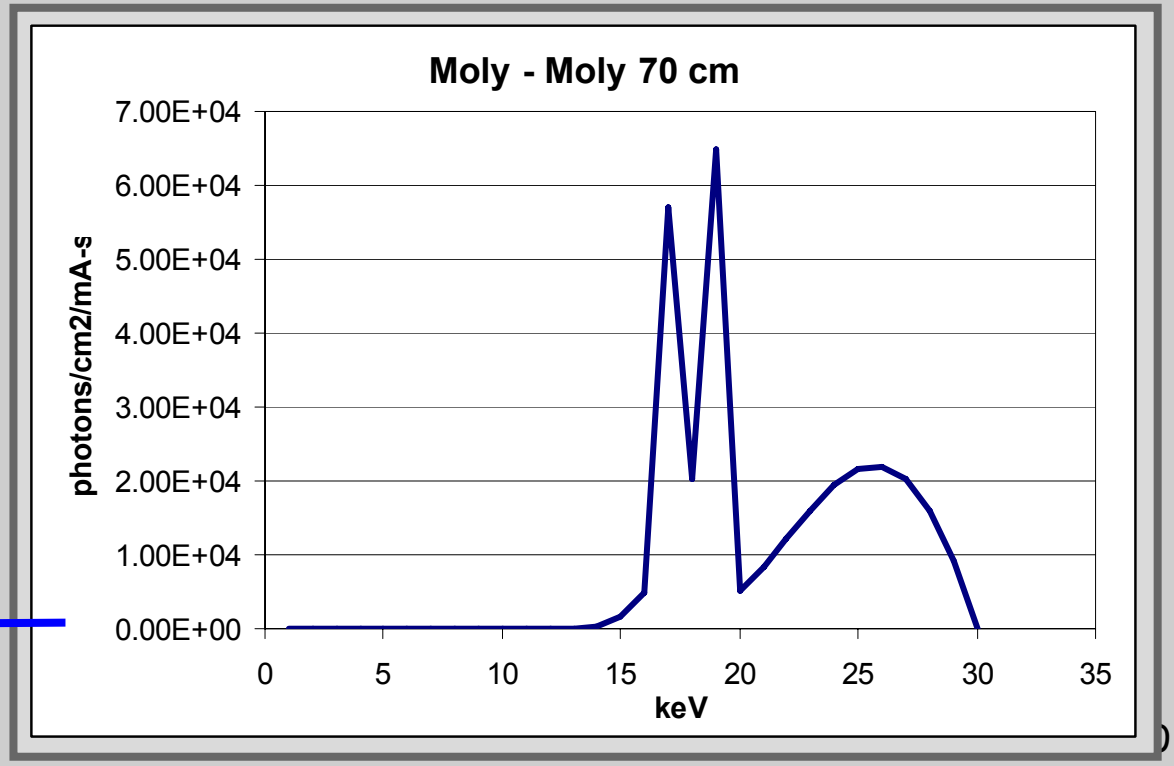

70 cm SDD

4.B.iv – Spectral Attenuation

The XSPECT 'atten' procedure attenuates the x-ray spectral data for a specified list of material.

For a typical glass envelope tungsten tube;

```
> atten
  3
  glass_pyrex   .148
  oil           .300
  al_1100       .1
```

'atten' appends an attenuation history to the spectral data structure

---

No. of materials
Material1 thickness1
Material2 thickness2
. .

```
# spect_gen: 74  12.000  1 120.00
#   120   1.0000      0.0000
#    1   1  (unit flags)
#  Energy        #/mAs-sr-keV
   1.000         0.0000E+00
   2.000         0.0000E+00
   .
   .
   119.000       3.1155E+08
   120.000       0.0000E+00
#  Attenuation History:
#  4
# glass_pyrex      1.4800E-01
# oil              3.0000E-01
# al_1100          1.0000E-01
# al_1100          3.0000E-01
```

4.B.iv – Material Composition Library

- A library of data files containing material composition in a standard format that is accessed by file name.
- 106 materials as of Jan 2004.
- The standardized data files are also used by the SKEPTIC Monte Carlo code (S. Wilderman) and the DETECT optical Monte Carlo code (A. Badano).

- line 1: no. of elements
- line 2: Z of each element
- line 3: either:
  - No. per molecule (int)
  - weight fraction (if < 1)
- line 4: density.
- line 5: Condensed or Gas
- line 6: Pressure for G

```
Parylene:

2
6 1
8 8
1.11
C

manufacturers data from
www.lebowcompany.com. Confirmed
at www.parylene.com. Density
varies depending on paraylene
type. Parylene N assumed due to
constant dielectric constant over
a wide range of temperatures
```

Computational Simulation of Radiation Imaging Systems using XSPECT*

A) X-ray Energy Spectrum.

B) Cross section & material composition.

C) xSpect: Exposure, Contrast, Noise, & Dose

i. xSpect script environment (pg 44)

ii. Exposure estimation (pg 47)

iii. Dose estimation (pg 49)

iv. Detector signal and noise (pg 51)

v. Contrast & normalized CNR (pg 59)

4.C.i - Tcl/tk scripted applications

- XSPECT routines can be invoked with tcl/tk scripts to simulate specific applications.
- XSPECT is supported on Unix & Windows lanquage systems.
- Tcl/tk is an advanced script that includes commands to form graphic window applications.
- XSPECT results can be presented using gnuplot.

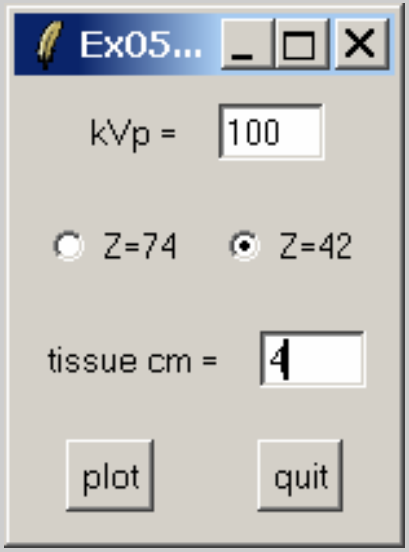

Lab #05 examines the tissue exit spectrum and exposure for varying amount of added filtration at the x-ray source.

Tissue exit spectrum vs added Mo filter thickness

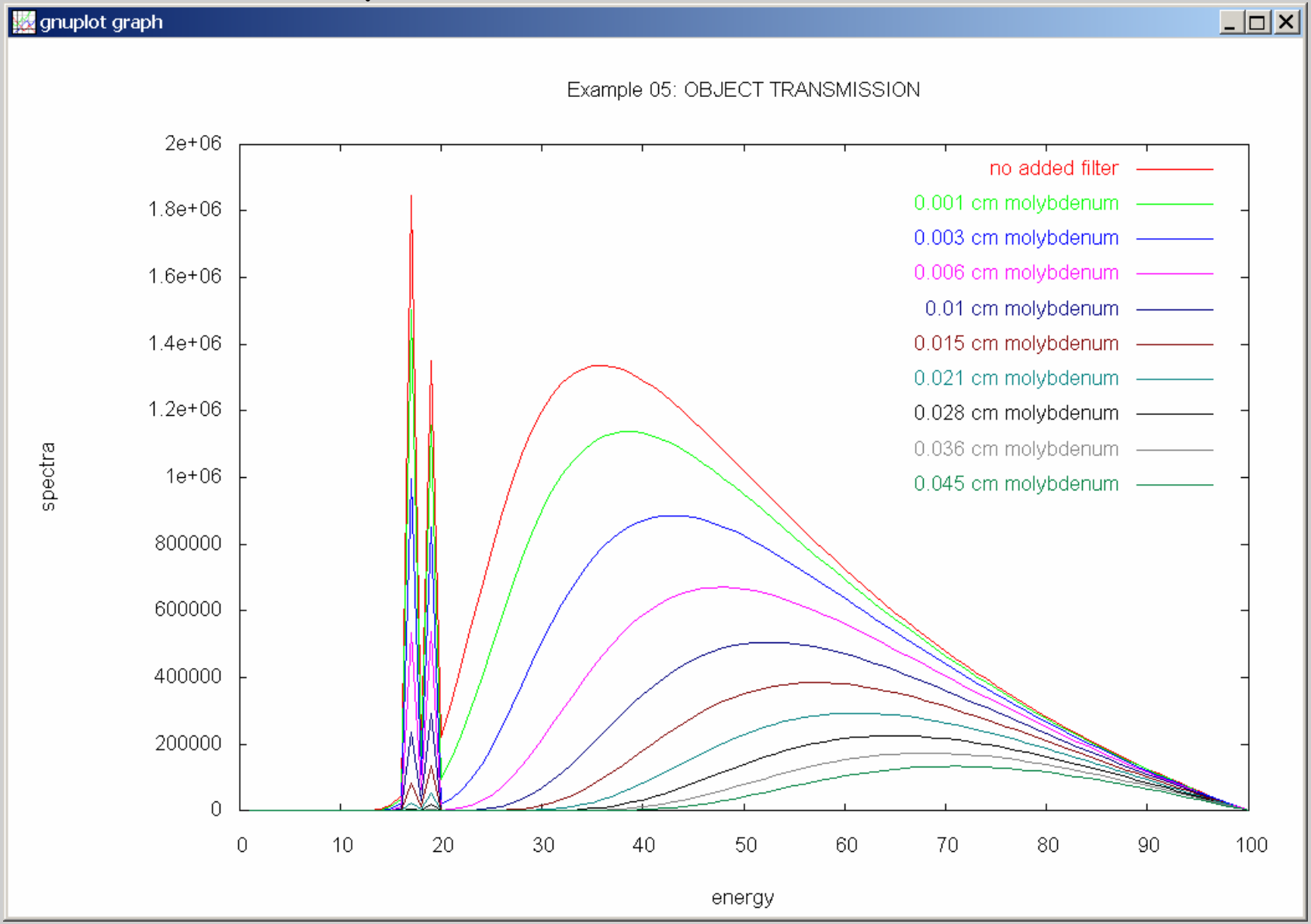

Tissue exit exposure vs added Mo filter thickness

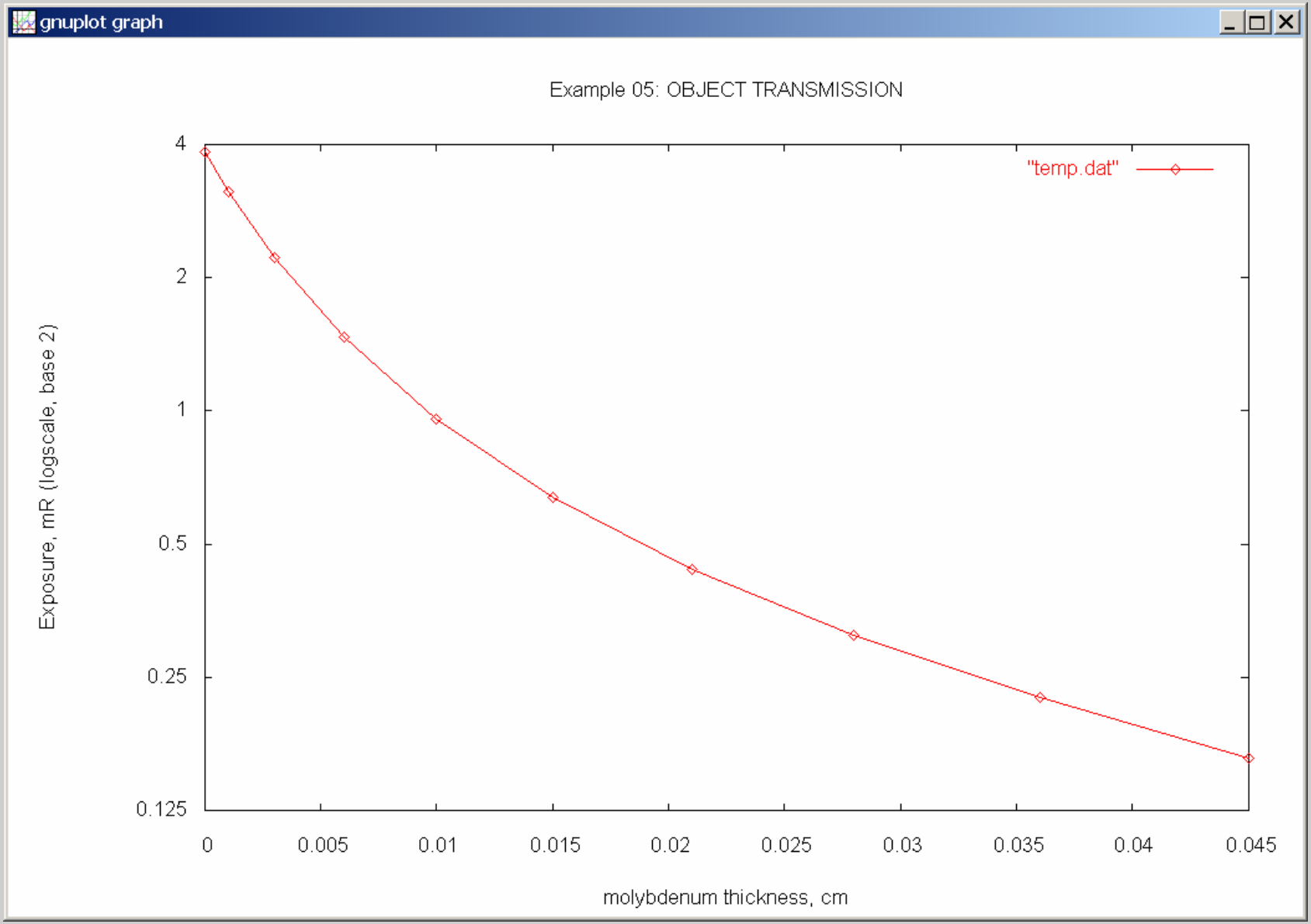

4.C.ii - Exposure – mR (coulombs/kg)

- Exposure is determined by an XSPECT script procedure that integrates the product of the energy spectrum (photons/cm^2/keV) and the air energy absorption coefficient (gms/ cm^2) to estimate the energy absorbed per gram;

$$g = \int \Phi(E) \frac{\mu_{en}}{\rho} dE$$

- The energy absorbed per gram, g (ergs/gm), is then converted to exposure using a conversion factor of 33.97 Joules/Coulomb (i.e. eV/ion, Boutillon 1987);

$$X = g/(33.97 \times 10^4) \ \ C/kg$$

$$X = g/87.643 \text{ Roentgens}$$

4.C.ii - Air energy absorption coef.

Tabulated air energy absorbtion data from NIST based on calculations by Seltzer (Radiation Research 136, 147; 1993) are interpolated using a log-log transformation.

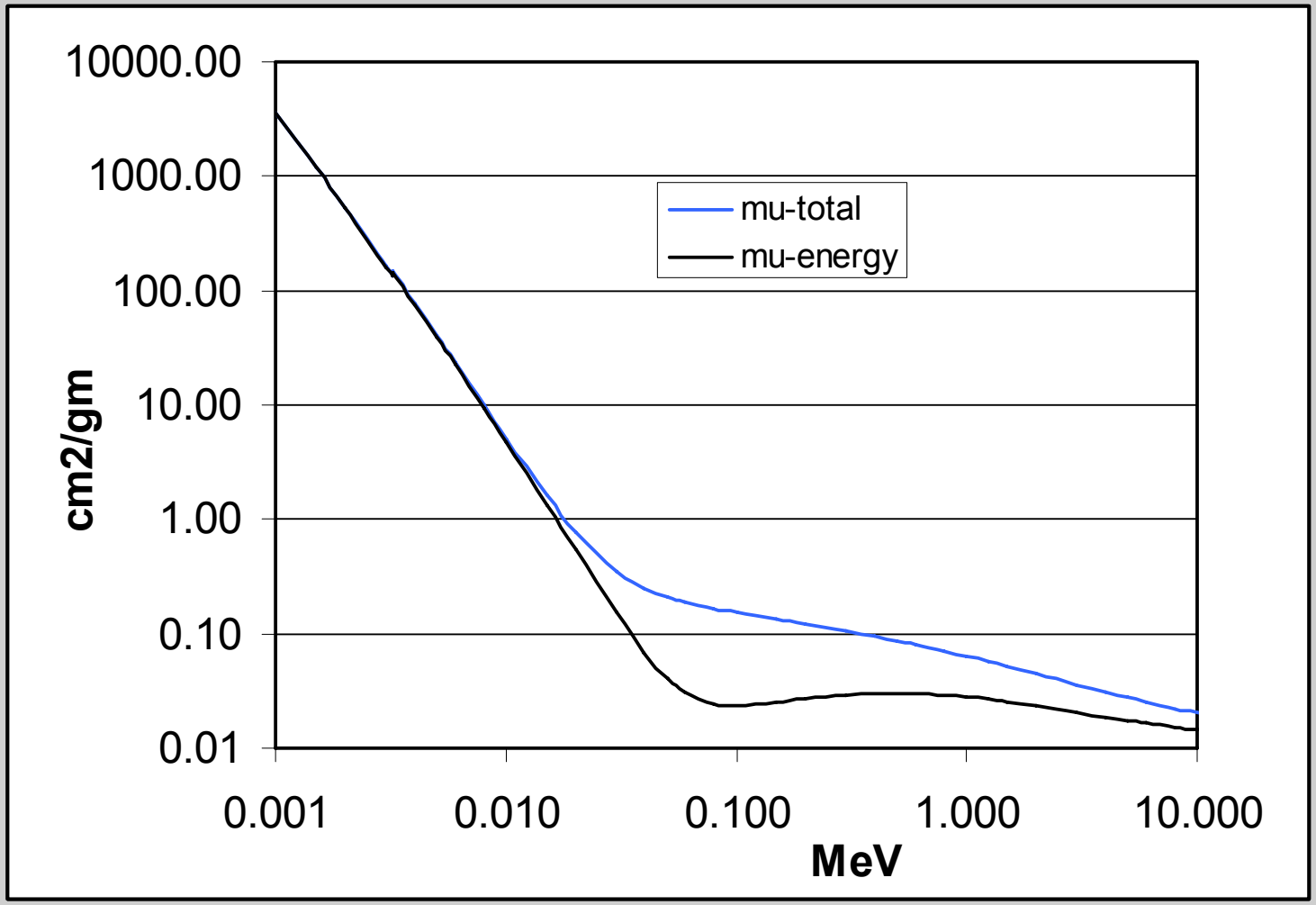

http://physics.nist.gov/PhysRefData

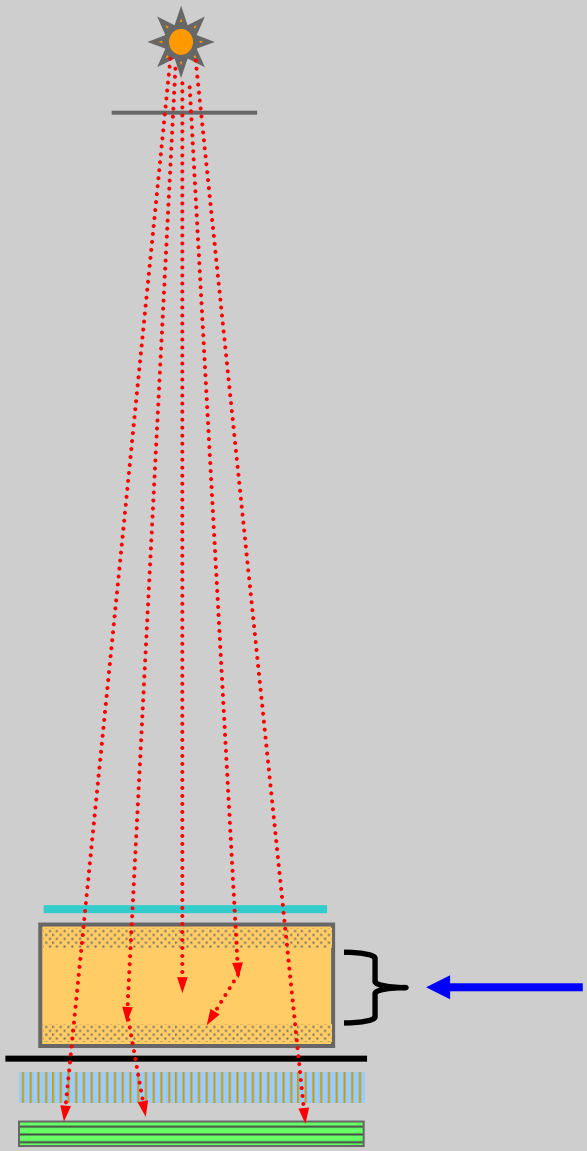

70 cm SDD

Absorbed dose is determined by an XSPECT script procedure that integrates the product of the energy spectrum and an energy dependant dose deposition function, ***G(E)*** ;

$$D = \int \Phi_{in}(E) G(E) dE$$

G(E) tables

- Monte Carlo computed tables.
- Must be computed for a specific object size using a geometry model that includes adjacent materials.
- Units of mGy/(photons/cm^2).

4.C.iii - Object specific Dose tables

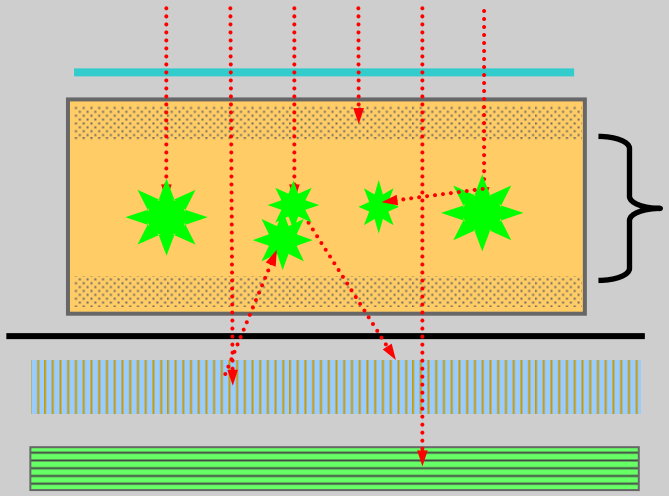

- G(E) is computed at 1 keV energy intervals using Monte Carlo simulation.
- For each energy, a many x-rays are tracked interaction by interaction through all materials.
- The energy depositions in the volume of interest are accumulated.
- The total energy binned is then normalized to the total number of photons/cm2 .

Breast phantom material

- BR12 50-50
- Excludes energy in top/bottom 5 mm

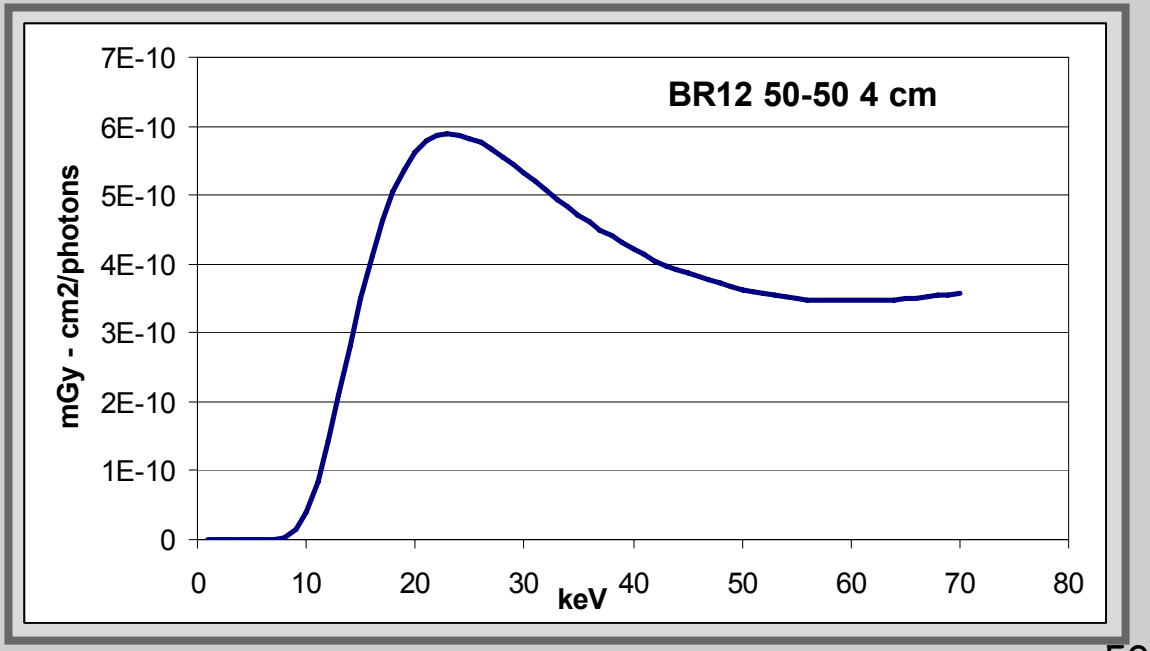

4.C.iv - Detector signal & noise

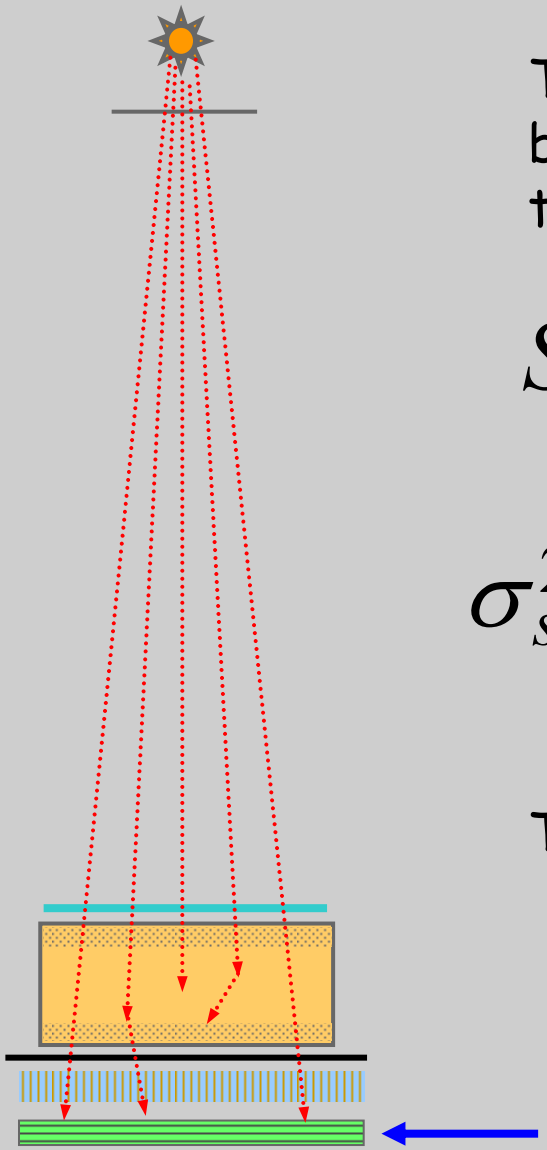

70 cm SDD

The detected signal and noise are determined by an XSPECT script procedure that integrates the product of the energy spectrum

$$S = A_p \bullet mA \bullet t \int \left(\varepsilon_s(E) \right) E \Phi_{\det}(E) dE$$

$$\sigma_s^2 = A_p \bullet mA \bullet t \int \left(\varepsilon_\sigma^2(E) \right) E^2 \Phi_{\det}(E) dE$$

Tabulated signal and noise transfer efficiencies

- Monte Carlo computed tables.
- Model includes all detector materials.
- Units of electrons/keV and (electrons/keV)^2 .

4.C.iv - 250 micron Se Detector

Detector materials

50 nm	ITO	<== layer 1
25 μm	parylene	<== layer 2
250 μm	a-Se	<== layer 3
100 nm	ITO	<== layer 4
200 nm	Si3N4	<== layer 5
50 nm	Cr	<== layer 6
1.1 mm	glass_1737	<== layer 7

Monte Carlo computation of energy deposition

P(e,E)de

The normalized energy deposition probability function is computed for layer 3, a-Se

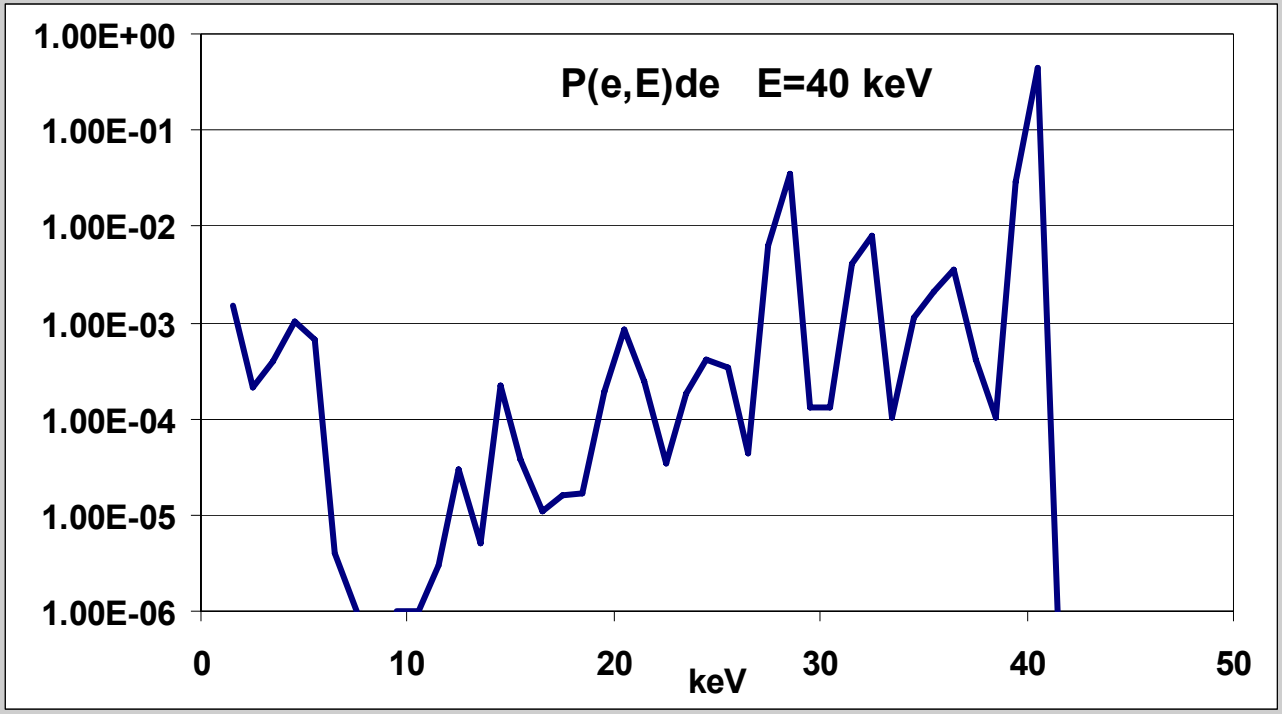

Electron production deduced from mean keV/e

The number of elections produced, $P(n,E)dE$ is computed as the integral of $P(n,e)\ P(e,E)de$

$P(n,e)\ de$ is a Poisson distibution function with mean n determinted from keV/e data.

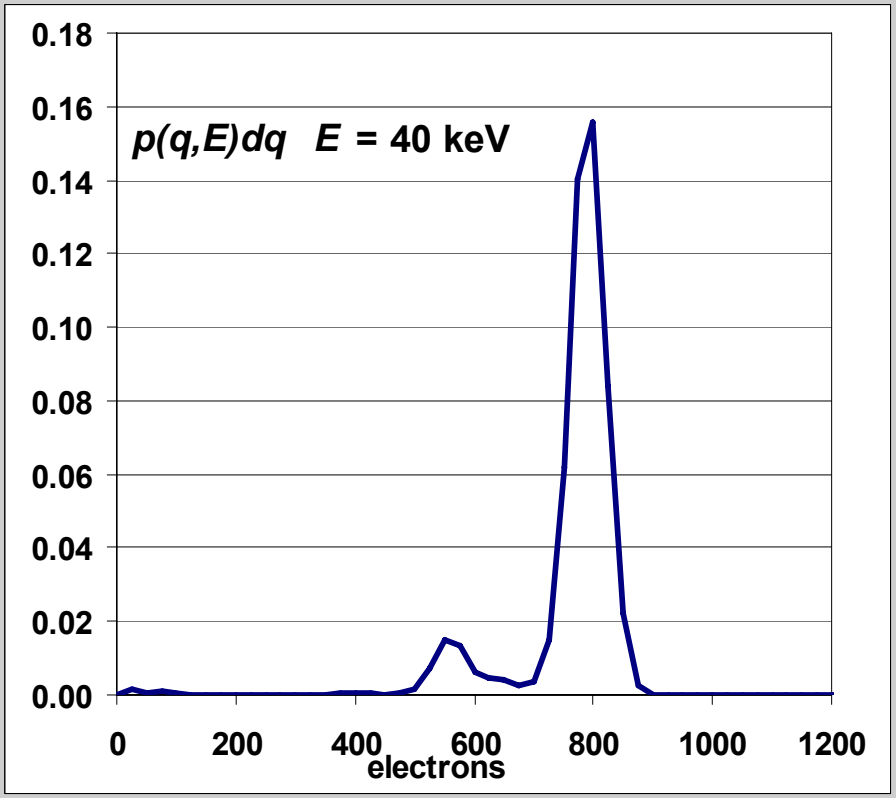

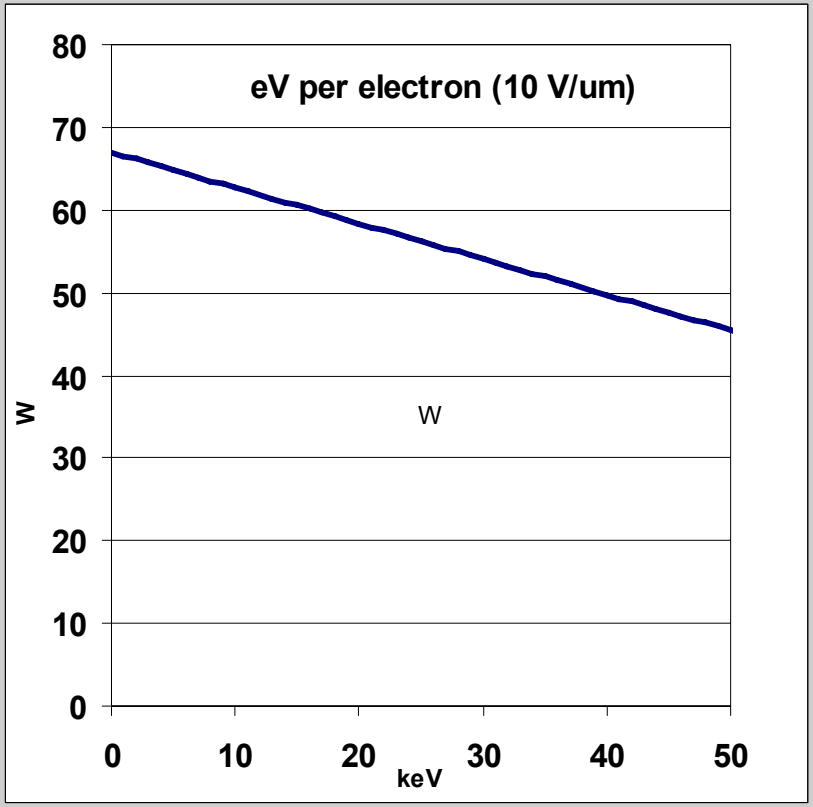

(see Blevis, Med.Phys.,1998)

Detector efficiency tables are computed from the first and second moments of the normalized electron deposition probability function

moments

$$M_0(E) = \int P(n,E)dn$$

$$M_1(E) = \int nP(n,E)dn$$

$$M_2(E) = \int n^2 P(n,E)dn$$

$$\varepsilon_S(E) = \frac{(M_1/M_0)}{E}$$

$$\varepsilon_\sigma^2(E) = \frac{(M_2/M_0)}{E^2}$$

$$DQE_E = \frac{(\varepsilon_n(E))^2}{\varepsilon_\sigma^2(E)} = \frac{(M_1)^2}{M_2 M_0}$$

Determining signal and noise using these transfer efficiencies provides a consistent solution to a Monte Carlo simulation that directly determines signal and noise from the charge deposited by H x-rays:

$$S = \sum n_i \Big/ H$$

$$\sigma^2 = \sum n_i^2 \Big/ H$$

Precomputing the efficiencies as tables avoids the need for repeating Monte Carlo calculations as the geometry or spectrum is changes.

4.C.iv - Detector DQE(E)

The computed DQE(E) for monoenergetic x-rays is a useful description of detector performance but can not be used for broad spectrum simulations.

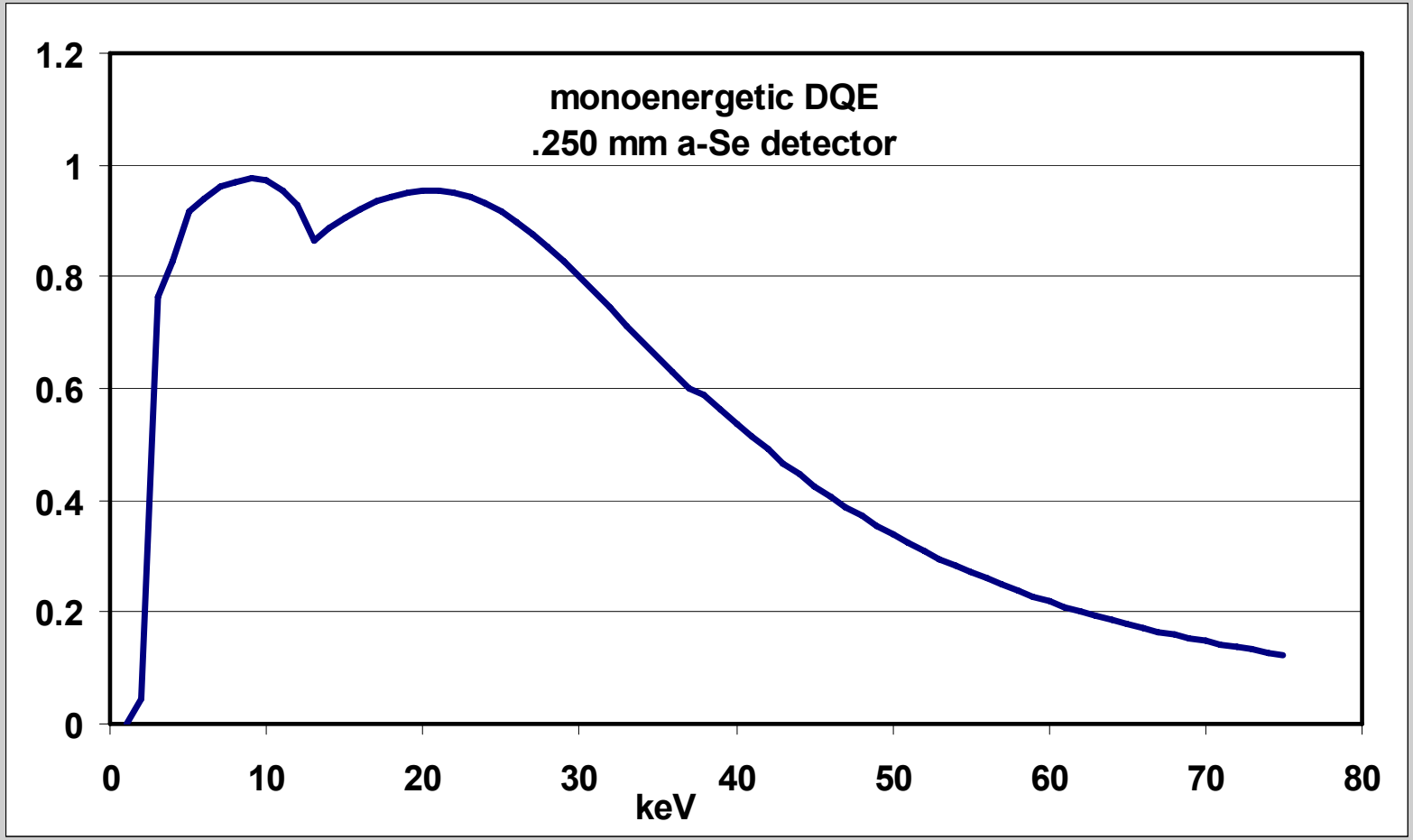

Lab07 – NEQ per mR, tungsten target, 1 inch Al-1100

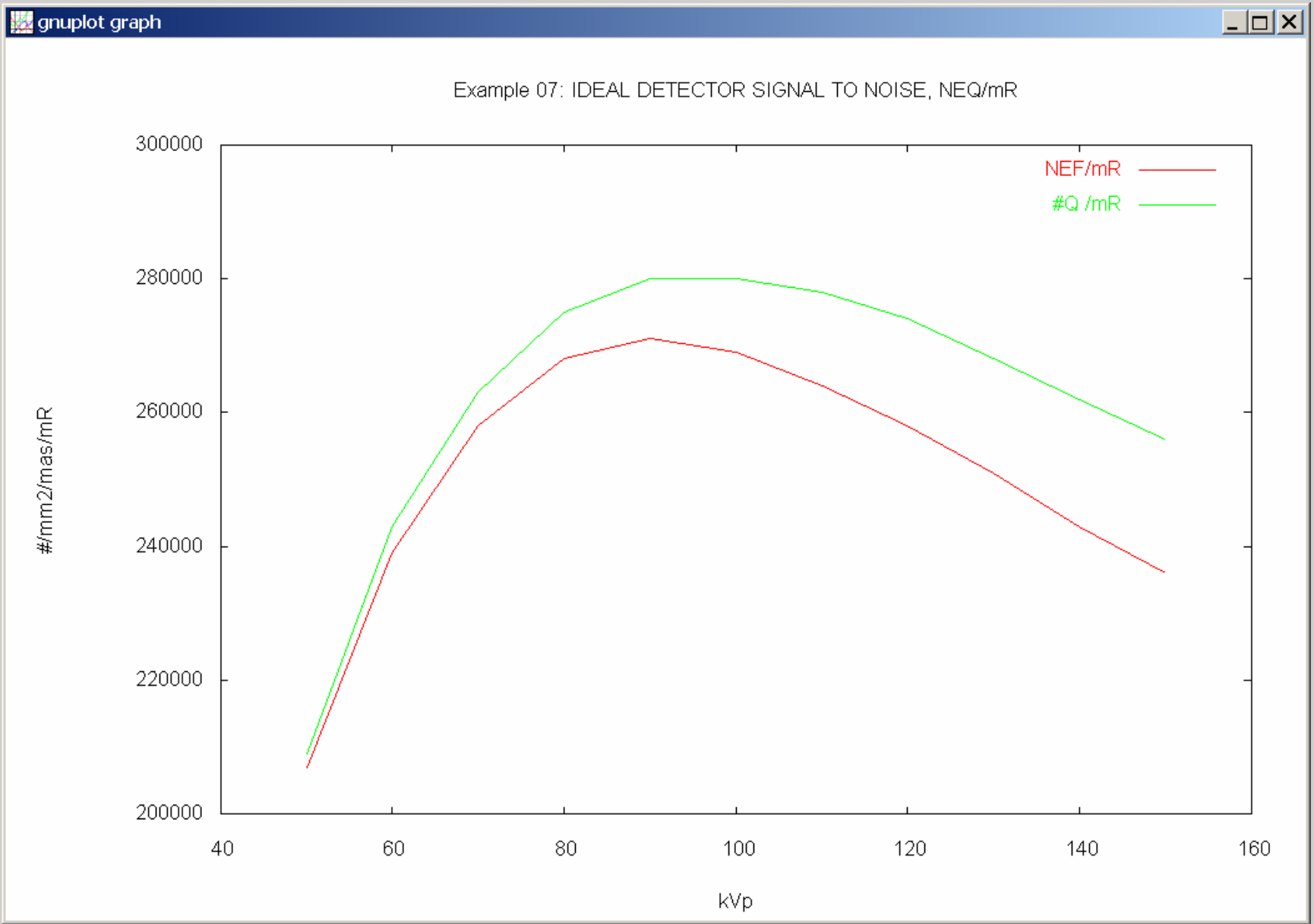

Lab08 – broad spectrum DQE vs kVp (Mo/.06mm Mo)

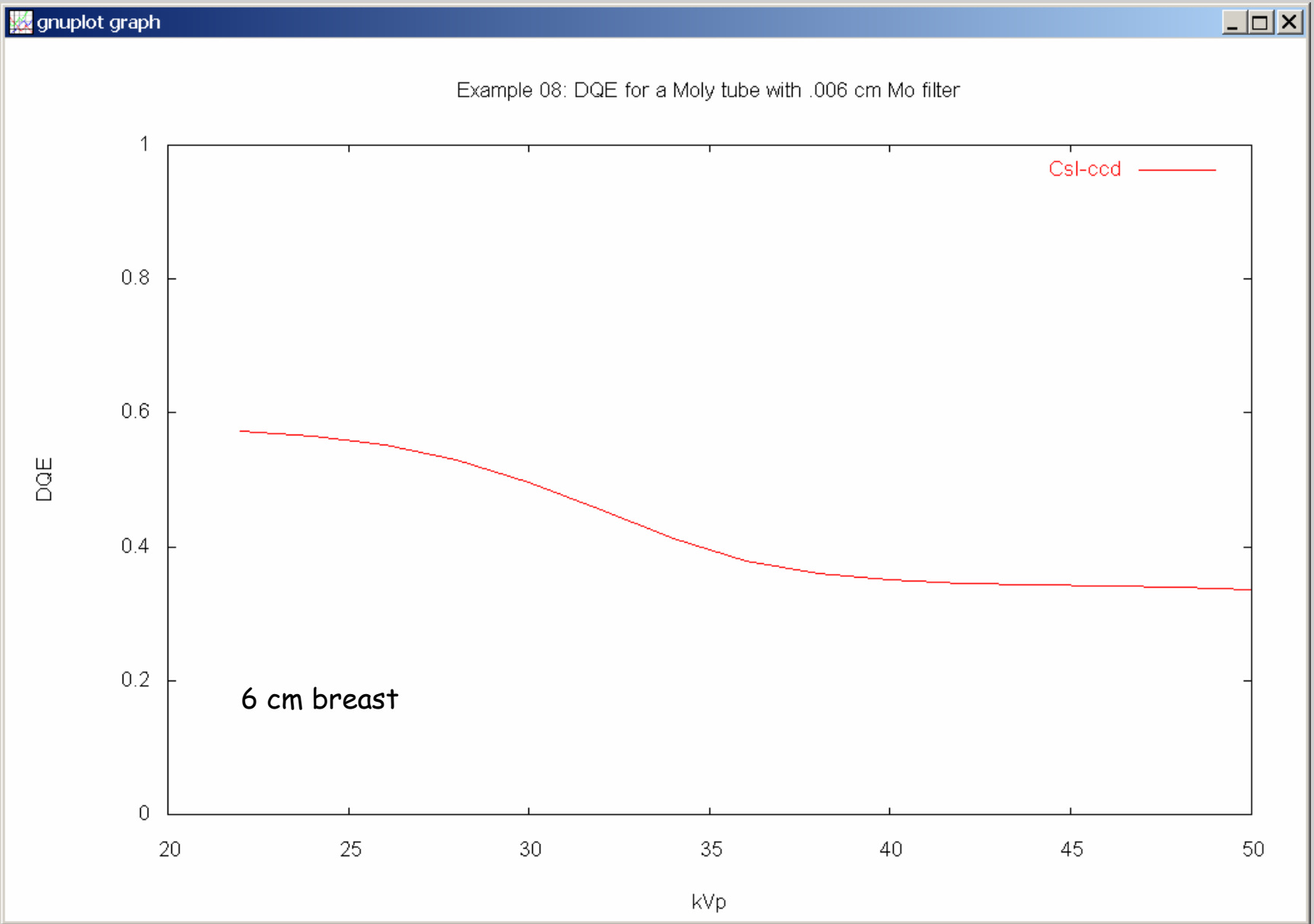

4.C.v - Relative Contrast

The relative contrast of a target structure is defined as the absolute signal difference between the target and the background divided by the background signal.

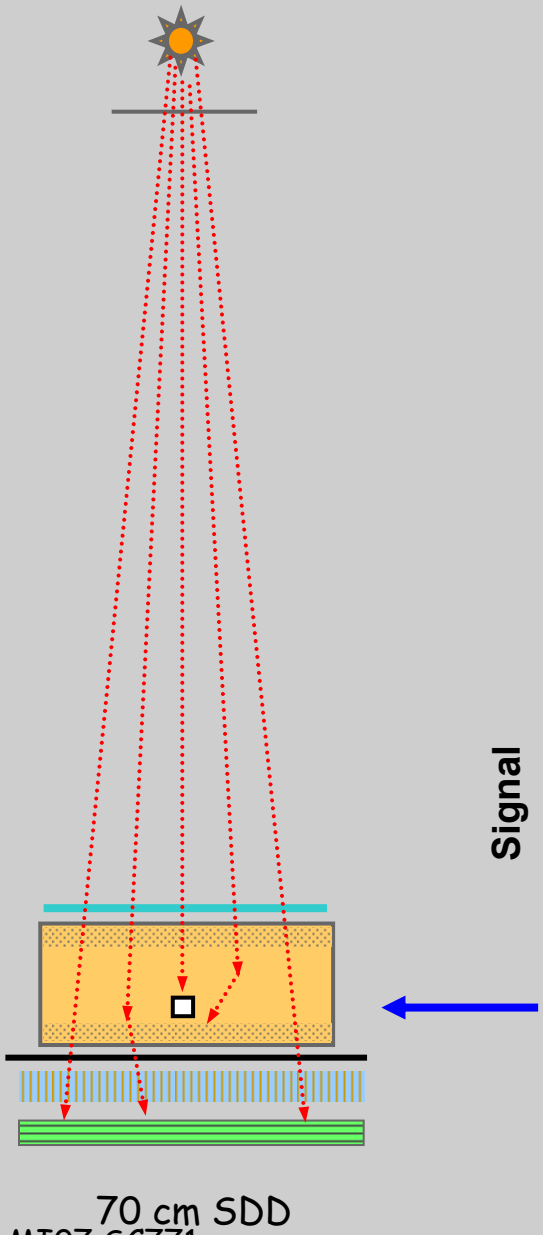

Relative Contrast

$$C_r = (St-Sb)/Sb$$

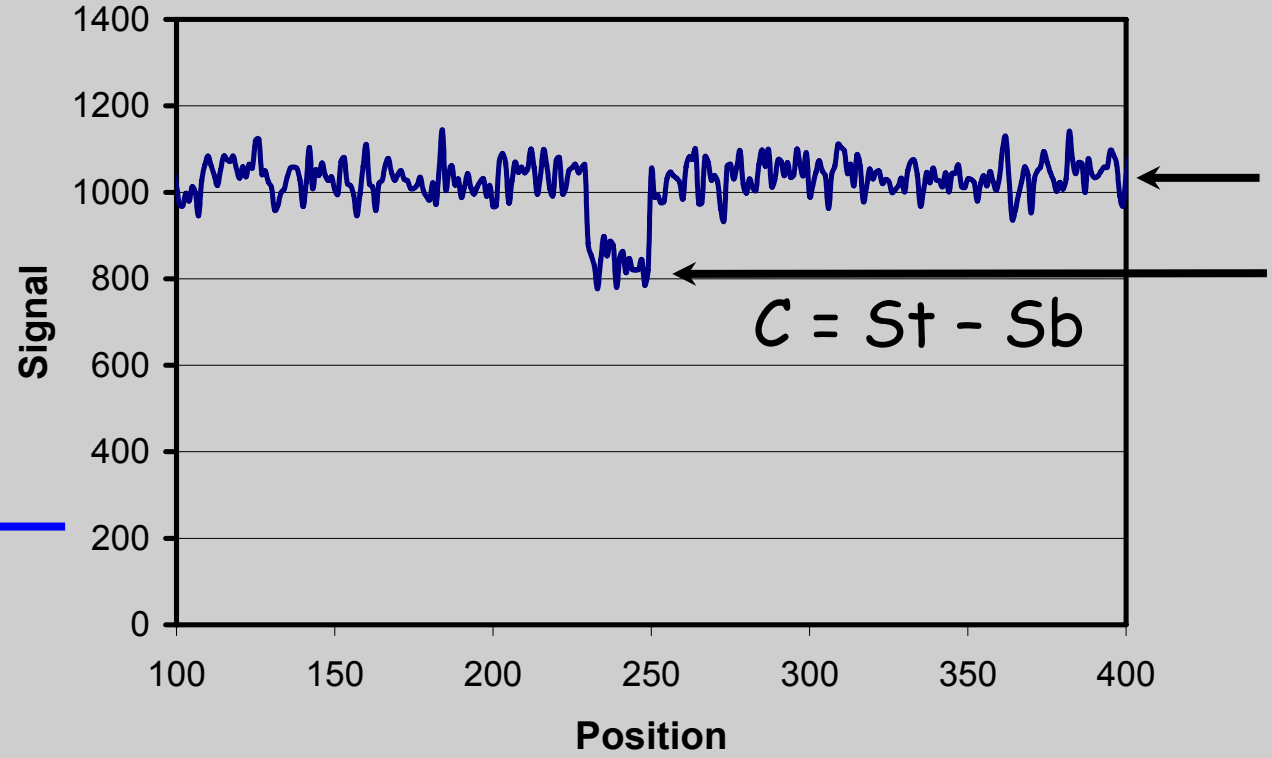

Signal difference to noise ratio

CNR

The ratio of the signal difference to the detectors background noise is the product of the relative contrast and the detector signal to noise ratio.

$$CNR = C_r \times SNR$$

CNR_t

The target contrast to noise ratio is estimated from the CNR by adjusting for the area of the target relative to the area of a detector pixel.

$$CNR_t = CNR(A_t/Ap)^{1/2}$$

FOM - Dose Normalized Contrast to Noise Ratio

$(CNR)^2$

The square of the contrast to noise ratio can be shown to be proportional to the equivalent number of detected x-ray quanta and thus is proportional to mA-s

$(CNR)^2$ / Dose

Since the absorbed dose in the subject is also proportional to mA-s, the ratio of contrast to noise squared to absorbed dose is a logical figure of merit for optimization.

$CNR/(mGy)^{1/2}$ mA-s/mGy

Flynn,Dodge, Peck.., SPIE 2003

Optimization of radiographic techniques for a .25 mm Se TFT detector (Lorad/Hologic).

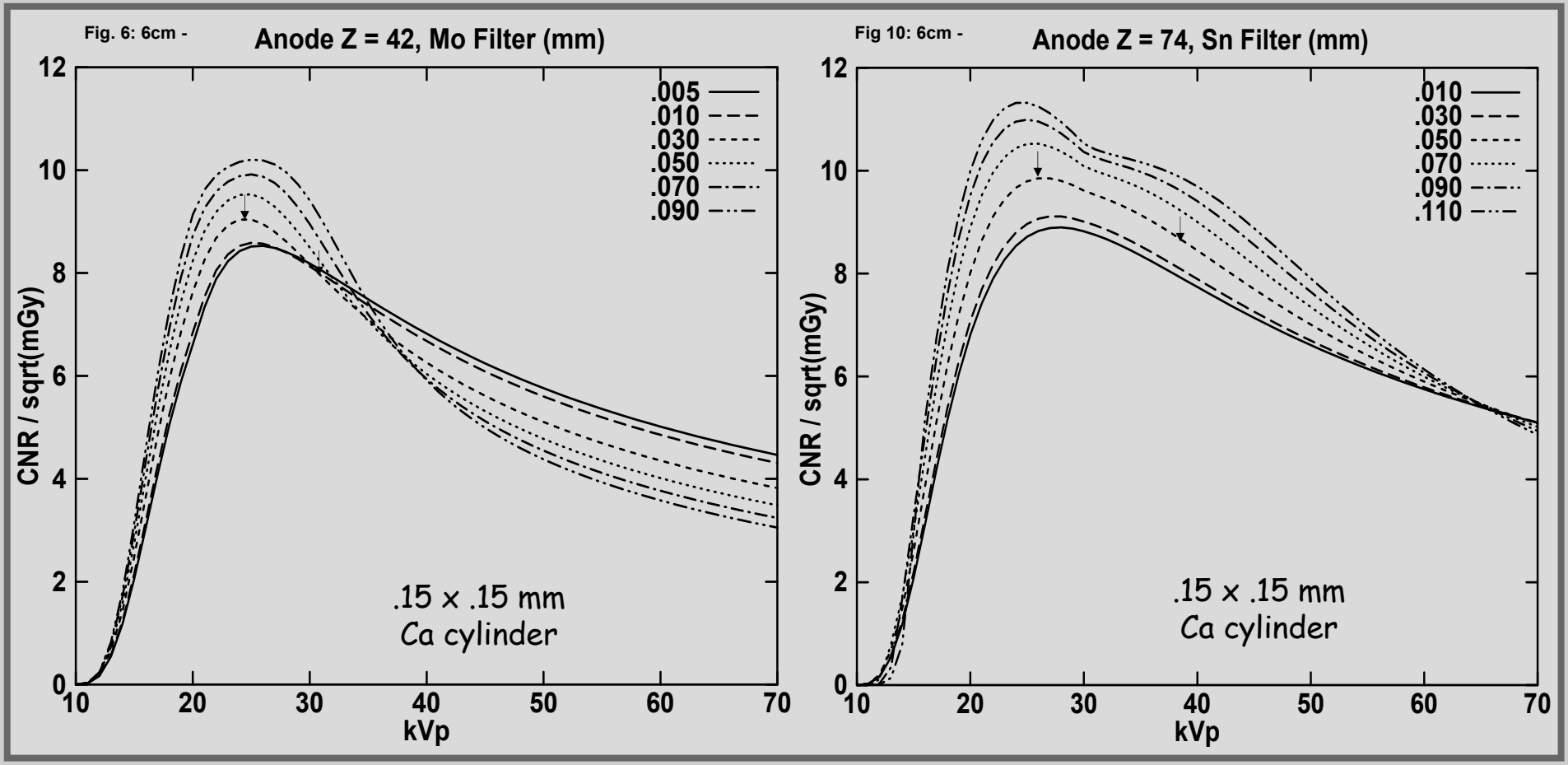

Dose and mA-s for a constant CNR = 10

Maximum CNR

	mGy		mA-s		kVp	
Thickness	Mo/Mo	W/Sn	Mo/Mo	W/Sn	Mo/Mo	W/Sn
4 cm	0.33	0.35	53	34	24.0	22
6 cm	1.2	1.0	215	77	24.5	26
8 cm	4.7	2.6	1086	120	25.0	31

High kVp at .9 times max CNR

	mGy		mA-s		$kVp_{90\%}$	
Thickness	Mo/Mo	W/Sn	Mo/Mo	W/Sn	Mo/Mo	W/Sn
4 cm	0.4	0.43	21	14	31	30
6 cm	1.52	1.3	114	27	31	38
8 cm	5.7	3.2	435	62	33	42

?

Supplemental material on the computation of XSPECT tables using Monte Carlo simulation

Diced slab geometry model

```
*******  Parameters for slab number 3 Carbon support:
3        <-  slab number, must be sequential
.150     <-  thickness, cm
1  1     <-  grid
F        <-  flag to repeat for next material
      10.084
12.604    2

*******  Parameters for slab number 4 lead grid:
4        <-  slab number, must be sequential
1.984    <-  thickness, cm
51 41    <-  grid
F        <-  flag to repeat for next material
      .004 .5 .004 .5 .004 .5 ....................... .004 .5 .004
.004    4   4   4   4   4   4  ....................... 4   4   4
.5      4   5   4   5   4   5  ....................... 4   5   4
.004    4   4   4   4   4   4  ....................... 4   4   4
.5      4   5   4   5   4   5  ....................... 4   5   4
.004    4   4   4   4   4   4  ....................... 4   4   4
.....................................................................
.....................................................................
.....................................................................
.....................................................................
.....................................................................
.5      4   5   4   5   4   5  ....................... 4   5   4
.004    4   4   4   4   4   4  ....................... 4   4   4
.5      4   5   4   5   4   5  ....................... 4   5   4
```

SKEPTIC Output – angular bins

P(e,E) for an angle bin

Angle Range from 20.000 to 30.000 degrees

Energy Range	Raw Number	Weighted Number (# / keV sr mAs)	Weighted Fraction
P(a,e) 1.00 - 2.00	0	0.0000E+00	0.0000E+00
P(a,e) 2.00 - 3.00	0	0.0000E+00	0.0000E+00
.			
.			
.			
P(a,e) 45.00-46.00	85	1.2606E+12	1.0865E-02
P(a,e) 46.00-47.00	81	1.2013E+12	1.0354E-02
P(a,e) 47.00-48.00	78	1.1568E+12	9.9706E-03
P(a,e) 48.00-49.00	93	1.3792E+12	1.1888E-02
P(a,e) 49.00-50.00	100	1.4830E+12	1.2783E-02
P(a,e) 50.00-51.00	90	1.3347E+12	1.1505E-02
P(a,e) 51.00-52.00	102	1.5127E+12	1.3038E-02
P(a,e) 52.00-53.00	125	1.8538E+12	1.5979E-02
P(a,e) 53.00-54.00	135	2.0021E+12	1.7257E-02
P(a,e) 54.00-55.00	167	2.4767E+12	2.1347E-02
P(a,e) 55.00-56.00	195	2.8919E+12	2.4926E-02
P(a,e) 56.00-57.00	196	2.9067E+12	2.5054E-02
P(a,e) 57.00-58.00	241	3.5741E+12	3.0807E-02
P(a,e) 58.00-59.00	329	4.8792E+12	4.2055E-02
P(a,e) 59.00-60.00	3862	5.7275E+13	4.9367E-01
P(a,e) 60.00-61.00	1343	1.9917E+13	1.7167E-01

SKEPTIC Output - energy bins

P(e,E) for active detector

```
 Material ==> a-Se
 Input Energy =   40.00 keV

Energy Bin        Raw Number     Prob/Inc Photon
     0.00 -    1.00            0        P(e,E, 1):    0.0000E+00
     1.00 -    2.00         1479        P(e,E, 1):    1.4790E-03
     2.00 -    3.00          214        P(e,E, 1):    2.1400E-04
     3.00 -    4.00          402        P(e,E, 1):    4.0200E-04
     4.00 -    5.00         1007        P(e,E, 1):    1.0070E-03
     5.00 -    6.00          662        P(e,E, 1):    6.6200E-04
     6.00 -    7.00            4        P(e,E, 1):    4.0000E-06
        .
    26.00 -   27.00           43        P(e,E, 1):    4.3000E-05
    27.00 -   28.00         6206        P(e,E, 1):    6.2060E-03
    28.00 -   29.00        34627        P(e,E, 1):    3.4627E-02
    29.00 -   30.00          133        P(e,E, 1):    1.3300E-04
    30.00 -   31.00          133        P(e,E, 1):    1.3300E-04
    31.00 -   32.00         4070        P(e,E, 1):    4.0700E-03
    32.00 -   33.00         8014        P(e,E, 1):    8.0140E-03
    33.00 -   34.00          105        P(e,E, 1):    1.0500E-04
    34.00 -   35.00         1121        P(e,E, 1):    1.1210E-03
    35.00 -   36.00         2120        P(e,E, 1):    2.1200E-03
    36.00 -   37.00         3489        P(e,E, 1):    3.4890E-03
    37.00 -   38.00          412        P(e,E, 1):    4.1200E-04
    38.00 -   39.00          103        P(e,E, 1):    1.0300E-04
    39.00 -   40.00        28873        P(e,E, 1):    2.8873E-02
    40.00 -   41.00       450839        P(e,E, 1):    4.5084E-01
```

Material Collision Statistics

Raw Photon Collisions

X-Sect #	Material	X-Sect Name	No. Coll.
1	a-Se	Compton Scattering	9373
2	a-Se	Coherent Scattering	30787
3	a-Se	K Photo-E, Z=34	469221
4	a-Se	L1 Photo-E, Z=34	36088
5	a-Se	L2 Photo-E, Z=34	77229
6	a-Se	L3 Photo-E, Z=34	146407
7	a-Se	M1 Photo-E, Z=34	0
8	a-Se	M2 Photo-E, Z=34	0
9	a-Se	M3 Photo-E, Z=34	0
10	a-Se	M4 Photo-E, Z=34	44340
11	a-Se	M5 Photo-E, Z=34	1706
12	a-Se	N1 Photo-E, Z=34	78

Active Detector Material: 12 collision types
TFT Glass: 50 collision types

MC spatial binning – Resolution and Noise

X-ray input:

- Distributed
- Pixel Center
- Pixel Edge
- Pixel Corner

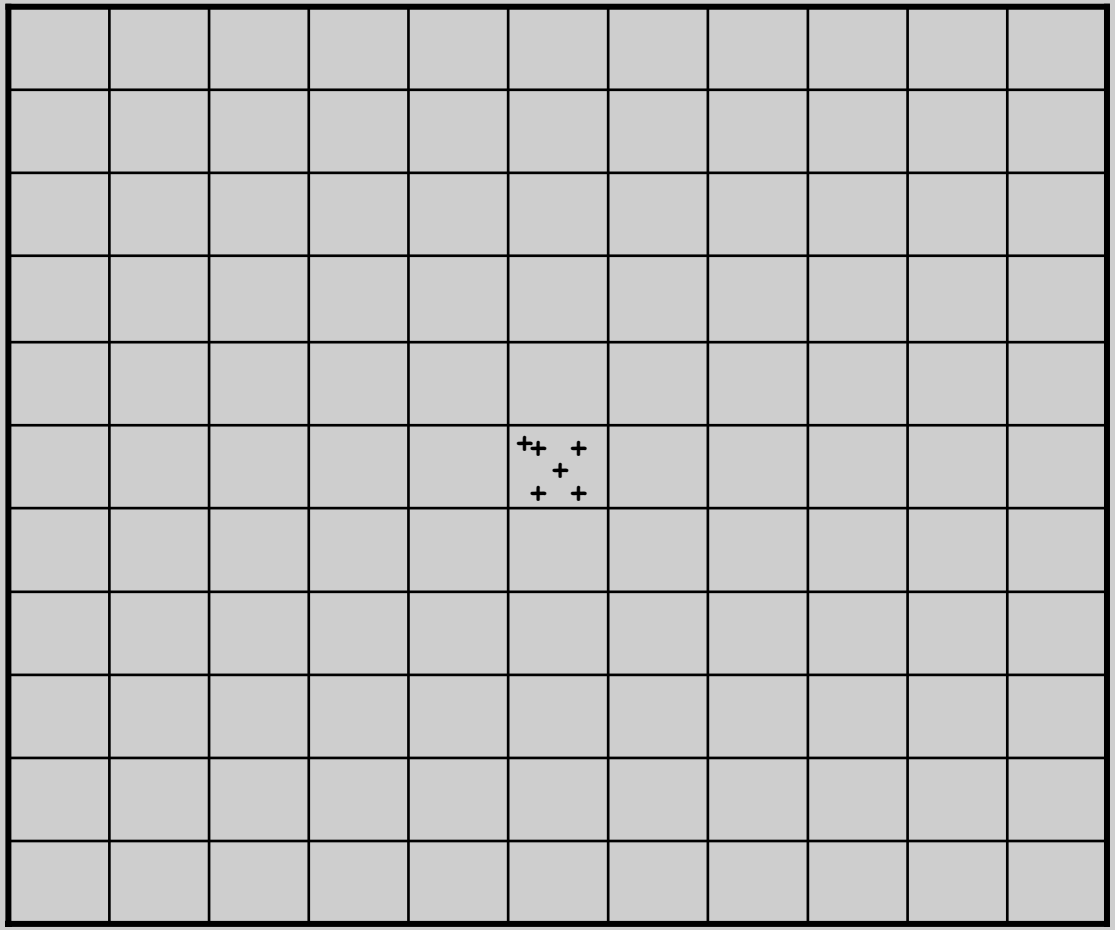

SKEPTIC output – spatial bins

Direct TFT detector

For each x-ray history, energy may be accumulated in one or more spatial bins

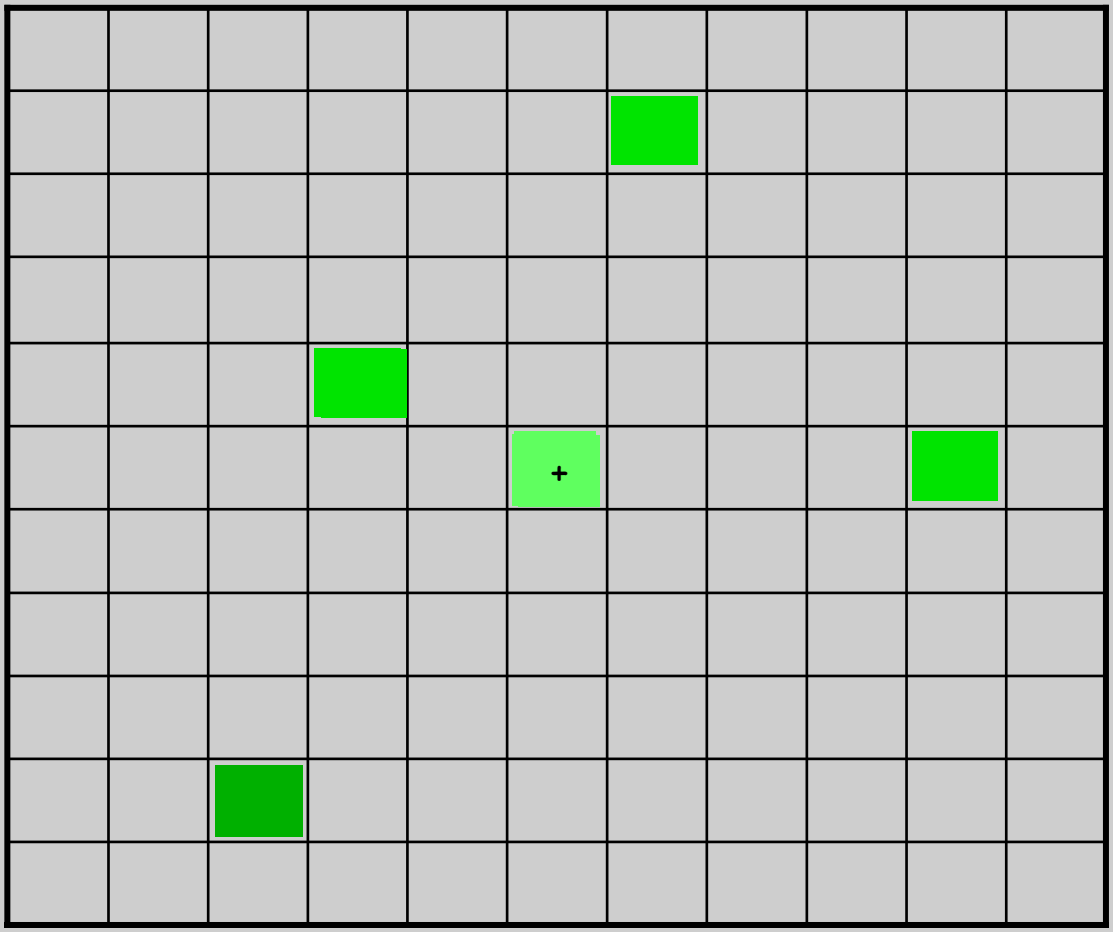

Energy deposition:

- cental
- Dual centered
- Triple off-center
- Single off-center
- Dual off-center

.

.

SKEPTIC output – spatial bins

Direct TFT detector

Average energy deposition distribution

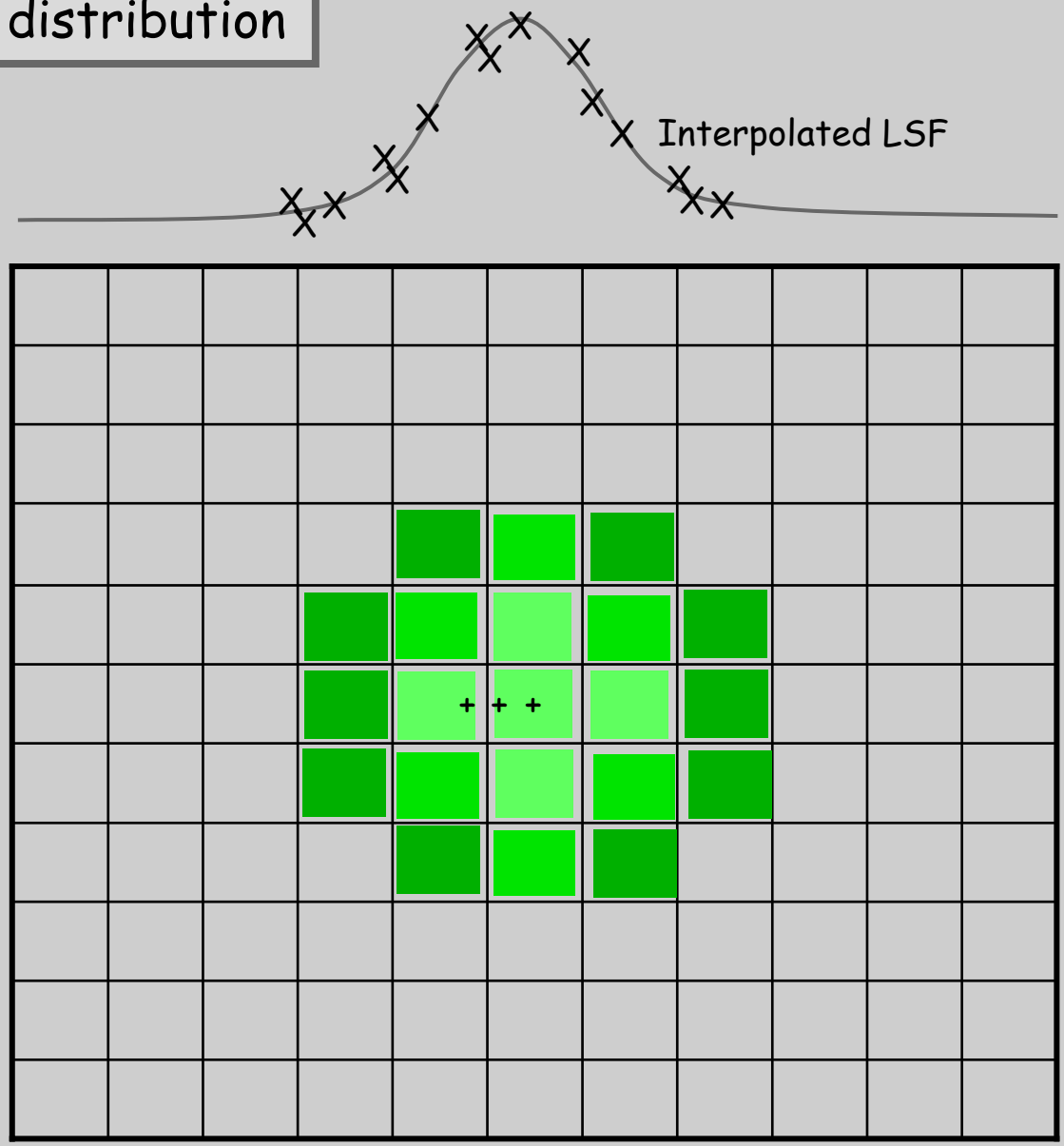

The detector point spread function is immediately obtained from the average of many x-ray histories

SKEPTIC output – spatial bins

Direct TFT detector

For each x-ray history, the energy deposited in multiple bins leads to noise correlation

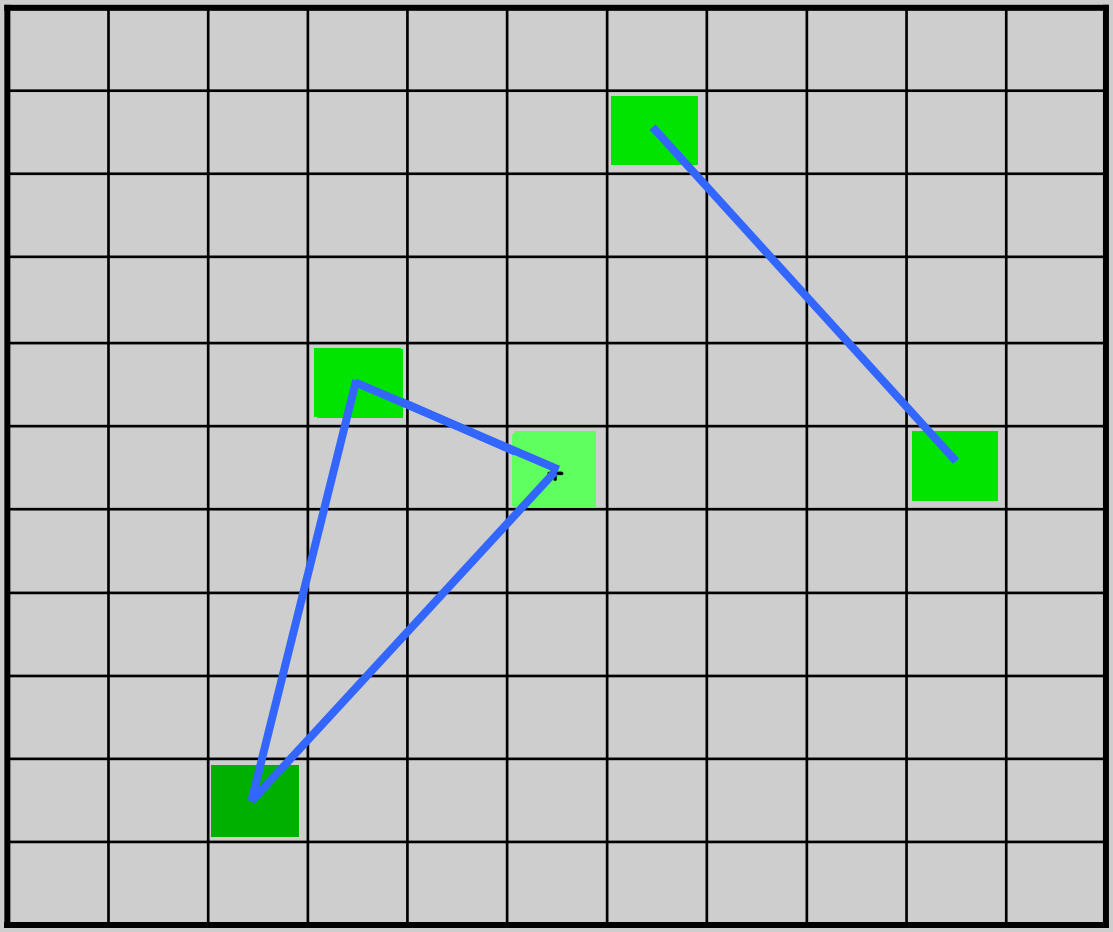

Energy deposition:

- cental
- Dual centered
- Triple off-center
- Single off-center
- Dual off-center

.

.

SKEPTIC output – spatial bins

Direct TFT detector

For each x-ray history, the cross products of the energy deposition components are accumulated at their correlation distance

Accumulation of the auto correlation matrix:

- Dual deposition
  - $2*E_1*E_2$ at R
  - $E_1^2 + E_2^2$ at 0,0
- Triple deposition
  - $2*E_1*E_2$ at R_1
  - $2*E_1*E_2$ at R_1
  - $2*E_1*E_2$ at R_1
  - $E_1^2 + E_2^2 + E_3^2$ at 0,0

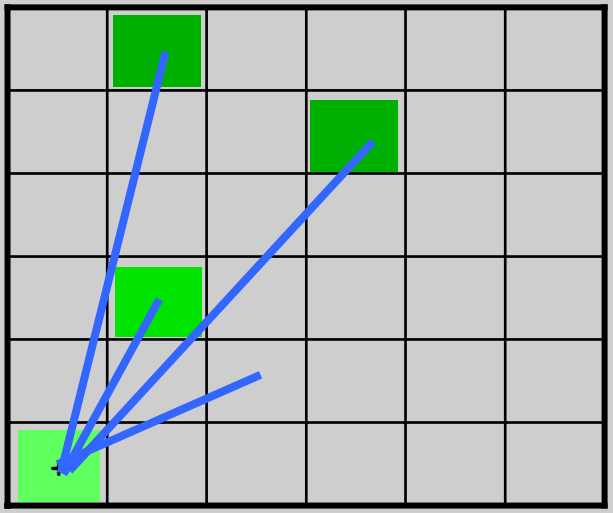

The sum of all elements in the auto-correlation matrix is equal to the sum of the square of the total energy deposition for all x-rays.

$$(E_1 + E_2)^2 + (E_1 + E_2 + E_3^2)^2 \; . \; . \; . \; . \; .$$

Direct Se MTF – deviation from sinc

Flynn, SPIE 1999 – Monte Carlo analysis indicates a ~10% reduction in MTF above 1 cycles/mm from x-ray fluorescence in the glass substrate.

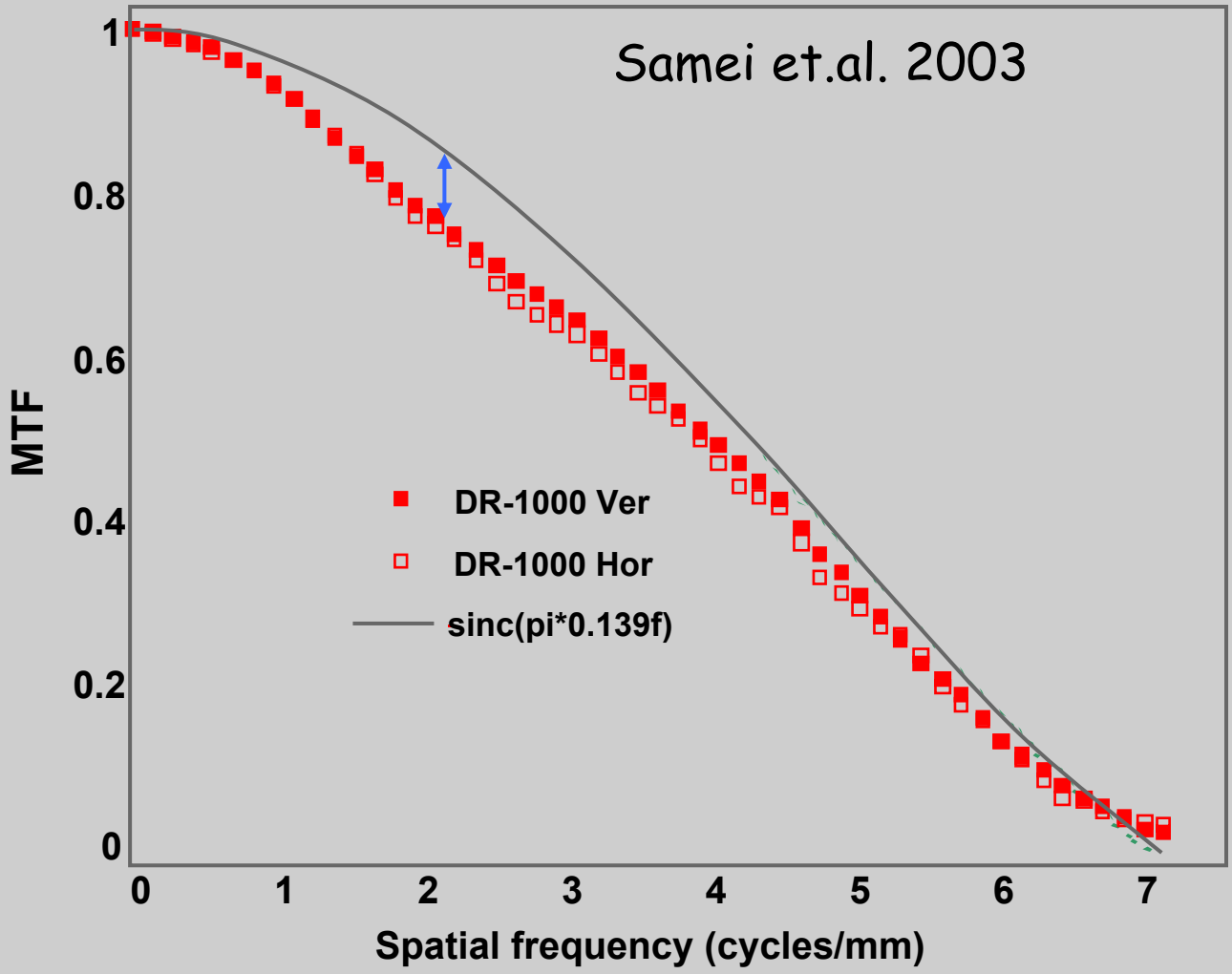

SKEPTIC output – spatial bins

inDirect TFT detector

Average energy deposition distribution

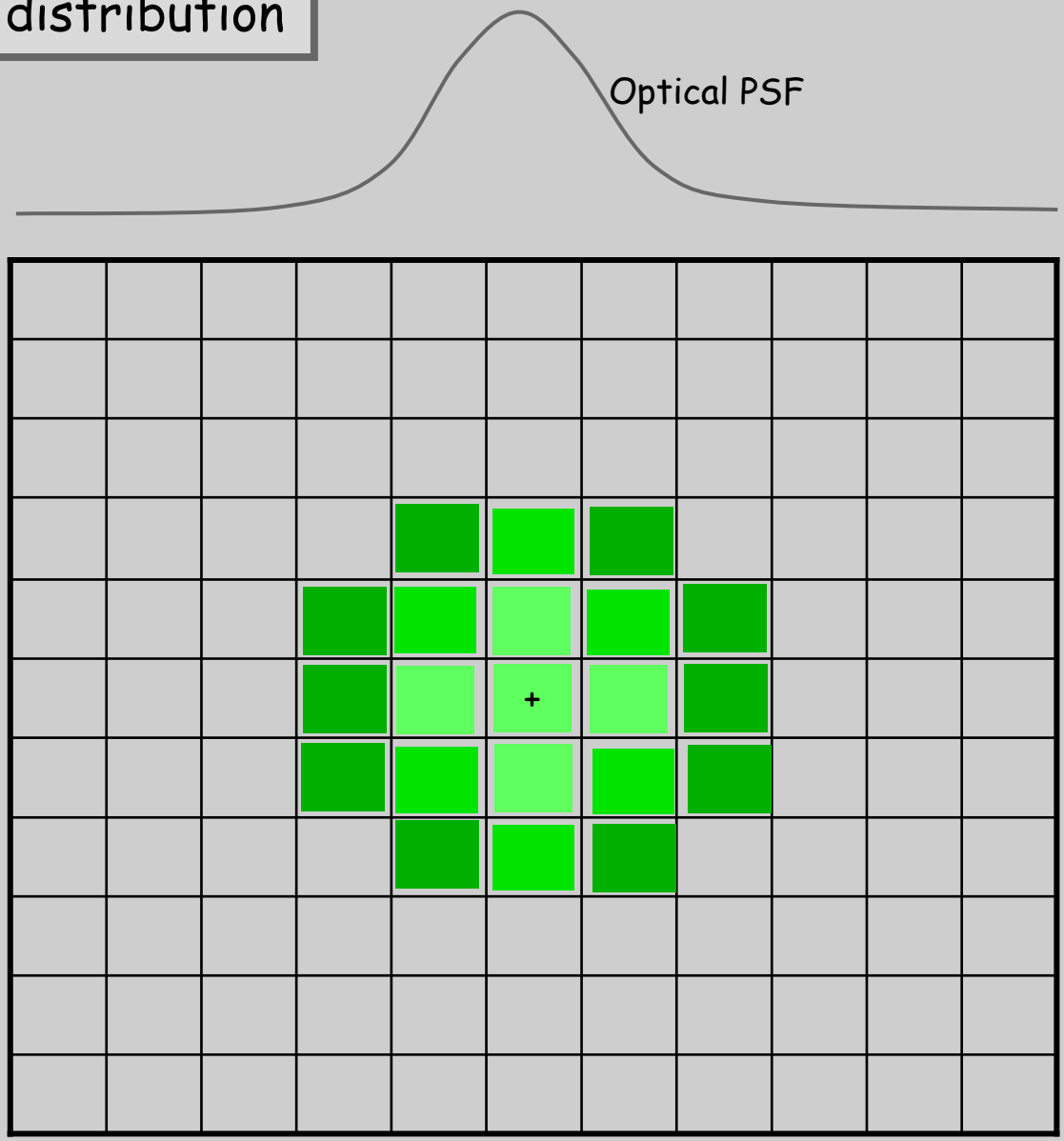

For detectors with optical scintillators, light spread occurs before sampling by the TFT detector.

For high light output per x-ray, this distribution is well shaped with low noise.

SKEPTIC output – spatial bins

inDirect TFT detector

Average energy deposition distribution

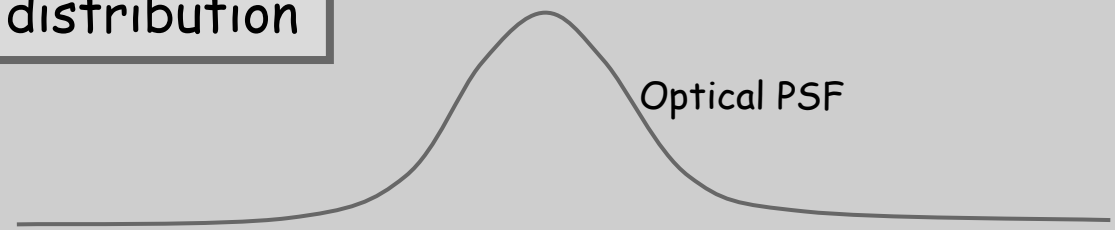

For low light output per x-ray, the number of electron created in each TFT photodiode can be small and significant noise is present.

This produces equivalent blur (on the average) but can contributes to noise correlation.

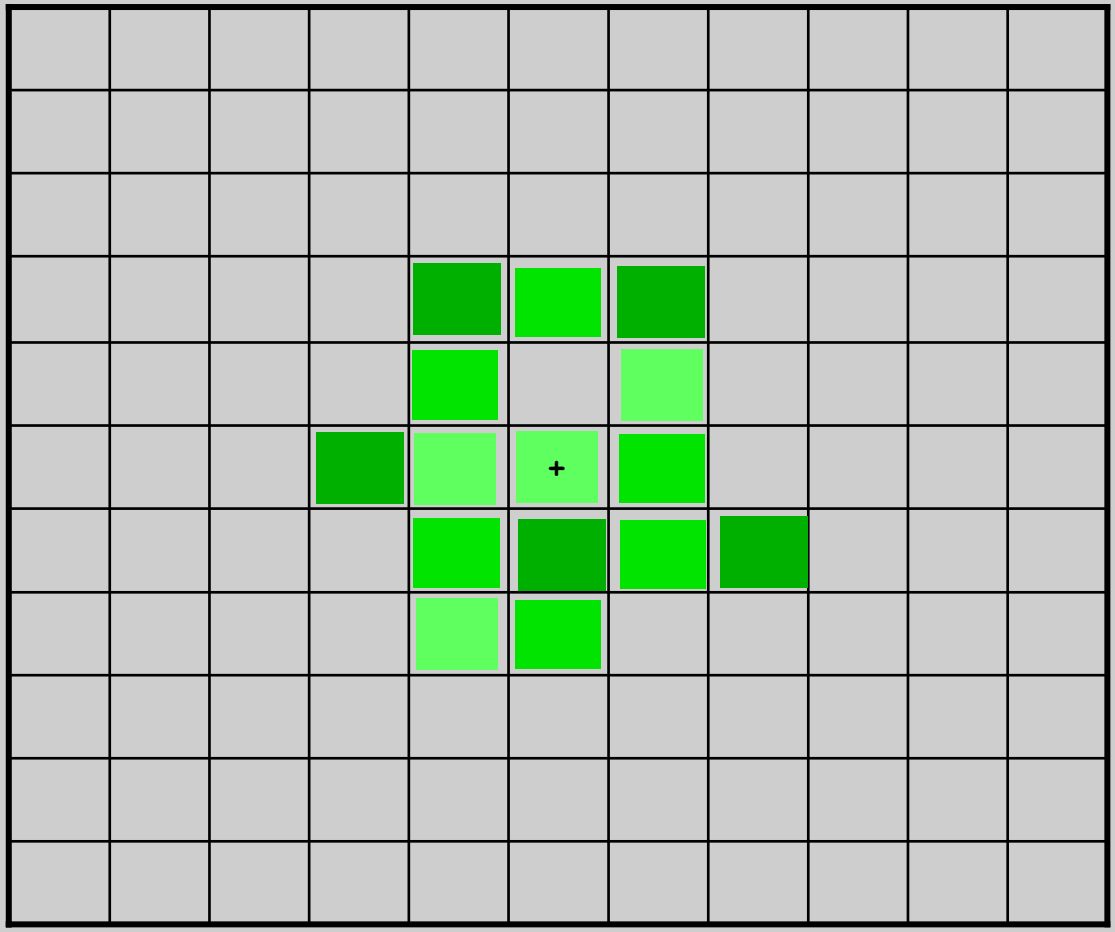

Outline

1. Fundamentals of Monte Carlo (40 min, AB)
   - Experiments, theory and numerical modeling
   - Components of the Monte Carlo method
   - The Monte Carlo method
   - Transport coefficients and cross sections
   - Random number generators
   - Variance reduction
2. PENELOPE (70 min, JS), *10-min break*
3. MANTIS (70 min, AB)
   - Introduction to MANTIS
   - Optical transport methods
   - Validation and examples
   - Applications in indirect x-ray imaging
   - Applications in display devices
   - Other applications
4. Imaging simulation using XSPECT (45, MJF)
5. **File list and description for the companion CD**
6. Hands-on demonstrations (afternoon session, AB/JS/MJF)

Description of the contents of the companion CD

PENELOPE directory

`penelope2006.zip` plus extras

MANTIS directory

MANTIS v2.0 distribution

- . FORTRAN source
- . \doc
- . \demo
- . \exercise1
- . \exercise2
- . \gnuplot_scripts

XSPECT directory

XSPECT package plus extras

Outline

1. Fundamentals of Monte Carlo (40 min, AB)
   - Experiments, theory and numerical modeling
   - Components of the Monte Carlo method
   - The Monte Carlo method
   - Transport coefficients and cross sections
   - Random number generators
   - Variance reduction
2. PENELOPE (70 min, JS), *10-min break*
3. MANTIS (70 min, AB)
   - Introduction to MANTIS
   - Optical transport methods
   - Validation and examples
   - Applications in indirect x-ray imaging
   - Applications in display devices
   - Other applications
4. Imaging simulation using XSPECT (45, MJF)
5. File list and description for the companion CD
6. **Hands-on demonstrations (afternoon session, AB/JS/MJF)**

Course syllabus

1. PENELOPE
2. MANTIS
   - Review of MANTIS
   - What's new in version 2?
   - Exercise 1: effect of x-ray energy on blur
   - Exercise 2: x-rays at an angle
3. XSPECT

Outline

1 PENELOPE

2 MANTIS
- Review of MANTIS
- What's new in version 2?
- Exercise 1: effect of x-ray energy on blur
- Exercise 2: x-rays at an angle

3 XSPECT

PENGEOM

Surfaces: basic concepts

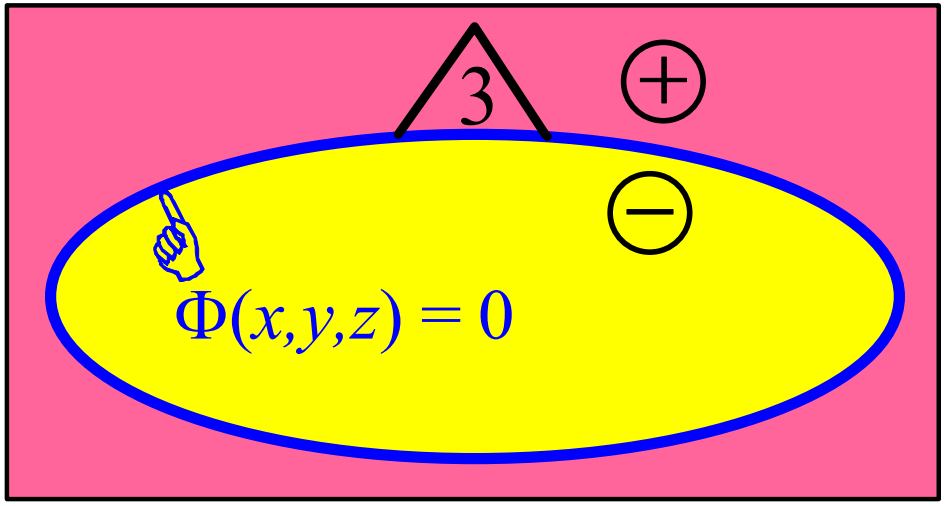

- The surface divides the space in three mutually exclusive regions;
  1) $\Phi(\mathbf{r}) = 0 \rightarrow$ the surface itself
  2) $\Phi(\mathbf{r}) > 0 \rightarrow$ "outside"
  3) $\Phi(\mathbf{r}) < 0 \rightarrow$ "inside"

- The "sign" of a region is not an absolute property.
  The eq. $-\Phi(\mathbf{r}) = 0$ defines the same surface but reverses the signs of the regions + and –

Quadrics

Any quadric can be generated from its reduced form:

$$\Phi(\mathbf{r}) = I_1 x^2 + I_2 y^2 + I_3 z^2 + I_4 z + I_5 = 0$$

Reduced form	Indices					Quadric
$z - 1 = 0$	0	0	0	1	-1	plane
$z^2 - 1 = 0$	0	0	1	0	-1	pair of parallel planes
$x^2 + y^2 + z^2 - 1 = 0$	1	1	1	0	-1	sphere
$x^2 + y^2 - 1 = 0$	1	1	0	0	-1	cylinder
$x^2 - y^2 - 1 = 0$	1	-1	0	0	-1	hyperbolic cylinder
$x^2 + y^2 - z^2 = 0$	1	1	-1	0	0	cone
$x^2 + y^2 - z^2 - 1 = 0$	1	1	-1	0	-1	one sheet hyperboloid
$x^2 + y^2 - z^2 + 1 = 0$	1	1	-1	0	1	two sheet hyperboloid
$x^2 + y^2 - z = 0$	1	1	0	-1	0	paraboloid
$x^2 - z = 0$	1	0	0	-1	0	parabolic cylinder
$x^2 - y^2 - z = 0$	1	-1	0	-1	0	hyperbolic paraboloid

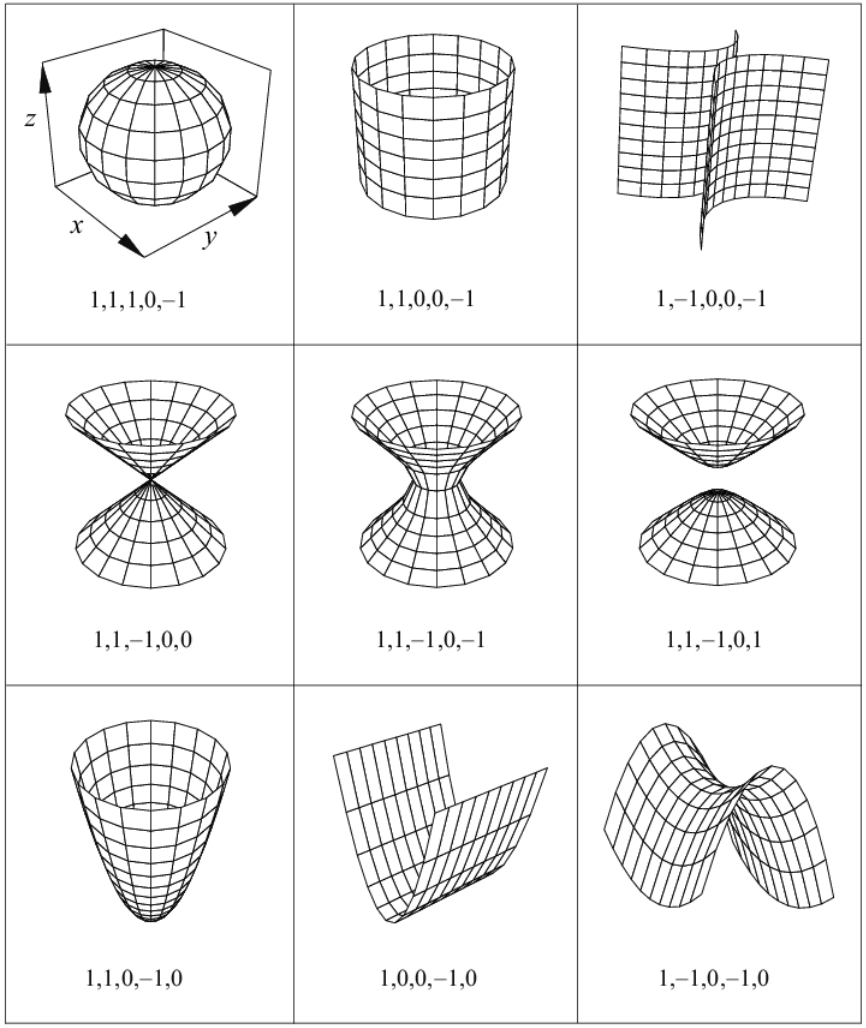

Non-planar reduced quadrics

Transformations

Any quadric can be generated by starting from its reduced form and applying a combination (in the quoted order) of the following transformations:

- Scaling of the coordinates axis

$$x \to ax \qquad y \to by \qquad z \to cz$$

- Rotation

$$\mathbf{r} \to R(\omega,\theta,\phi)\,\mathbf{r} = R_z(\phi)\,R_y(\theta)\,R_z(\omega)\,\mathbf{r}$$

- Translation

$$\mathbf{r} \to \mathbf{r} + \mathbf{a}$$

Syntax

```
0000000000000000000000000000000000000000000000000000000000000000
SURFACE (    )   reduced form
INDICES=( 1, 1, 1, 1, 1)
X-SCALE=(+1.000000000000000E+00,  0)                (DEFAULT=1.0)
Y-SCALE=(+1.000000000000000E+00,  0)                (DEFAULT=1.0)
Z-SCALE=(+1.000000000000000E+00,  0)                (DEFAULT=1.0)
  OMEGA=(+0.000000000000000E+00,  0) DEG            (DEFAULT=0.0)
  THETA=(+0.000000000000000E+00,  0) DEG            (DEFAULT=0.0)
    PHI=(+0.000000000000000E+00,  0) RAD            (DEFAULT=0.0)
X-SHIFT=(+0.000000000000000E+00,  0)                (DEFAULT=0.0)
Y-SHIFT=(+0.000000000000000E+00,  0)                (DEFAULT=0.0)
Z-SHIFT=(+0.000000000000000E+00,  0)                (DEFAULT=0.0)
0000000000000000000000000000000000000000000000000000000000000000
SURFACE (    )   implicit form
INDICES=( 0, 0, 0, 0, 0)
    AXX=(+0.000000000000000E+00,  0)                (DEFAULT=0.0)
    AXY=(+0.000000000000000E+00,  0)                (DEFAULT=0.0)
    AXZ=(+0.000000000000000E+00,  0)                (DEFAULT=0.0)
    AYY=(+0.000000000000000E+00,  0)                (DEFAULT=0.0)
    AYZ=(+0.000000000000000E+00,  0)                (DEFAULT=0.0)
    AZZ=(+0.000000000000000E+00,  0)                (DEFAULT=0.0)
     AX=(+0.000000000000000E+00,  0)                (DEFAULT=0.0)
     AY=(+0.000000000000000E+00,  0)                (DEFAULT=0.0)
     AZ=(+0.000000000000000E+00,  0)                (DEFAULT=0.0)
     A0=(+0.000000000000000E+00,  0)                (DEFAULT=0.0)
```

Definition of bodies

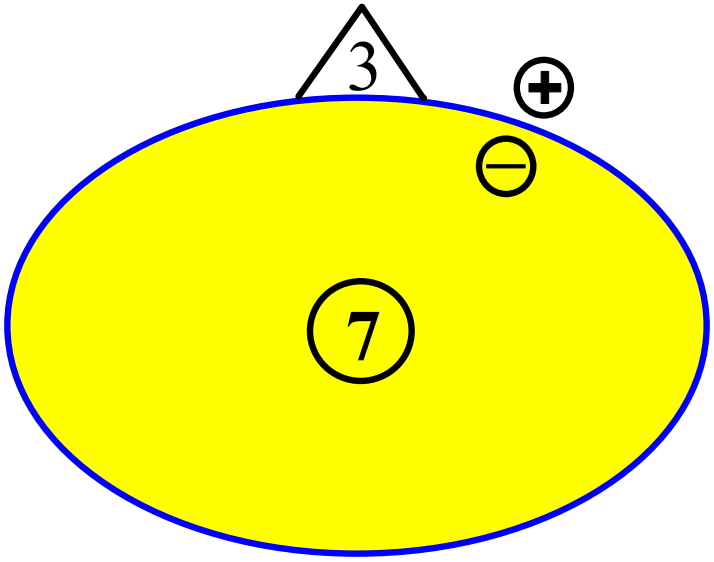

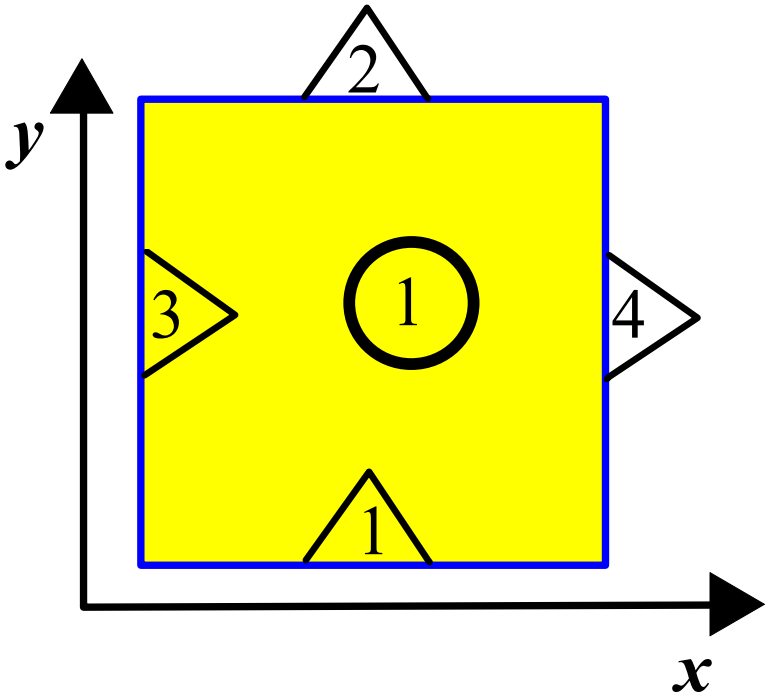

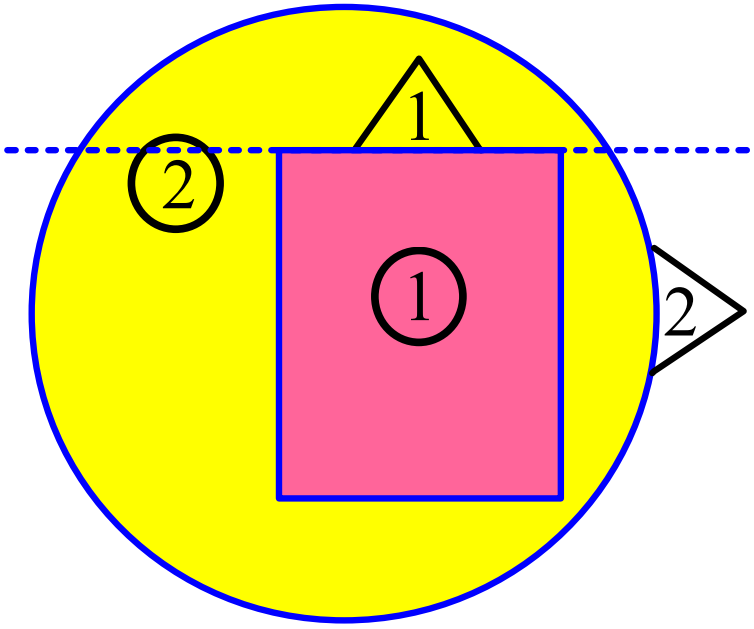

Some bodies require more than surfaces

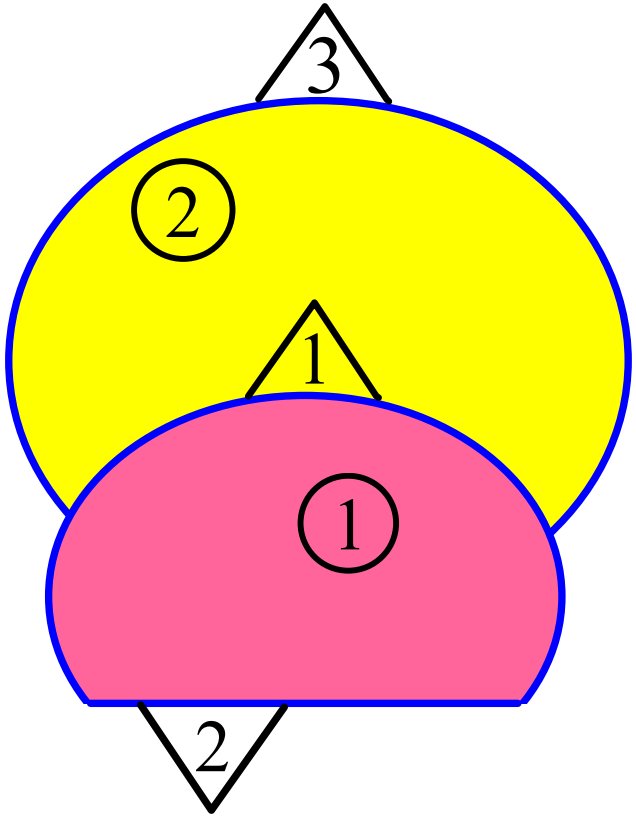

Avoid substractions if there are simpler definitions

Syntax

```
0000000000000000000000000000000000000000000000000000000000000000000000
BODY     (     )   text
MATERIAL(     )
SURFACE (     ), SIDE POINTER=( 1)
BODY     (     )
MODULE   (     )
```

etc...

Lines defining default values can be removed from the definition file

Other options

```
0000000000000000000000000000000000000000000000000000000000000000000000
CLONE    (     )   copies one module and moves it
MODULE   (     )   original module
1111111111111111111111111111111111111111111111111111111111111111111111
  OMEGA=(+0.000000000000000E+00,  0) DEG          (DEFAULT=0.0)
  THETA=(+0.000000000000000E+00,  0) DEG          (DEFAULT=0.0)
    PHI=(+0.000000000000000E+00,  0) RAD          (DEFAULT=0.0)
X-SHIFT=(+0.000000000000000E+00,  0)              (DEFAULT=0.0)
Y-SHIFT=(+0.000000000000000E+00,  0)              (DEFAULT=0.0)
Z-SHIFT=(+0.000000000000000E+00,  0)              (DEFAULT=0.0)
```

```
0000000000000000000000000000000000000000000000000000000000000000000000
INCLUDE
FILE=   (filename.ext)
```

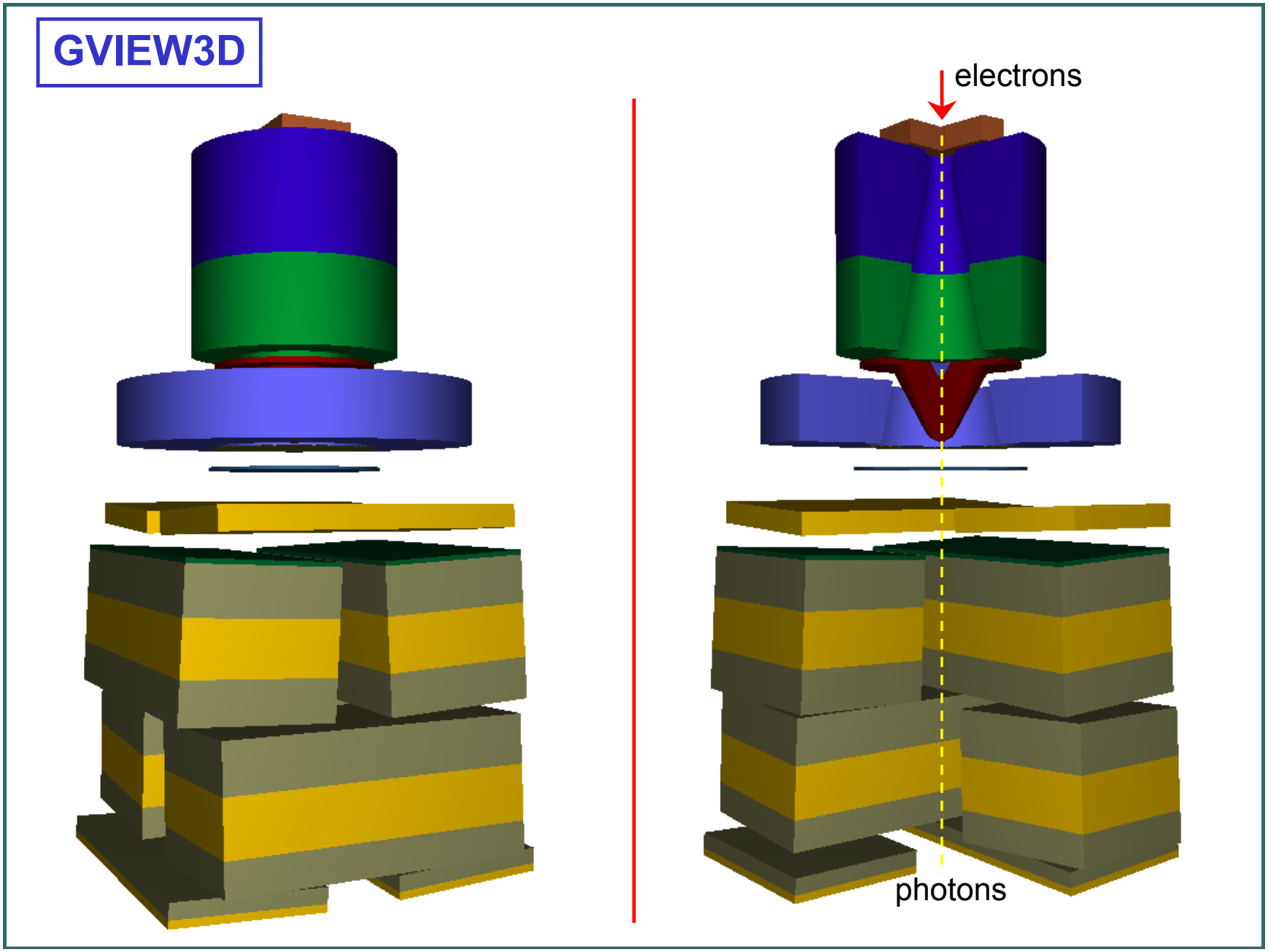
GVIEW3D
electrons
photons

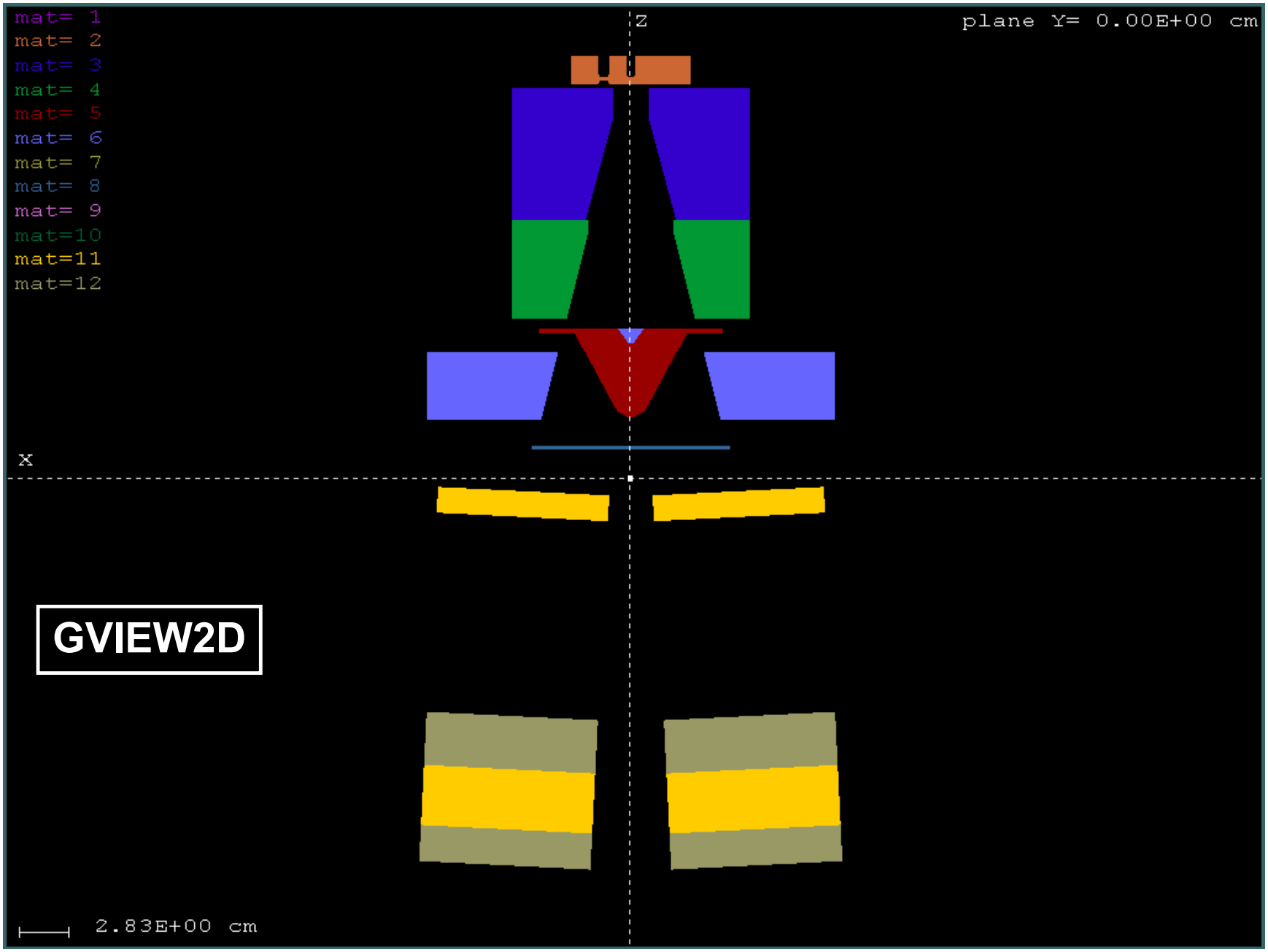
mat= 1
mat= 2
mat= 3
mat= 4
mat= 5
mat= 6
mat= 7
mat= 8
mat= 9
mat=10
mat=11
mat=12
Z
plane Y= 0.00E+00 cm
X
GVIEW2D
2.83E+00 cm

End

Exercise:
NaI detector

Overview

- Calculate the distribution $p(E)$ of energy deposition events (that is, the spectrum) produced by a ^{60}Co beam in a NaI detector

- Introduce an on-the-fly convolution of $p(E)$ with a Gaussian to account for the widening of the peaks observed in a real detector.

Geometry

A 3 in $\times$ 3 in cylindrical NaI detector:

- The crystal is 7.62×7.62 cm^2 in size. Choose its base to be the plane $z = 0$ and its axis of symmetry along the positive z axis.

- The crystal is encased in a 0.24-cm-thick aluminum cover(*)

- An aluminum slab with a thickness of 2 cm is located behind (downstream) the crystal, to model the effect of the photocathode and the photomultiplier tube.

(*) Usually, there is a reflector coating (e.g. Al_2O_3) between the crystal and the cover. For simplicity, we have assumed that its material is equivalent to Al and considered it as part of the cover.

SEE NEXT SLIDE

Cylindrical 3in × 3in NaI detector

2D view

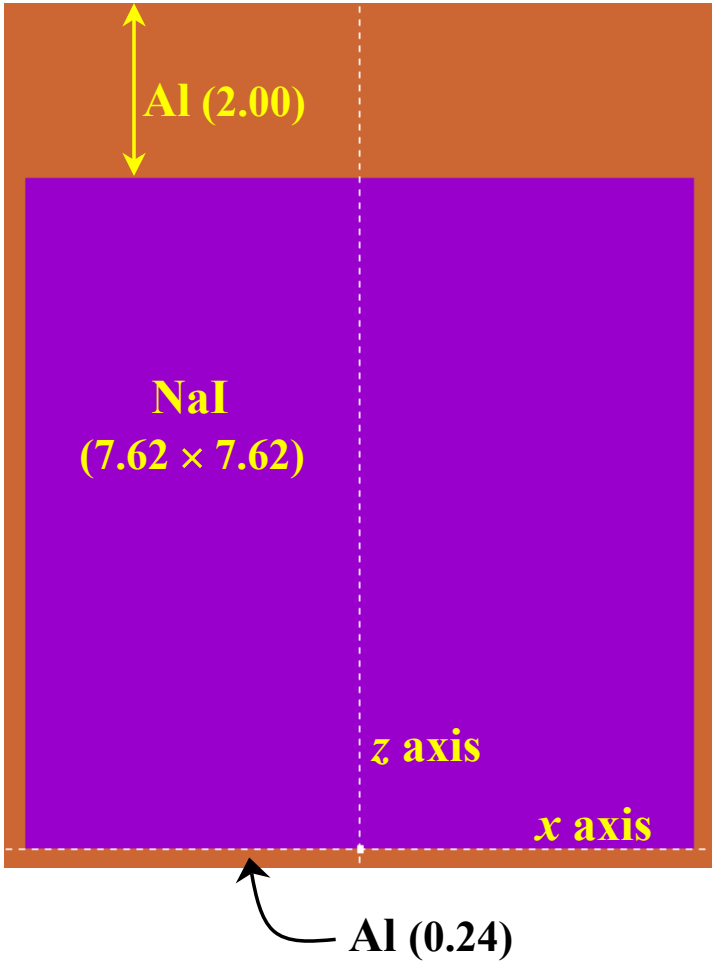

3D view

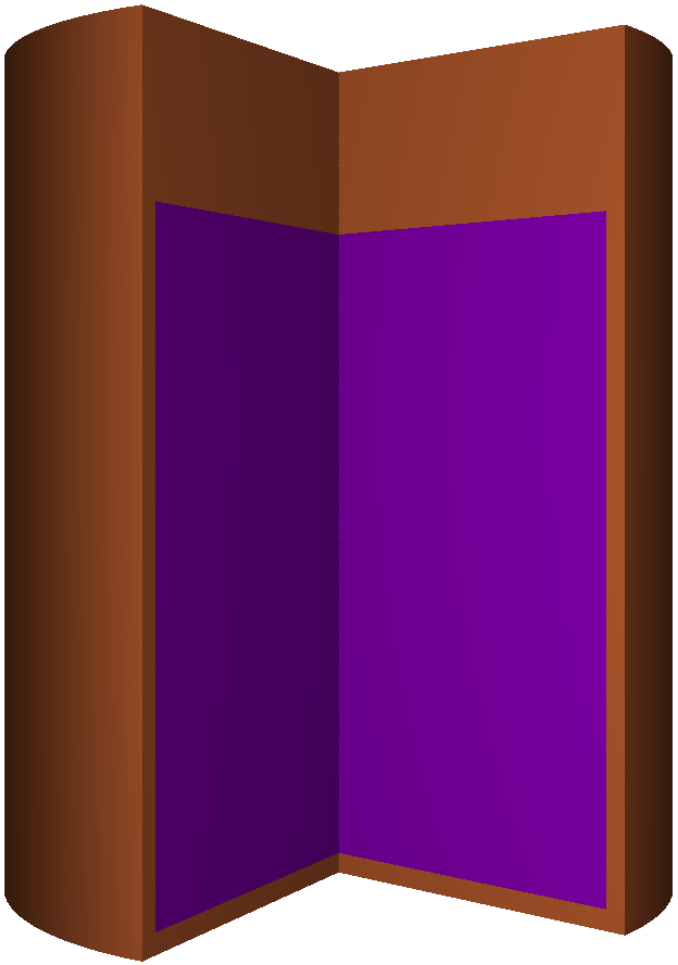

Case 1

Source

- ^{60}Co, i.e. 1173 and 1333 keV photons with equal probability
- Point source, position: (0,0,-20), direction: (0,0,1)
- Angular aperture: enough to “illuminate” the detector front face

Tallies

- Energy deposition spectrum in the crystal

  E in [0,1.5] MeV, N_{bin} = 150
- Cylindrical dose distribution in the crystal

  $N_{\text{r-bin}}$ = 20 , $N_{\text{z-bin}}$ = 20

Configuration

- **`EABS(e-,γ,e+)`** = (+∞, 1, +∞) keV (no $e^{\pm}$ transport)
- **`C1`**,**`C2`**,**`WCC`**,**`WCR`**,**`DSMAX`** are irrelevant
- Simulation time = 60 s

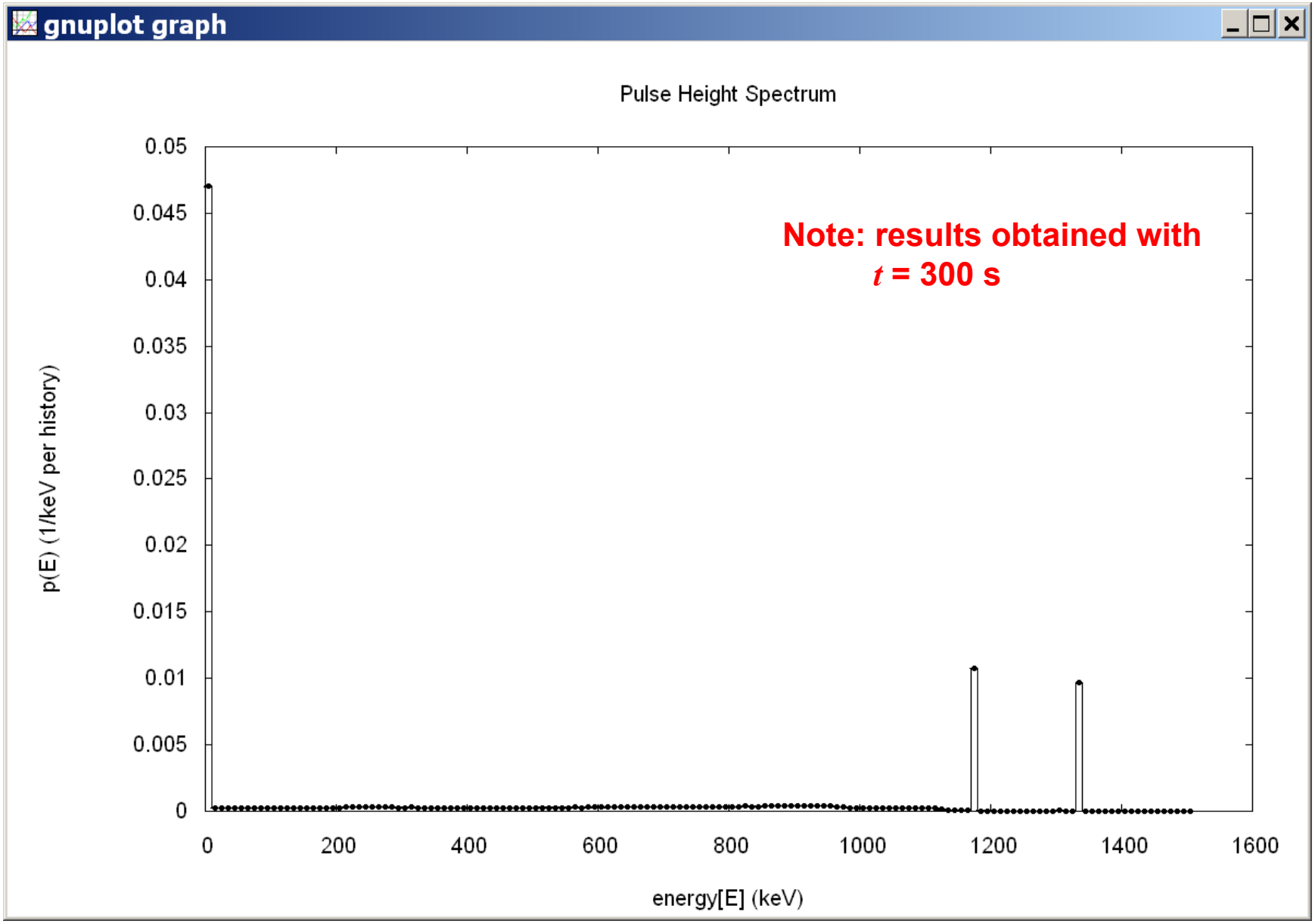
gnuplot graph
Pulse Height Spectrum
Note: results obtained with
t = 300 s
p(E) (1/keV per history)
0.05
0.045
0.04
0.035
0.03
0.025
0.02
0.015
0.01
0.005
0
0
200
400
600
800
1000
1200
1400
1600
energy[E] (keV)

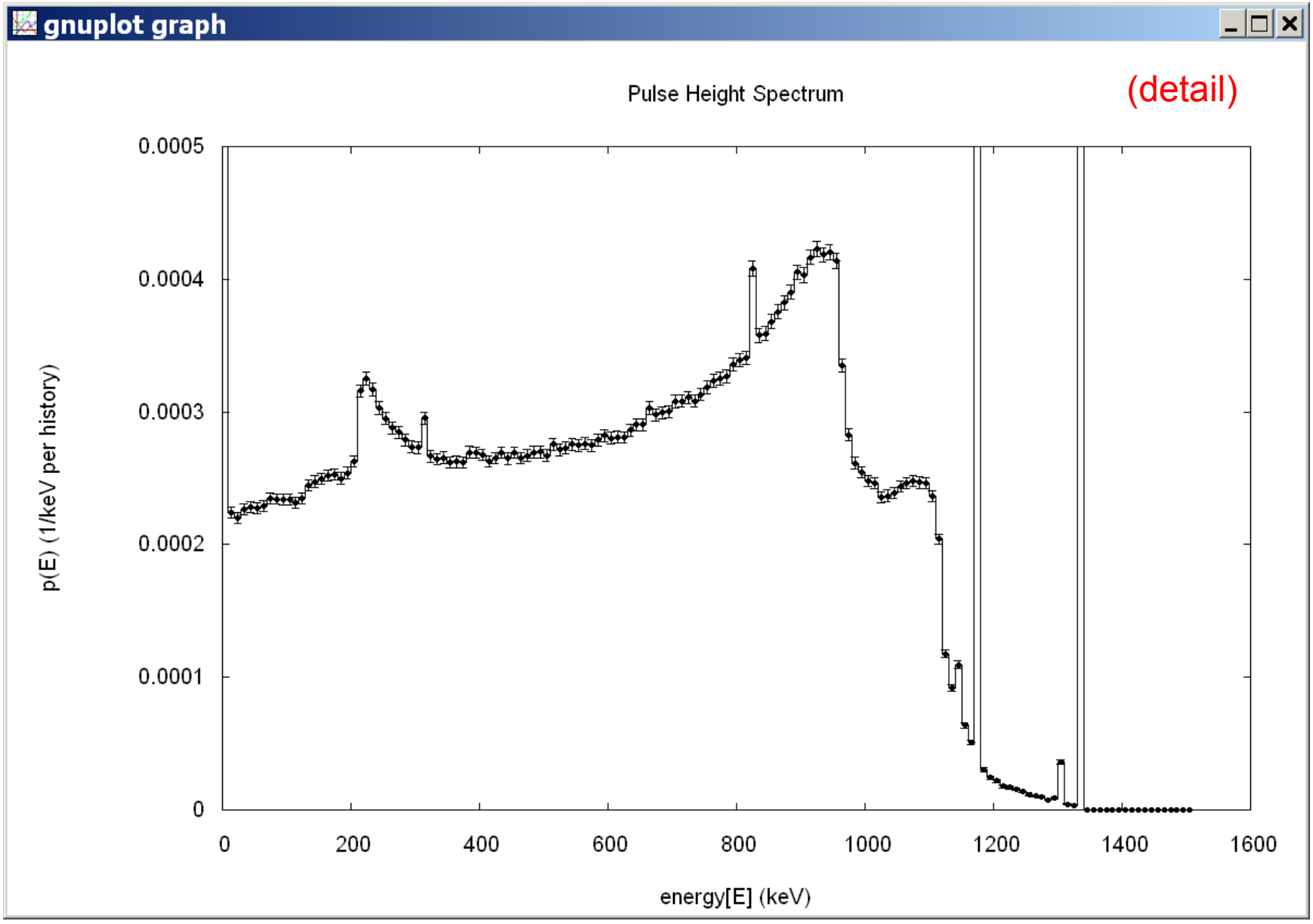
gnuplot graph
Pulse Height Spectrum
(detail)
0.0005
0.0004
0.0003
0.0002
0.0001
0
p(E) (1/keV per history)
0
200
400
600
800
1000
1200
1400
1600
energy[E] (keV)

gnuplot graph

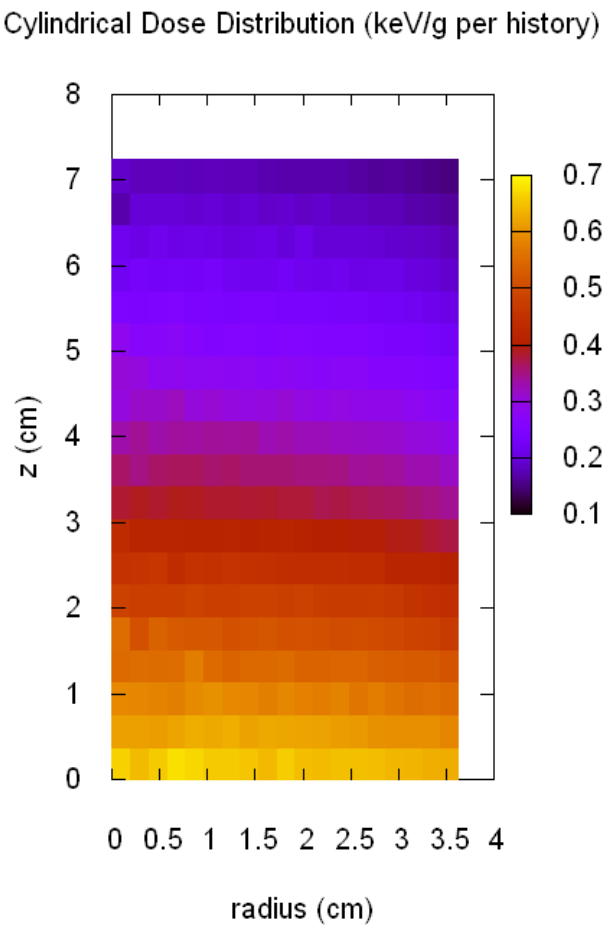

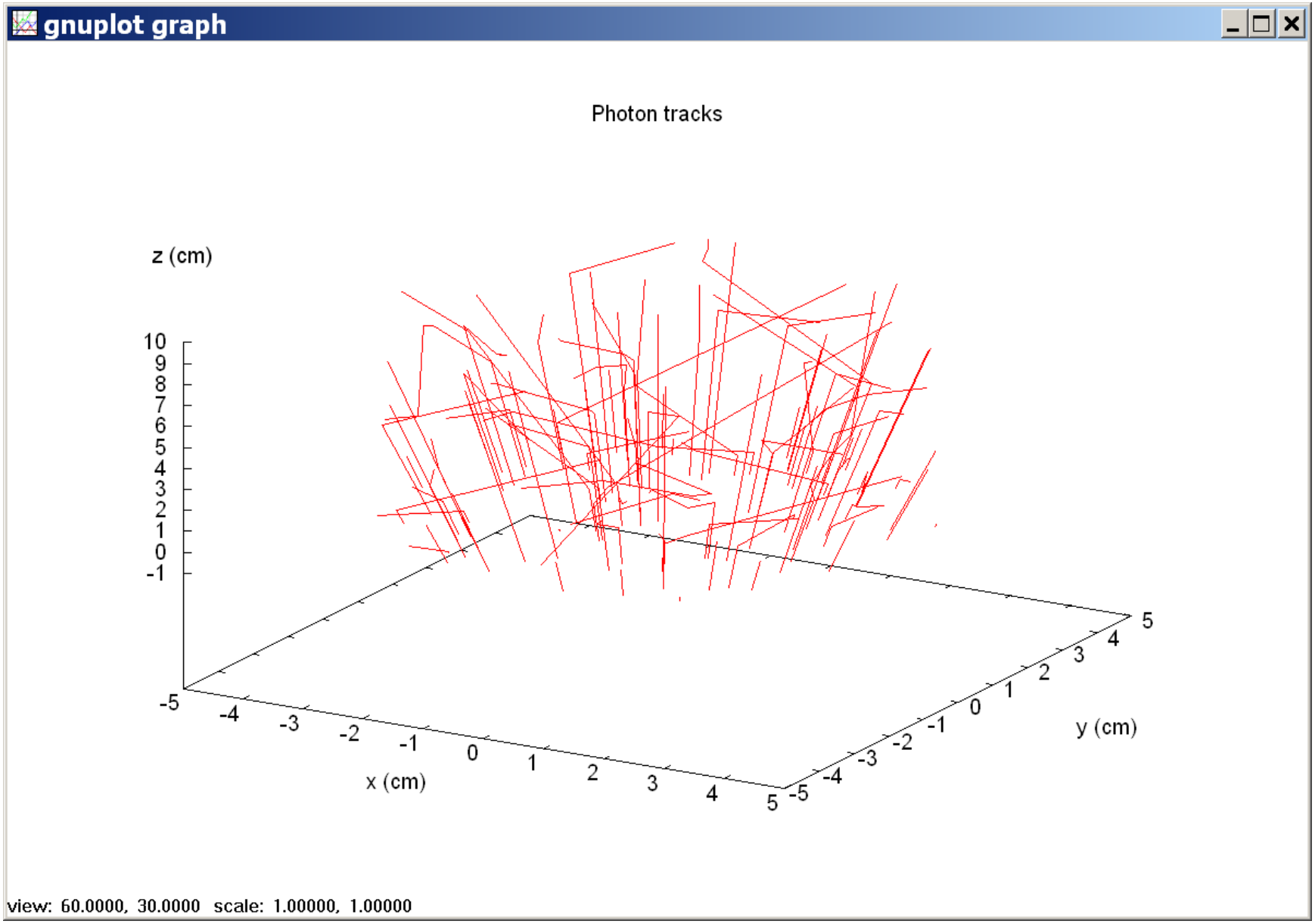
gnuplot graph
Photon tracks
z (cm)
10
9
8
7
6
5
4
3
2
1
0
-1
-5
-4
-3
-2
-1
0
1
2
3
4
5
x (cm)
-5
-4
-3
-2
-1
0
1
2
3
4
5
y (cm)
view: 60.0000, 30.0000 scale: 1.00000, 1.00000

Case 2

Source

Same as case 1

Tallies

Same as case 1, but performing an on-the-fly **convolution with a Gaussian** with a std deviation of

$$\sigma = 34.6\sqrt{E_{\text{dep}}} \quad (\text{in eV})$$

Hint: use the Box-Müller method to sample a Gaussian:

$$\Delta E = \sigma \ \sin(2\pi\xi_1) \ \sqrt{-2\ln\xi_2}$$

Configuration

Same as case 1

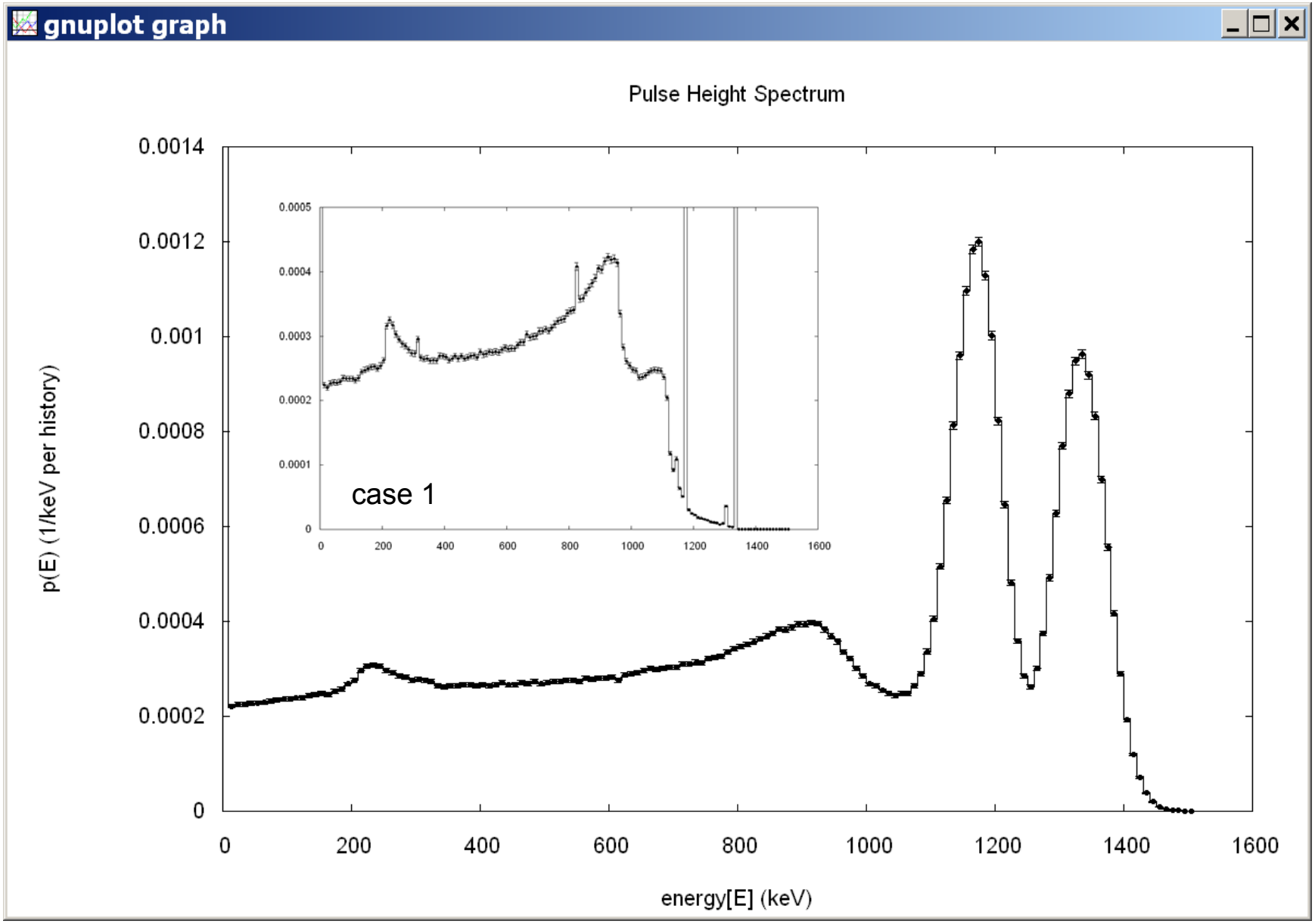
gnuplot graph
Pulse Height Spectrum
p(E) (1/keV per history)
energy[E] (keV)
0.0014
0.0012
0.001
0.0008
0.0006
0.0004
0.0002
0
0
200
400
600
800
1000
1200
1400
1600
case 1
0.0005
0.0004
0.0003
0.0002
0.0001
0
0
200
400
600
800
1000
1200
1400
1600

End

penEasy

PENELOPE made easy

penEasy is a structured general-purpose main program for PENELOPE developed by J. Sempau. It intends to accomplish two goals:

- To provide a set of ready-made source models and tally schemes that are directly applicable to a large variety of practical situations. Users must only provide an input data file, **no programming** is required

- To supply a **structured and modular code** that facilitates its adaptation in case it is needed, reducing the programming effort to a minimum

penEasy, like PENELOPE, is **free and open** software written in Fortran 77. penEasy has also recourse to some extensions supported by g77 and included in Fortran 95 (in particular, the time routines)

penEasy can be downloaded from
http://www.upc.es/inte/downloads/penEasy.htm

What you get

After unzipping, the penEasy directory should contain:

- Windows executable: **`penmain.exe`**
- **`README.txt`** file. This is the user's manual.
- A set of Fortran (*.f) files. Only **`penmain.f`** needs to be compiled.
- Sample geometry file for PENELOPE: **`sample.geo`**
- Input file: **`penmain.in`**
- Command input file: **`command.in`**
- **`documentation/`**
- **`gnuplotScripts/`**

How to use it (Unix)

1- Copy penEasy files into a directory, e.g. `~/penEasy/`.

2- Copy `penelope.f, pengeom.f, penvared.f` from PENELOPE to `penEasy/`.

3- Compile and link penmain: `$ g95 penmain.f -o penmain.x -O -Wall`

1- Create a directory (`~/mySimul`) to store your job. Keep the originals in `penEasy/`

2- Copy the following files from `penEasy/` to `mySimul/`

```
penmain.x, penmain.in, gnuplotScripts/*
```

The geometry and material files need also be in `mySimul/`

3- Edit `penmain.in` and adapt it to your case. In case of doubt, `documentation/`.

4- To run penmain, execute this

```
$ penmain.x < penmain.in > penmain.out &
```

5- If necessary, control the simulation by sending commands through `command.in`

6- Simulation results are in `penmain.out` (in the example). Each tally is also written in a *.dat file used by the Gnuplot scripts. Partial results are updated periodically. All uncertainties are 2 sigma.

End. Thank you.

Outline

1 PENELOPE

2 MANTIS
- Review of MANTIS
- What's new in version 2?
- Exercise 1: effect of x-ray energy on blur
- Exercise 2: x-rays at an angle

3 XSPECT

MANTIS - from the Greek *prophet* or *oracle*

Project goal and description

- An efficient[ab] and flexible[cd] simulation tool for R&D and optimization of radiation imaging systems that includes realistic source, object, and detector modules, and can be used for γ, x rays, $e^{\pm}$ and optical modalities.
- MANTIS features [1]:
  - PENELOPE (x ray and $e^{\pm}$) + DETECT-II (optical)
  - Particle energy range 100 eV - 1 GeV
  - All x-ray scattering included, analog or condensed transport
  - 3D optical blur with realistic columnar model
  - List-mode operation at interaction level, with simultaneous scoring of dose and imaging performance

[a] Detail of simulation can be tailored to the demands of the study.
[b] No added user interphase for efficient calculations in parallel environments.
[c] Free, open source, modular programming.
[d] Ability to model different key geometric scenarios involved in volumetric imaging.

What is MANTIS?

Components

- Requires full PENELOPE2005 distribution[a].
- Requires additional subroutines unique to MANTIS[b].
- Main program structure based on PENEASY package, a general-purpose main program for configuring and running PENELOPE.[c]
- Requires a current FORTRAN compiler.[d]

[a] Available from OECD Nuclear Energy Agency Data Bank (`http://www.nea.fr`).
[b] MANTIS is free, open source software. Requests should be sent to `aldo.badano@fda.hhs.gov`.
[c] Available free from `http://www.upc.es/inte`.
[d] A free compiler successfully used for MANTIS is G95 (`http://www.g95.org`).

Useful components (not required)

- GNUPLOT, a command-driven interactive plotting program.[a]

[a] Available multi-platform, free from `http://www.gnuplot.info`.

Physics in MANTIS

Particle interactions [2]:

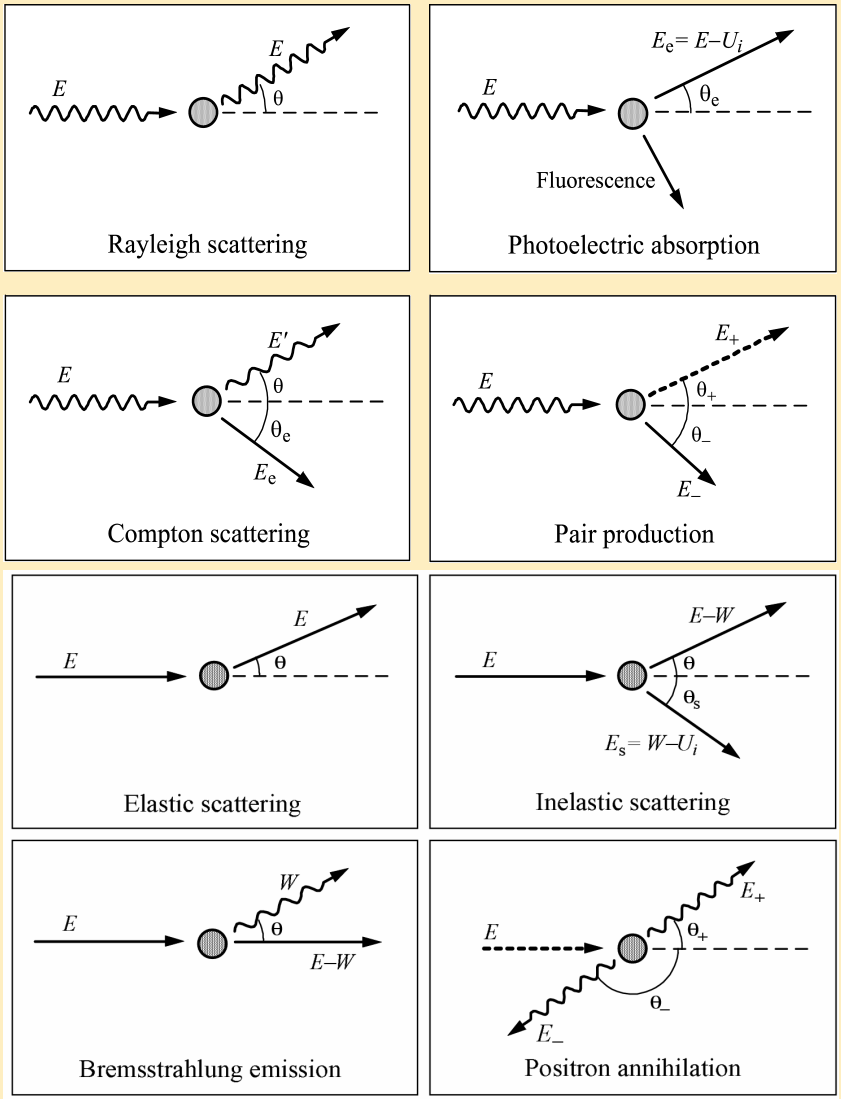

Optical transport methods

- Geometrical optics treatment neglects effect of finite wavelength.
- Light ray is assumed to carry one single quanta (reflection coefficients interpreted as probabilities)
- Materials and emission considered isotropic.
- Refraction (Snell's) law: $n_1 \sin\theta_1 = n_2 \sin\theta_2$.
- Transmission and reflection probabilities:

$$P_{\parallel,trans} = \frac{\sin(2\theta_1)\sin(2\theta_2)}{\sin^2(\theta_1+\theta_2)\cos^2(\theta_1-\theta_2)}$$

MANTIS **tutorial**

Tutorial for MANTIS

Aldo Badano and Josep Sempau

I. Introduction

MANTIS is an efficient and flexible simulation tool for R&D and optimization of radiation imaging systems that use x-ray, γ, $e^{\pm}$ and optical photons. The physics models in MANTIS are described in Ref. [1]. This tutorial describes the contents of the Monte Carlo code MANTIS distribution (version 1.0) and guides first-time users through the demonstration examples.[1] Please read the entire document before starting to use the package. Since MANTIS is an extension to PENELOPE [2], familiarity with the PENELOPE2005 package is needed.

II. Distribution package

The files included in this distribution of MANTIS are listed below.

- \. FORTRAN source:
  MANTIS.F
  DETECT2.F90
  PENELOPE.F
  PENAUX.F
  PENGEOM.F
  PENVARED.F
  SOURCEBOXISOTROPICGAUSSSPECTRUM.F
  SOURCEPHASESPACEFILE.F
  TALLYDETECT2.F
  TALLYENERGYDEPOSITION ...
  ...PULSEHEIGHTSPECTRUM.F
  TALLYPARTICLECURRENTSPECTRUM.F
  TALLYPHASESPACEFILE.F
  TALLYSPATIALDOSEDISTRIB.F
  TALLYSPATIALDOSEDISTRIB_C1.F
  TALLYSPATIALDOSEDISTRIB_C2.F
  TALLYSPATIALDOSEDISTRIB_C3.F
  TIMING.F
  This directory also includes a workspace and project file associated with Visual Studio:
  MANTIS.DSW
  MANTIS.DSP
  not needed if you don't use that software package.
- \demo Files needed to run the demo example described in Section V. More information about the input files can be found in the file header.
  Optical transport material properties:
  abs-vacuum.dm2
  backing.dm2
  csi.dm2
  diode.dm2
  gas.dm2
  pseudo-vacuum.dm2
  substrate.dm2
  Configuration for demonstration examples with wild character ? stands for R or L (see Section V for details):
  mantis_demo_CsI_H?.d2c contains general optical Monte Carlo configuration parameters
  mantis_demo_CsI_H?.d2d contains detector spectral sensitivity
  mantis_demo_CsI_H?.d2m contains material list
  mantis_demo_CsI_H?.d2s contains surface definitions
  mantis_demo_CsI_H?.d2x contains emission spectrum for scintillator
  mantis_demo_CsI_H?.pen contains general Monte Carlo configuration parameters for ionizing radiation transport (see PENELOPE documentation)
  Material file (for particle transport): dixid.mat
  Geometry file: dixid00.level4.geo
  Jobname file: mantis.job
  Output files (you can generate the same output files by running the example cases; useful to compare results): *.out, *.dat.
- \doc This tutorial, TUTORIAL_mantis.pdf.
- \gnuplot_scripts A few Gnuplot scripts for MANTIS output.
- \release Intermediate compilation files obtained

AB is from the CDRH/NIBIB Laboratory for the Assessment of Medical Imaging Systems, Division of Imaging and Applied Mathematics, Office of Science and Engineering Laboratories, Center for Devices and Radiological Health, U.S. Food and Drug Administration. 12720 Twinbrook Parkway, Rockville, MD 20857, telephone (301) 443-5020, fax (301) 443-9101, email aldo.badano@fda.hhs.gov. The mention of commercial products herein is not to be construed as either an actual or implied endorsement of such products by the Department of Health and Human Services. This is a contribution of the U.S. Food and Drug Administration, and is not subject to copyright. JS is with the Universitat Politècnica de Catalunya, Barcelona, Spain, email josep.sempau@upc.es.

[1] MANTIS is free, open source software. Requests for the version 1.0 package should be sent to aldo.badano@fda.hhs.gov.

MANTIS TUTORIAL, VERSION 1.0, JANUARY 30, 2006 1

Tutorial for MANTIS

Aldo Badano and Josep Sempau

I. Introduction

MANTIS is an efficient and flexible simulation tool for R&D and optimization of radiation imaging systems that use x-ray, γ, $e^{\pm}$ and optical photons. The physics models in MANTIS are described in Ref. [1]. This tutorial describes the contents of the Monte Carlo code MANTIS distribution (version 1.0) and guides first-time users through the demonstration examples.[1] Please read the entire document before starting to use the package. Since MANTIS is an extension to PENELOPE [2], familiarity with the PENELOPE2005 package is needed.

II. Distribution package

The files included in this distribution of MANTIS are listed below.

- \. FORTRAN source:
  MANTIS.F
  DETECT2.F90
  PENELOPE.F
  PENAUX.F
  PENGEOM.F
  PENVARED.F
  SOURCEBOXISOTROPICGAUSSSPECTRUM.F
  SOURCEPHASESPACEFILE.F
  TALLYDETECT2.F
  TALLYENERGYDEPOSITION ...
  ...PULSEHEIGHTSPECTRUM.F
  TALLYPARTICLECURRENTSPECTRUM.F
  TALLYPHASESPACEFILE.F
  TALLYSPATIALDOSEDISTRIB.F
  TALLYSPATIALDOSEDISTRIB_C1.F
  TALLYSPATIALDOSEDISTRIB_C2.F
  TALLYSPATIALDOSEDISTRIB_C3.F
  TIMING.F
  This directory also includes a workspace and project file associated with Visual Studio:
  MANTIS.DSW
  MANTIS.DSP
  not needed if you don't use that software package.
- \demo Files needed to run the demo example described in Section V. More information about the input files can be found in the file header.
  Optical transport material properties:
  abs-vacuum.dm2
  backing.dm2
  csi.dm2
  diode.dm2
  gas.dm2
  pseudo-vacuum.dm2
  substrate.dm2
  Configuration for demonstration examples with wild character ? stands for R or L (see Section V for details):
  mantis_demo_CsI_H?.d2c contains general optical Monte Carlo configuration parameters
  mantis_demo_CsI_H?.d2d contains detector spectral sensitivity
  mantis_demo_CsI_H?.d2m contains material list
  mantis_demo_CsI_H?.d2s contains surface definitions
  mantis_demo_CsI_H?.d2x contains emission spectrum for scintillator
  mantis_demo_CsI_H?.pen contains general Monte Carlo configuration parameters for ionizing radiation transport (see PENELOPE documentation)
  Material file (for particle transport): dixid.mat
  Geometry file: dixid00.level4.geo
  Jobname file: mantis.job
  Output files (you can generate the same output files by running the example cases; useful to compare results): *.out, *.dat.
- \doc This tutorial, TUTORIAL_mantis.pdf.
- \gnuplot_scripts A few Gnuplot scripts for MANTIS output.
- \release Intermediate compilation files obtained

AB is from the CDRH/NIBIB Laboratory for the Assessment of Medical Imaging Systems, Division of Imaging and Applied Mathematics, Office of Science and Engineering Laboratories, Center for Devices and Radiological Health, U.S. Food and Drug Administration. 12720 Twinbrook Parkway, Rockville, MD 20857, telephone (301) 443-5020, fax (301) 443-9101, email aldo.badano@fda.hhs.gov. The mention of commercial products herein is not to be construed as either an actual or implied endorsement of such products by the Department of Health and Human Services. This is a contribution of the U.S. Food and Drug Administration, and is not subject to copyright. JS is with the Universitat Politècnica de Catalunya, Barcelona, Spain, email josep.sempau@upc.es.

[1] MANTIS is free, open source software. Requests for the version 1.0 package should be sent to aldo.badano@fda.hhs.gov.

What's new in version 2?

New features in MANTIS version 2

1. Unified Mersenne Twister RNG
2. Allows larger number of surfaces and bodies (columns)
3. Normalized and non-normalized output options
4. Fixed multiple bugs

Objective of the exercises

- The exercises are designed to get you started in running simulations.
- The exercises are drawn from the published literature. Therefore, some additional details are available in the respective papers.
- The exercises are not designed to model a particular brand or model of columnar CsI(Tl) screens. The cases are set up to be representative of current designs.
- The exercises are a good platform to build new models if new or more detailed information is available regarding the geometrical and material properties of the many components of a phosphor screen.
- This evolution of the distributed model (files included in the CD) is entirely up to the user. Therefore, the results obtained with the modified set of files becomes his work and responsability.

Exercise 1: effect of x-ray energy on blur

During this exercise we will replicate the results of Fig. 4a-b of Ref. [3]. Files in the directory allow replication of many other results in that paper.
We'll obtain point-response functions for a CsI(Tl) columnar screen (the details of the model are in the paper) for a monoenergetic x-ray beam of 19 and 79 keV.

X-ray and optical Monte Carlo simulations for imaging 1551

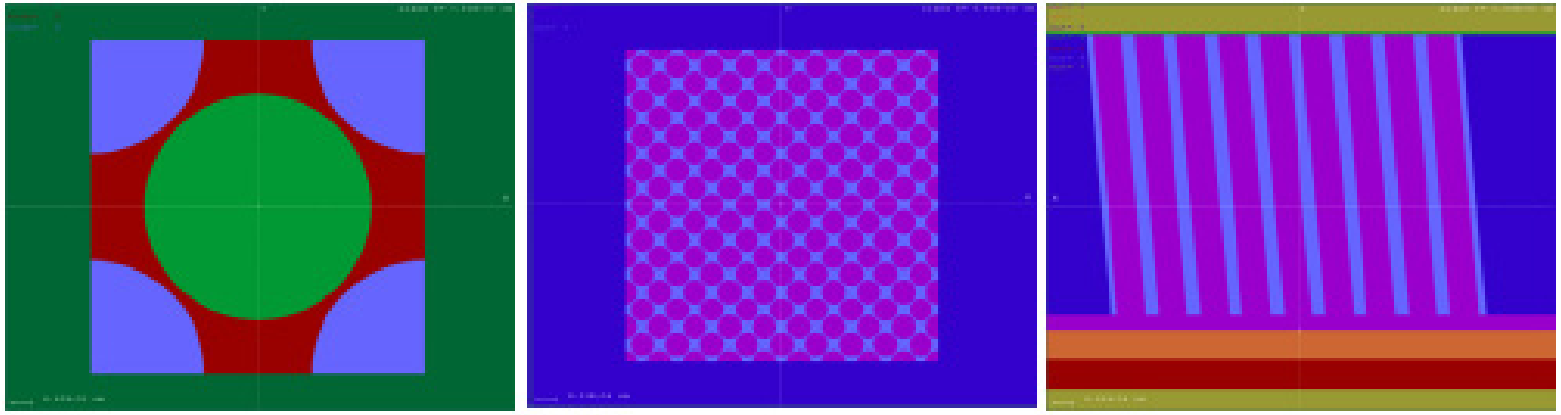

(a) (b) (c)

Figure 4. Cross sections of the basic phosphor screen model containing a columnar layer with arbitrary tilt: (a) basic cell for columnar array, (b) top-view of perpendicular column array and (c) array of 5°-tilted columns. Figures obtained with GVIEW (available with PENELOPE's distribution).

Exercise 1: effect of x-ray energy on blur

Procedure:

1. Script `ipar.pl` generates input files (requires PERL, so done already)
2. Batch file `i.tch` copies common files for all cases (done)
3. Execute case `../mantis_v2 filename.par > filename.log &`
4. Plot the results using gnuplot file `allplots.gnu`

2703 Badano, Kyprianou, and Sempau: Anisotropic imaging performance in indirect x-ray imaging detectors 2703

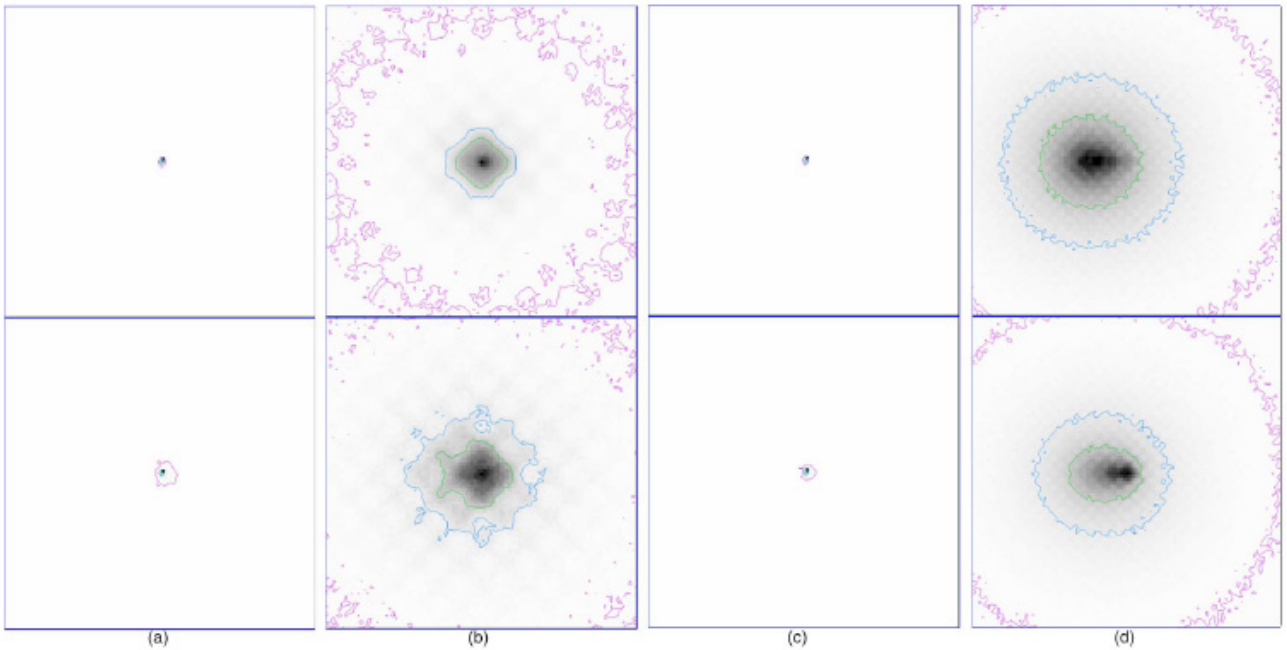

FIG. 4. Point-response functions at 19 (top row) and 79 keV (bottom row) under the normal x-ray incidence angle (θ_x=0°). For our basic phosphor screen model, the columns are tilted to θ_c=5° and ϕ_c=180° (unless otherwise noted, for instance, in Fig. 8). The pixel size in these 100 by 100 images is 1 μm for the 100-μm phosphor thickness, and 3 μm for the 500-μm thick phosphor. Contour lines are indicated for 0.25, 0.1, and 0.01 of the maximum. (a) and (c) are energy deposition maps for 100 and 500 μm thickness. (b) and (d) are the corresponding 2D-PRF including optical transport.

Exercise 1: effect of x-ray energy on blur

Results:

- `*3det.out` contain images at the photo-detector array binned in xsize and ysize in `*.d2c`:

  ```
  &binarraysize xsize=100, ysize=100, imgdx=1.0,
  imgdy=1.0 /
  ```

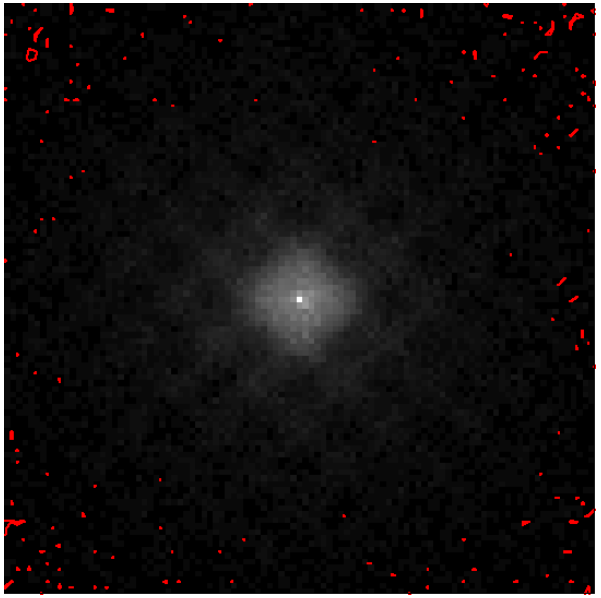

19 keV

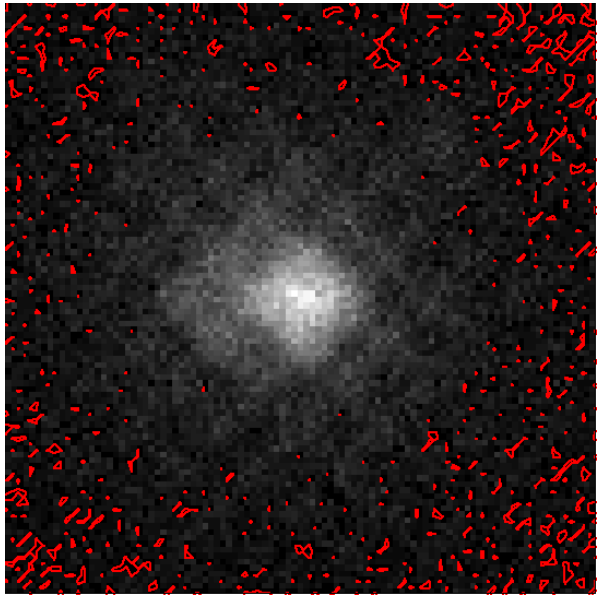

79 keV

Exercise 1: effect of x-ray energy on blur

Results:

- `*collect.out` contain histograms of events per particle (optical pulse-height spectrum):

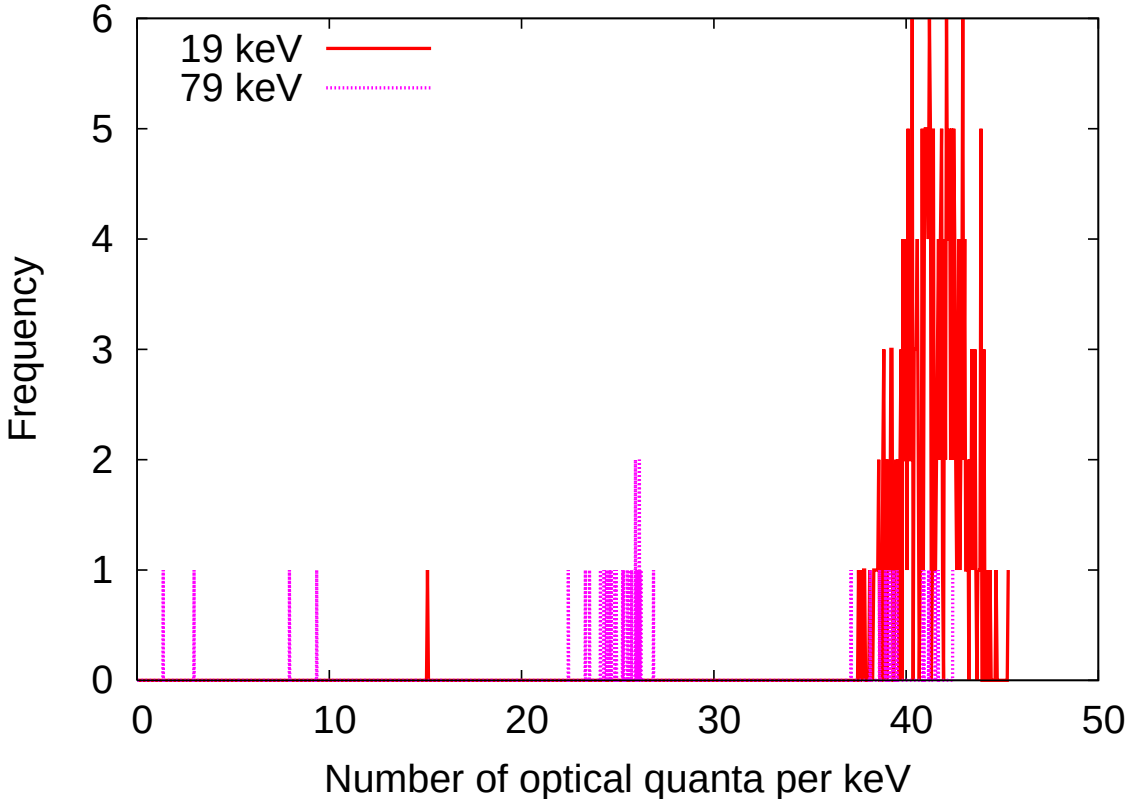

Exercise 2: x-rays at an incidence angle

During this exercise we will replicate the results of Fig. 4a-b of Ref. [3]. Files in the directory allow replication of many other results in that paper.
We'll obtain point-response functions for a CsI(Tl) columnar screen (the details of the model are in the paper) for a monoenergetic x-ray beam of 19 and 79 keV.

X-ray and optical Monte Carlo simulations for imaging 1551

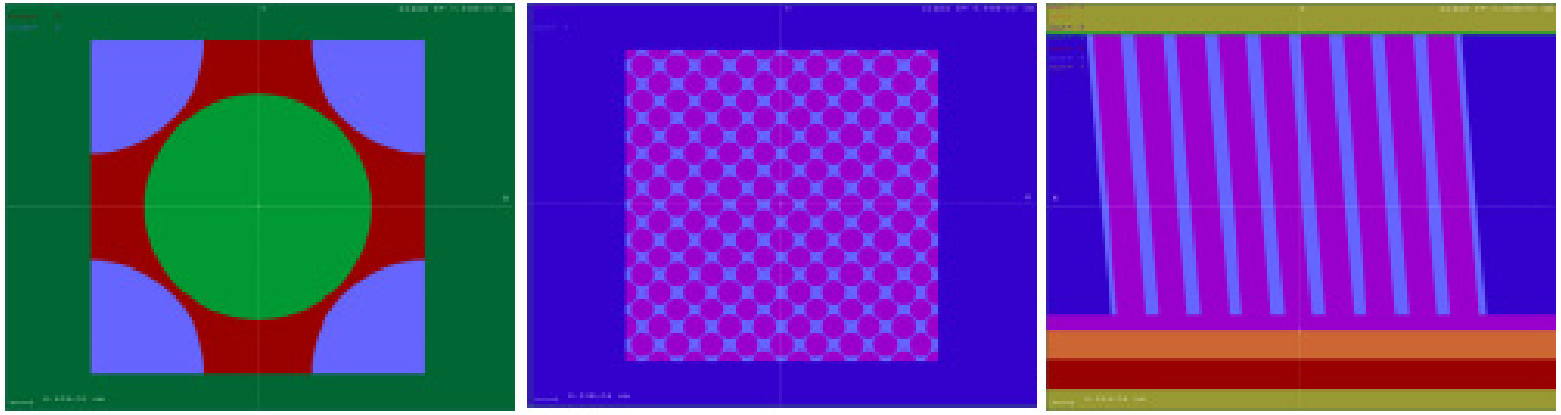

(a) (b) (c)

Figure 4. Cross sections of the basic phosphor screen model containing a columnar layer with arbitrary tilt: (a) basic cell for columnar array, (b) top-view of perpendicular column array and (c) array of 5°-tilted columns. Figures obtained with GVIEW (available with PENELOPE's distribution).

Exercise 2: x-rays at an incidence angle

Procedure:

1. Script `ipar.pl` generates input files (requires PERL, so done already)
2. Batch file `i.tch` copies common files for all cases (done)
3. Execute case `../mantis_v2 filename.par > filename.log &`
4. Plot the results using gnuplot file `allplots.gnu`

2703 Badano, Kyprianou, and Sempau: Anisotropic imaging performance in indirect x-ray imaging detectors 2703

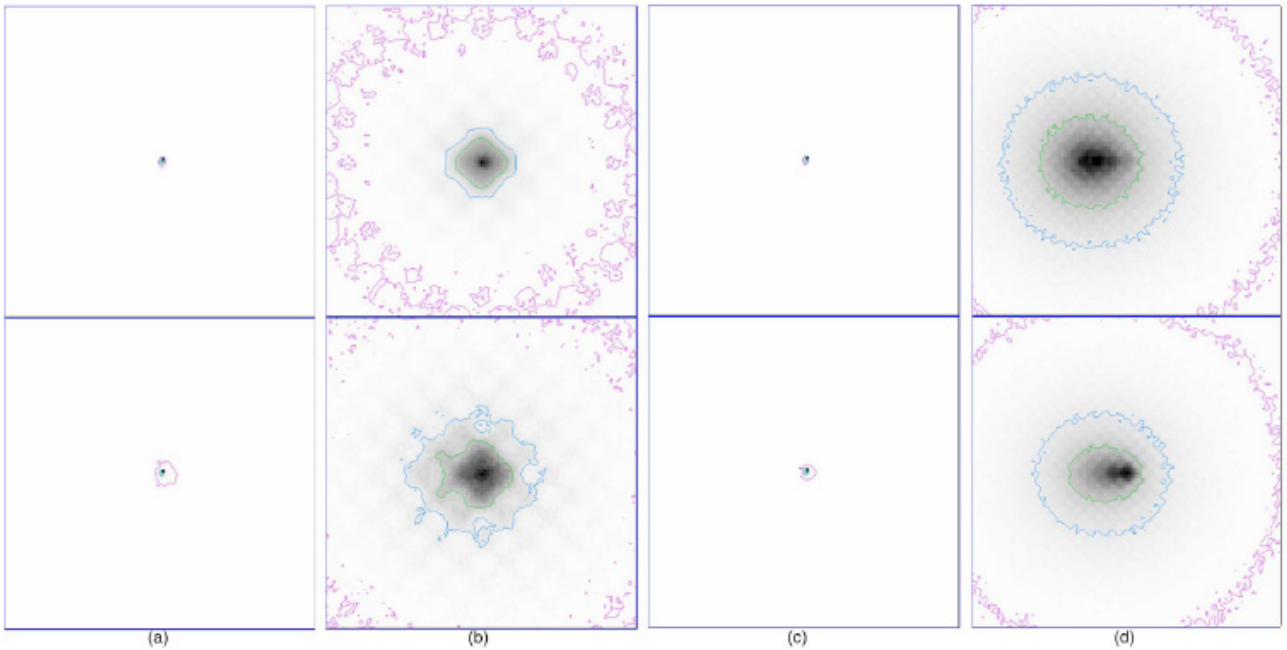

FIG. 4. Point-response functions at 19 (top row) and 79 keV (bottom row) under the normal x-ray incidence angle (θ_x=0°). For our basic phosphor screen model, the columns are tilted to θ_c=5° and ϕ_c=180° (unless otherwise noted, for instance, in Fig. 8). The pixel size in these 100 by 100 images is 1 μm for the 100-μm phosphor thickness, and 3 μm for the 500-μm thick phosphor. Contour lines are indicated for 0.25, 0.1, and 0.01 of the maximum. (a) and (c) are energy deposition maps for 100 and 500 μm thickness. (b) and (d) are the corresponding 2D-PRF including optical transport.

Exercise 2: x-rays at an incidence angle

Results:

- `*3det.out` contain images at the photo-detector array binned in xsize and ysize in `*.d2c`:

  ```
  &binarraysize xsize=100, ysize=100, imgdx=1.0,
  imgdy=1.0 /
  ```

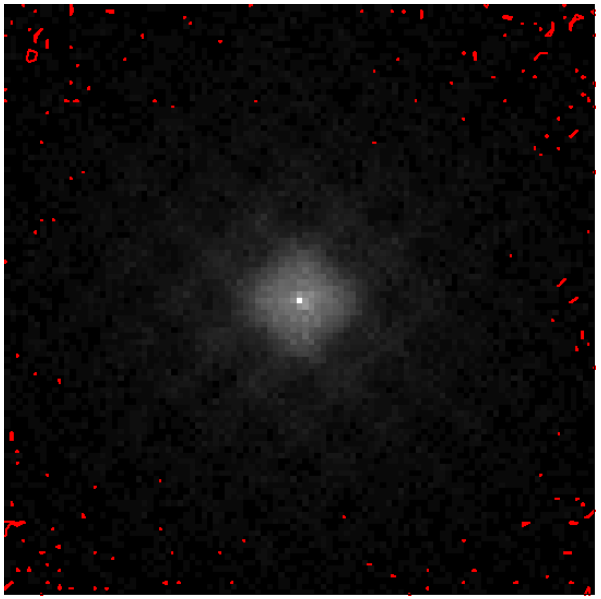

19 keV, normal incidence

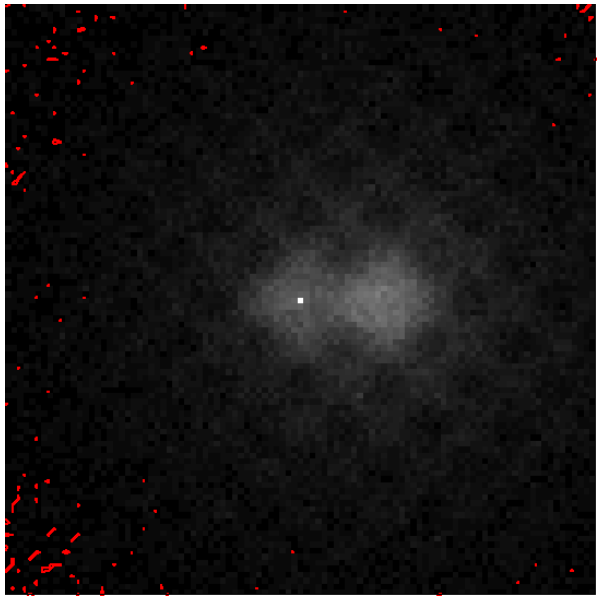

19 keV, 15°

References I

A. Badano and J. Sempau.

Combined x-ray, electron, and optical Monte Carlo simulations of indirect radiation imaging systems.

Phys. Med. Biol., 51:1545–1561, 2006.

F. Salvat, J. M. Fernández-Varea, and J. Sempau.

PENELOPE, A Code System for Monte Carlo Simulation of Electron and Photon Transport.

OECD Nuclear Energy Agency, Issy-les-Moulineaux, France, 2003.

Available in pdf format at `http://www.nea.fr`.

A. Badano, I. S. Kyprianou, and J. Sempau.

Anisotropic imaging performance in indirect x-ray imaging detectors.

Med. Phys., -:In press, 2006.

Outline

1 PENELOPE

2 MANTIS
- Review of MANTIS
- What's new in version 2?
- Exercise 1: effect of x-ray energy on blur
- Exercise 2: x-rays at an angle

3 XSPECT